Sonogashira Reactions on Dimolybdenum Paddlewheel Complexes at the Ligand Periphery

Ilias Alexopoulos

MSc By Research

University of York

Chemistry

January 2023

Abstract

Dimolybdenum paddlewheel complexes (Mo_2PWCs) are well-known and appreciated for their fascinating photophysical and electrochemical properties. These complexes can be linked together *via* an organic linker to form so-called "dimers of dimers", which have been investigated in the literature to improve our understanding of through-bond electronic communication between two redox-active metal cores. Additionally, due to their desirable properties, Mo_2PWCs are seen as potential candidates for synthons towards molecular assemblies such as molecular wires and molecular diodes. However, molecular diodes require an element of asymmetry, which cannot be introduced through traditional self-assembly methodologies due to the formation of undesirable side products, which cannot be separated. To work around this limitation, reactivity at the ligand periphery is proposed as a new, highly selective way of linking two Mo_2PWCs together. In this project, a series of Mo_2PWCs bearing an iodo- or terminal alkyne functionality at the periphery of their ligands have been prepared. These Mo_2PWCs are able to undergo the Sonogashira reaction on their ligands to expand their functionality and to link together two Mo_2PWCs towards the synthesis of a symmetric Mo_2 dimer of dimers. The synthesis of asymmetric dimers of dimers was attempted using two Mo_2PWCs bearing different ancillary ligands. The product was observed but could not be isolated due to ligand scrambling taking place between the two starting materials while in solution. This work therefore proves that performing reactions at the ligand periphery is a plausible way of introducing asymmetry to Mo_2-based molecular assemblies, so long as synthetic limitations unrelated to the reactions themselves are addressed. Finding a way around these limitations will be the subject of future work.

List of Figures

List of Schemes

List of Tables

Acknowledgements

I will try to keep this section brief. After all, it is good practice.

This work was written during what was a transition period for myself as I was starting my PhD studies at the University of Leicester. Especially under these circumstances, I know that without a robust support network, I could not have made it alone.

First and foremost, I would like to thank my supervisor, Dr Luke Wilkinson. His unwavering enthusiasm and support have allowed me to truly push above and beyond my original capabilities when I started my studies here at York. It was thanks to him that I could understand how to tell a story, that "paddlewheels are awesome" and that Times New Roman is a poor choice of font. I would also like to thank my second supervisor, Dr William Unsworth, for his support, advice and contributions throughout my studies.

I would also like to thank the past and present members of the Wilkinson group, as well as all staff and students in the E214 lab, for providing some invaluable company and unforgettable memories inside the lab and in various socials. I would like to especially thank Dr Christopher Goult for providing me with some useful insight in handling air-sensitive chemistry and in using the SolariX for MALDI-MS, Caitlin Fulton for sharing a fume hood and tolerating my clamp-stealing tendencies and, last but not least, Imogen Squire and Benedict Thompson (along with Dr Christopher Goult and Dr Luke Wilkinson) for their massive contributions towards our publication at ACS Inorganic Chemistry. I would also like to thank Dr Iman Khazal for running the lab, Dr Alex Heyam and Heather Fish for keeping the NMR spectrometers running, Karl Heaton for running samples for ESI-MS and APCI-MS and Dr Graeme McAllister for running samples for elemental analysis.

This acknowledgements section would not be complete without a mention of the new people that I am currently working with. I would like to thank in particular my new supervisor, Dr. Fabrizio Ortu, for being incredibly patient while I was working on this thesis and for allowing me to spend some office hours to make sure that I finish strong. I would also like to thank the members of the Ortu group for the warm welcome into the group, helping me settle in and generally being around during a particularly stressful period for me.

Finally, I would like to thank my close family, extended family and friends across cities and countries for their support throughout the years.

Declaration

I declare that, unless otherwise stated, this thesis is a presentation of original work, and I am the sole author. This work has not previously been presented for an award at this, or any other, university. All sources are acknowledged as references.

Abbreviations

CuAAC: Copper Azide-Alkyne Cycloaddition

CV: Cyclic Voltammetry

DAniF: Di-p-Anisyl Formamidinate

DarF: Diphenyl Formamidinate [$(PhNC(H)NPh)^-$]

DFArF: 3,5-Difluorophenyl Formamidinate

DFT: Density Functional Theory

DOSY: Diffusion Ordered Spectroscopy

DPV: Differential Pulse Voltammetry

DSSC: Dye-Sensitised Solar Cell

IR: Infrared

MALDI TOF: Matrix Assisted Laser Desorption Ionisation Time-of-Flight

MLCT: Metal Ligand Charge Transfer

MO: Molecular Orbitals

MOF: Metal-Organic Framework

Mo_2PWCs: Dimolybdenum Paddlewheel Complexes

PWC: Paddlewheel Complex

r.t.: Room Temperature

Rh_2PWCs: Dirhodium Paddlewheel Complexes

Ru_2PWCs: Diruthenium Paddlewheel Complexes

SEC: Size Exclusion Chromatography

UV-Vis: Ultra Violet-Visible

Table of Contents

Introduction

Molecular Assemblies

Supramolecular chemistry is a discipline which deals with the organised assembly of more than one molecule, often facilitated by non-covalent interactions. Despite their weaker nature, these interactions are crucial in keeping certain molecular systems together. One core example of the integral role of such interactions would be human and animal DNA, whose iconic double helical structure is kept in place due to the hydrogen bonding interactions between the nitrogenous bases attached to each strand. Such non-covalent interactions are also responsible for the structure of every protein, whose variation is based on the sequence of amino acids in their peptide chains. These interactions keep our world together, so it is only natural that they would pique scientific interest, which has manifested into a field that is exponentially growing in popularity.[1] However, it is not just sheer curiosity that fuels this field of research. By enhancing our understanding of supramolecular chemistry, it is possible to develop new technologies that can contribute towards solving some of humanity's greatest challenges. For example, MOFs (metal-organic frameworks) can help with CO_2 capture and environmental remediation,[2,3] while the host-guest chemistry of molecular cages has been shown to have potential in drug delivery and treatment of cancers.[4,5]

Types of Molecular Assemblies and their Application

Metal Organic Frameworks (MOFs)

Metal-organic frameworks (MOFs) are solid materials that consist of repeating units of metal nodes, often referred to as "secondary building units" (SBUs), coordinated and connected by organic linkers.[6] They are most commonly made by "self-assembly", a highly efficient method of utilising the innate properties of their constituents to construct frameworks with highly organised geometries (Figure 1). The properties that determine their capacity to self-assemble and the structure of the final product are the coordination geometry of the metal centre, as well as the geometric shape of the organic linker. MOFs typically consist of a porous, three-dimensional structure. Properties such as porosity, surface-area and crystallinity can be fine-tuned based on the choice of starting materials, making them excellent materials for the sorption of small molecules. Furthermore, their capacity to absorb gases within their pores has spiked interest for their applications in gas storage and separation.[7]

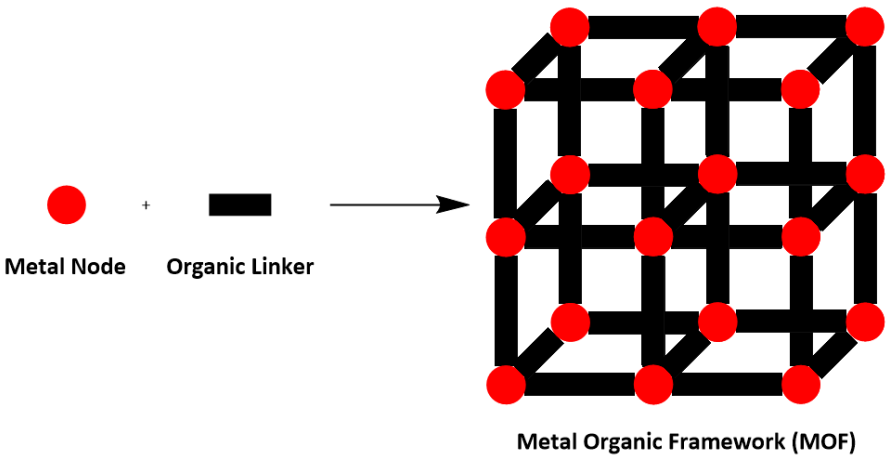

Figure 2 General schematic for the construction of a MOF.

The structural features of MOFs also make them ideal candidates for applications in heterogeneous catalysis.[8] Catalysts must contain active sites to function, and the organic-inorganic hybrid nature of MOFs means that active sites can be placed on either the metal node or the organic linker unit. For example, iron (III) porphyrin MOFs can heterogeneously catalyse the Diels-Alder reaction through the iron coordination site, whereas thiourea-functionalised organic linkers have been used as part of a zinc-MOF to utilise hydrogen-bonding interactions for the catalysis of Friedel-Crafts reactions.[9,10] The capacity to choose the metal atom for its coordination mode, as well as the organic linkers for their functionality, give rise to a host of possibilities for MOF engineering towards sustainable heterogeneous catalysts.

The presence of redox centres within MOFs amplifies the potential for their use as electrical conductors.[11] Metal centres in MOFs can act as charge carriers and, based on the structural and electronic properties of the ligands and their capacity to communicate with the metal centres, can allow for electron- and hole-transport through the framework, making them potentially conductive materials. For example, when nodes are coordinated with organic linkers *via* thiol groups over hydroxy groups, MOFs show higher conductivity, due to greater orbital overlap between metal and chalcogen.[12] In conductive MOFs, an electronic charge can be transferred in a number of ways:[11] through organic linkers *via* bonding; through expanding the conjugation in an organic system by orbital overlap with the metal centre; *via* through-space conductivity facilitated by π-π stacking interactions; through redox-hopping interactions; through guest-promoted hopping interactions, which is possible for MOFs containing guest molecules in their pores. This versatility in potential electron charge transfer pathways makes MOFs excellent candidates for the development of molecular electronics, such as supercapacitors.[13]

Molecular Cages

Molecular cages are three-dimensional molecular frameworks that, unlike MOFs, do not span infinitely. Instead, they are closed assemblies consisting of smaller molecular systems. At their core, these assemblies contain an empty space which can be occupied by a guest molecule (Figure 2). Similar to the usability of pores in MOFs, the encapsulation of a "guest" molecule can pave the way for applications in, for example, drug delivery.[14] Based on the size of the cavity, organic molecules can also be trapped within it by interacting with the host in a manner similar to how enzymes trap molecules in their active site. Accordingly, it seems plausible to expect that molecular cages can take part in homogeneous catalysis by encapsulating and activating molecules that would be otherwise unreactive under most other conditions. Indeed, self-assembled molecular cages have been used as catalysts for commonly used organic reactions such as the Diels-Alder reaction,[15,16] the Nazarov cyclisation,[17] and the acid-catalysed hydrolysis of orthoformates.[18] The acceleration of reaction rates is often owed to the stabilisation of a transition state by binding a reactant within the cage host.[15] The degree of acceleration in reaction rates attainable by the use of molecular cages as catalysts can be comparable to that observed in some naturally-occurring enzymes.[17]

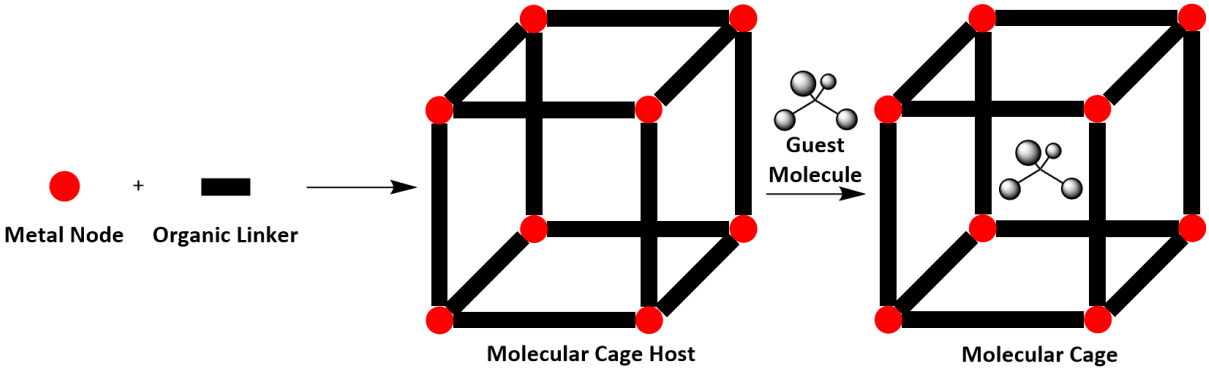

Figure 3 General schematic for the construction of a molecular cage.

2-Dimensional Nanosheets

The world of materials science was revolutionised in 2004 when graphene was discovered and, in 2010, the Nobel prize in physics was awarded to the scientists responsible for its discovery.[19] Since then, the interdisciplinary field of 2D nanomaterials has been growing rapidly, with one of the branches of this field being metal-organic nanosheets.[20] They can be constructed either from a top-down or a bottom-up approach (Figure 3). A top-down approach involves the exfoliation of layered MOFs to leave behind only one layer. A "bottom-up" approach involves the synthesis of MOFs whilst preventing their growth along one direction. Such materials have found extended use in heterogeneous catalysis, electrocatalysis and photocatalysis, utilising the considerably larger available surface area compared to their three-dimensional analogues in conjunction with the catalytically active metal sites, which are more exposed as a result.[21] The large surface area has also fuelled research towards the development of light-harvesting devices.[22] Thus, 2D nanosheets are starting to play a vital role in amplifying the capabilities and therefore application of MOFs.

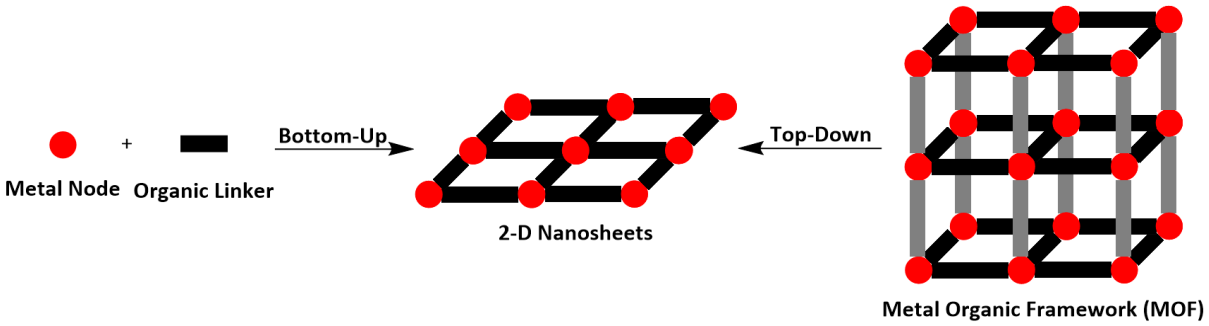

Figure 4 General schematic for the construction of a 2D nanosheet.

Other Supramolecular Structures of Note

In some cases, non-covalent interactions can facilitate the self-assembly of "pseudorotaxanes" which comprise a linear molecule threaded through the centre of a cyclic host. These compounds can be capped by bulky organic groups or inorganic metal centres *via* directed assembly to give rise to rotaxanes, which are host-guest molecules where the guest is trapped within the cavity due to steric constraints. A guest molecule possessing the right template to undergo a ring-closing mechanism can participate in a template-directed assembly process where the guest ring is closed, interlocking the host and the guest together. This gives rise to a catenane, defined as two macrocyclic structures interlocked together. All of these molecules play an important role in the large field of molecular machines in the form of molecular switches and molecular shuttles.[23–25] Rotaxanes

have also been developed into molecular materials by designing polymers as well as metal-organic rotaxane frameworks (MORFs) using metal centres to impose the desired geometry.[26]

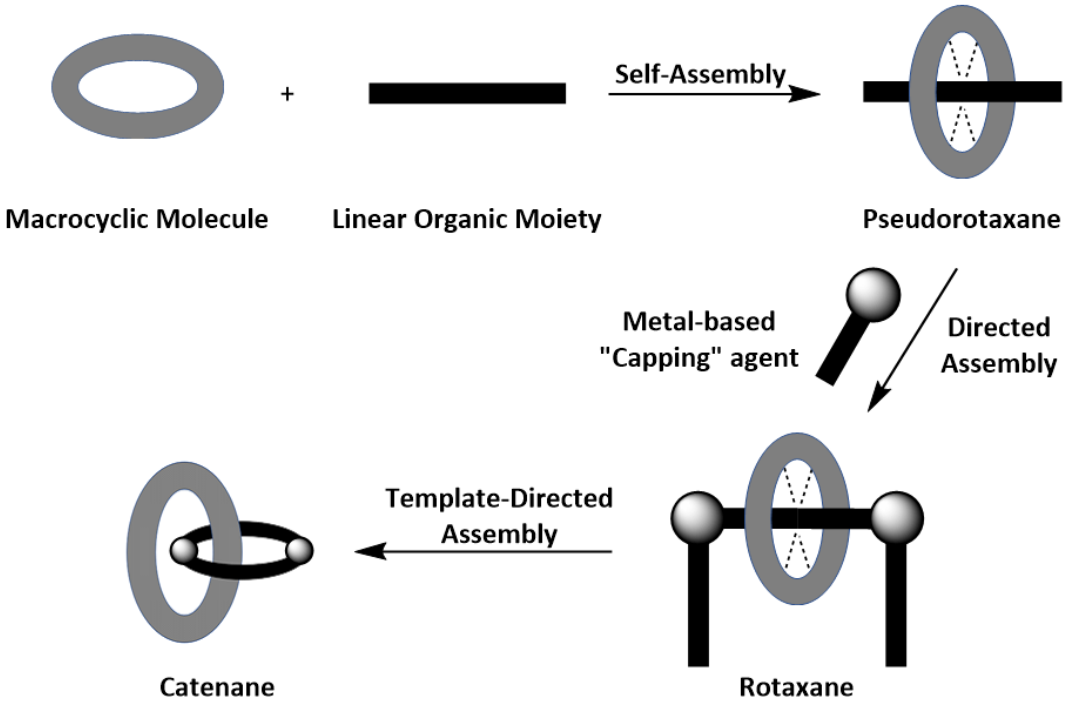

Figure 5 General schematic for one way of constructing rotaxanes and catenanes.

Building Molecular Assemblies: Self-assembly vs Directed Assembly

Most of the above supramolecules are built either by self-assembly or by directed assembly. Self-assembly involves the construction of supramolecular architectures from their constituents through the fluxional, intermolecular interactions taking place between them. In an environment where all required constituents are in place, no human intervention is required, and supramolecular assemblies form as the thermodynamically favoured outcome. Conversely, directed assembly takes place through the "irreversible" (in relative terms) formation of non-fluxional covalent bonds. Although this approach is less commonly observed in nature, proteins use directed assembly to combine amino acids into a peptide chain. Self-assembly is the most commonly employed method for constructing supramolecular assembles since large molecules containing repeating units can be prepared in one step, making the synthetic process much more facile. Nevertheless, both strategies can be highly efficient but require careful consideration when it comes to choosing the appropriate starting materials and reaction conditions.

One highly-predictable way of bringing molecules together is coordination-based self-assembly (Figure 5, left).[27] While coordination bonds are considered covalent, they are often kinetically labile and an equilibrium can be established, leading to the thermodynamically favoured products. Transition-metal elements can adopt different coordination geometries based on their electronic configuration and to some extent on the binding geometry of the ligand used. For example, d^8 metal centres such as Pd(II) prefer a square planar geometry, whereas low-spin d^6 metals such as $Ru^{(II)}$ may prefer octahedral coordination environments. Such geometries are typically well known, meaning that they can be leveraged to add the proper directionality of the starting materials for the construction of supramolecular assemblies such as $Pt^{(II)}$-based coordination cages.[14,28–30]

Another strategy for self-assembly involves utilising hydrogen bonding interactions to bring molecules together (Figure 5, centre). Similar to how DNA stores genetic information through the maintenance of its double helical structure, selected molecules that can donate or accept hydrogen atoms *via* appropriate functional groups can come together to form larger molecular assemblies. One fascinating example of such systems involves hydrogen bonding self-assembled polymers, where monomers are polymerised *via* hydrogen-bonding interactions.[31,32] The polymer properties can be modified by solvent, temperature and concentration.

Self-assembly can also be driven by π-π stacking interactions, caused by weak interactions between two separate planar π-systems (Figure 5, right). This particular strategy is less reliable on its own due to the possibility of π-stacking interactions taking place on two different phases, meaning that symmetric starting materials need to be used to avoid obtaining a statistical mixture of isomers. Despite this challenge, highly symmetrical cages have been designed using this strategy.[33]

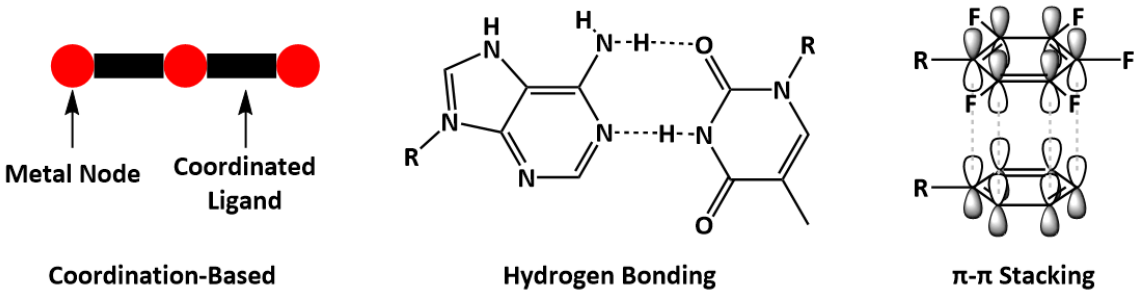

Figure 6 Different Types of self-assembly.
Coordination-based between metals and bridging ligands (left), hydrogen-bonding between adenine and thymine (middle), π-π stacking between an arene and pentafluoroarene ring (right).

Although most supramolecular systems are constructed through self-assembly, an alternative approach to construct such moieties would be directed assembly. As described above, this approach involves the construction of more rigid,kinetically inert linkers (i.e. C-C bonds) between appropriately selected building blocks through a chemical reaction. Typically, reactions employed for such systems involve those that can form covalent bonds under mild conditions with few side products. Examples of such reactions may involve cross-coupling chemistry (Heck, Suzuki, Sonogashira *etc*.), imine condensation, "click" chemistry (such as the copper-catalysed alkyne-azide cycloaddition, CuAAC). To perform these reactions, a suitable functionality needs to be present on the starting materials. Furthermore, to obtain a desired supramolecular structure, building blocks with the correct molecular geometry need to be selected. This method is often used for the construction of molecular cages, and a large database consisting of starting materials has been amassed over the last few decades.[34] One downside to self-assembly is its inability to introduce variety to its supramolecular structures. Proteins made by nature are vastly more complicated than any supramolecular cage built by self-assembly, particularly when forming assemblies which include an advanced functionality at a targeted spot (*i.e.* an enzyme active site); self-assembly generally does not allow for this type of addition. This can be a challenge for directed assembly as well. For example, when trying to add more than one organic linker to form supramolecular cages with Pd on their edges, large superstructures of the formula $[Pd_{12}L_{24}]^{24+}$ have over 350,000 potential isomers.[35] Of course, there is a preference for certain isomers, but with increasing complexity, introducing asymmetry appears to be a considerable challenge due to the increased thermodynamic stability of symmetric structures.

There are many instances where introducing asymmetry into smaller molecular assemblies could unlock certain applications. For example, a 2011 study developed a multi-component organic

molecule containing an electron-donating dithiophene component on one end and an electron-withdrawing naphthalene diimide component on the other end (Figure 6, top). These two structural features enforce the directionality of the electron transport in the junction, acting as a molecular diode or rectifier.[36] The introduction of asymmetry can also be beneficial towards the development of dye-sensitised solar devices.[37] Adding an electron-donating organic component on one *meso* position of a zincated porphyrin and an electron withdrawing organic component on the opposite *meso* position of said porphyrin can introduce a "push-pull mechanism", which would enhance charge transfer from the photoactive porphyrin moiety onto the semiconductor support in the cell (Figure 6, bottom).[38]

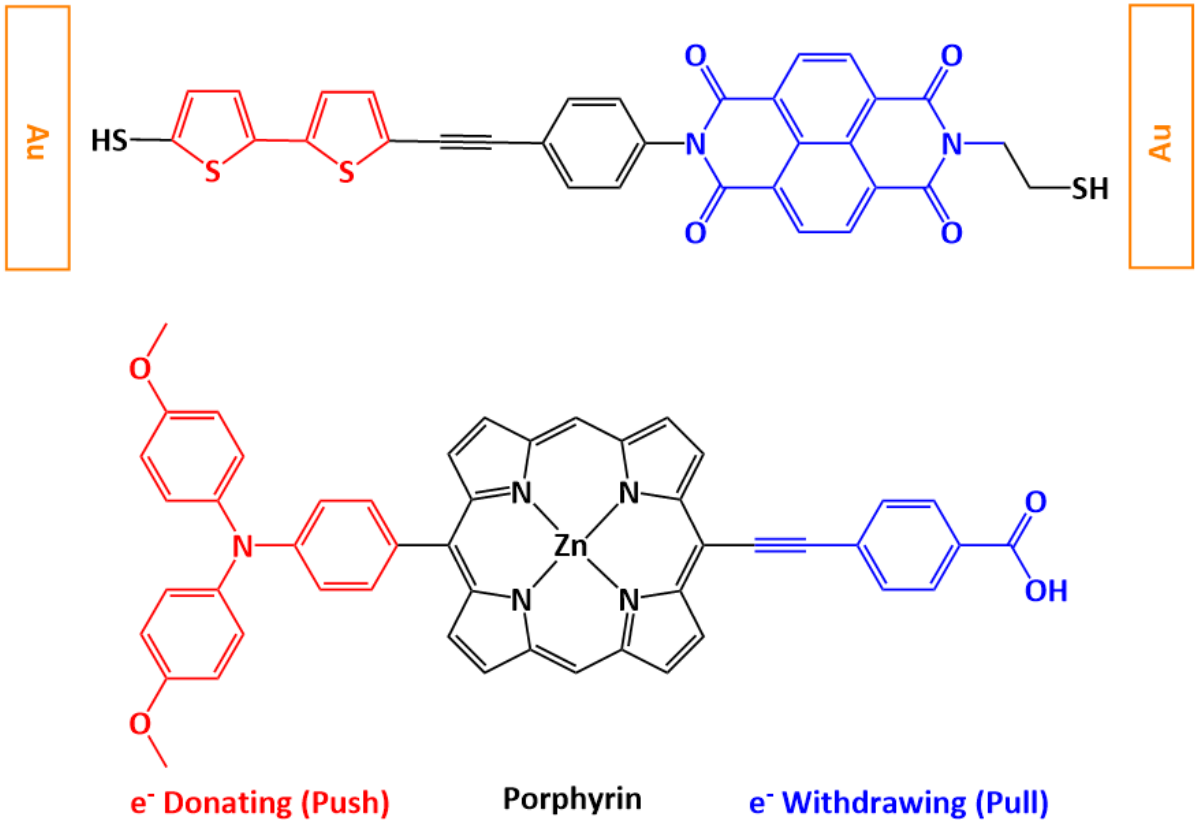

Figure *7 Asymmetric donor-bridge-acceptor systems*.[36,38]

With these applications in mind, one of the major challenges that this project aims to address is the development of "push-pull" type transition-metal complexes with precise synthetic control through a directed assembly approach. The complexes of particular interest herein are the MM quadruply-bonded dimolybdenum paddlewheel complexes (Mo_2PWCs), which have exceptional electron-transfer properties (*vide infra*) and have recently shown considerable promise in the field of molecular electronics.[39,40]

Mo_2PWCs and the Quadruple Bond

The first reported instance of a transition-metal complex consisting of two metal centres bound together by a quadruple bond was in 1964 after a series of investigations surrounding rhenium clusters.[41] The compound of interest, $[Re_2Cl_8]^{2-}$, had its chloride ligands arranged in an eclipsed conformation (as found in a subsequent study) and exhibited an "ultra-short" metal-metal distance of 2.24 Å (Figure 7, left).[42] This geometrical shape defines a category of complexes known as "Paddlewheel Complexes" (PWCs). Since their initial discovery, a plethora of PWCs with varying bond

orders have been observed based on a variety of d-block metals such as Rh,[43] Mo,[44] W,[45] Ru,[46,47] Cu,[48] Co,[49] and more.

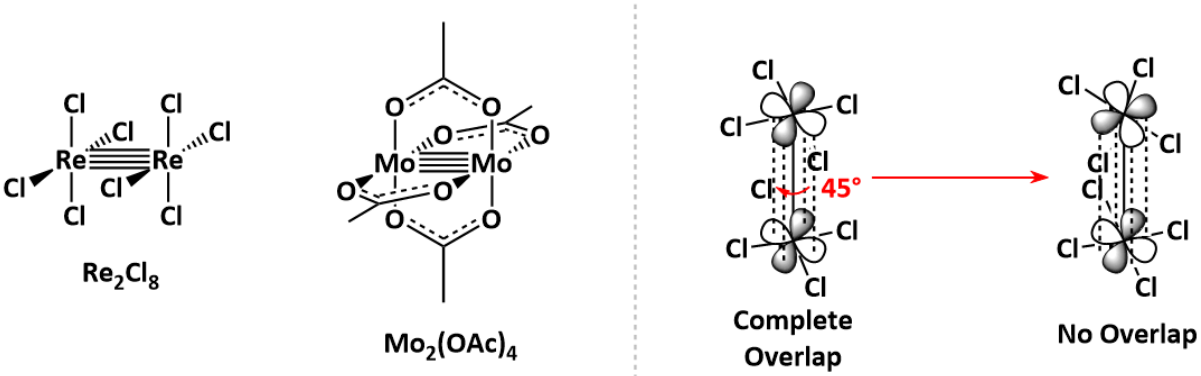

Figure 8 Geometrical structures of Re_2Cl_8 and $Mo_2(OAc)_4$ (left).
Depiction of loss of δ-orbital bonding character after a 45° rotation along the M-M bond axis (right).

Dimolybdenum paddlewheel complexes (Mo_2PWCs) consist of a central dimolybdenum Mo_2^{4+} unit, where the two molybdenum atoms are bound together by a quadruple bond (Figure 7, left, $Mo_2(OAc)_4$). The Mo atoms are found in the Mo^{2+} oxidation state, giving each a d^4 configuration which is isoelectronic to the Re^{3+} atoms in $[Re_2Cl_8]^{2-}$. For both Re_2 and Mo_2 complexes, the bond formed between them has the configuration of $\sigma^2\pi^4\delta^2$, owed to the overlap of d_{z^2} orbitals (σ^2), d_{xz} and d_{yz} orbitals ($2 \times \pi^2$) and d_{xy} orbitals (δ^2). These four types of orbital overlap give rise to the quadruple bond, whose strength places the two Mo atoms in close proximity with an average Mo-Mo bond length of 2.06-2.12 Å. A molecular orbital diagram describing the origin of the quadruple bond is illustrated (Figure 8). The last pair of atomic orbitals, $d_{x^2-y^2}$, does not participate in the quadruple bond, but instead contributes to metal-ligand bonding.[50] Upon rotation around the z axis (i.e. the M-M bond), the σ bond remains unchanged and the two orthogonal π bonds rotate into each other, resulting in no net loss of σ or π bonding character. However, the δ bond is sensitive to internal rotation around the z axis, with a 45° rotation leading to complete loss of bonding character and a 30° rotation leading to the loss of 50% of the bonding character (Figure 7, right). The extra stability provided by the retention of the quadruple bond leads to the unusually stable eclipsed arrangement of the ligands.[51]

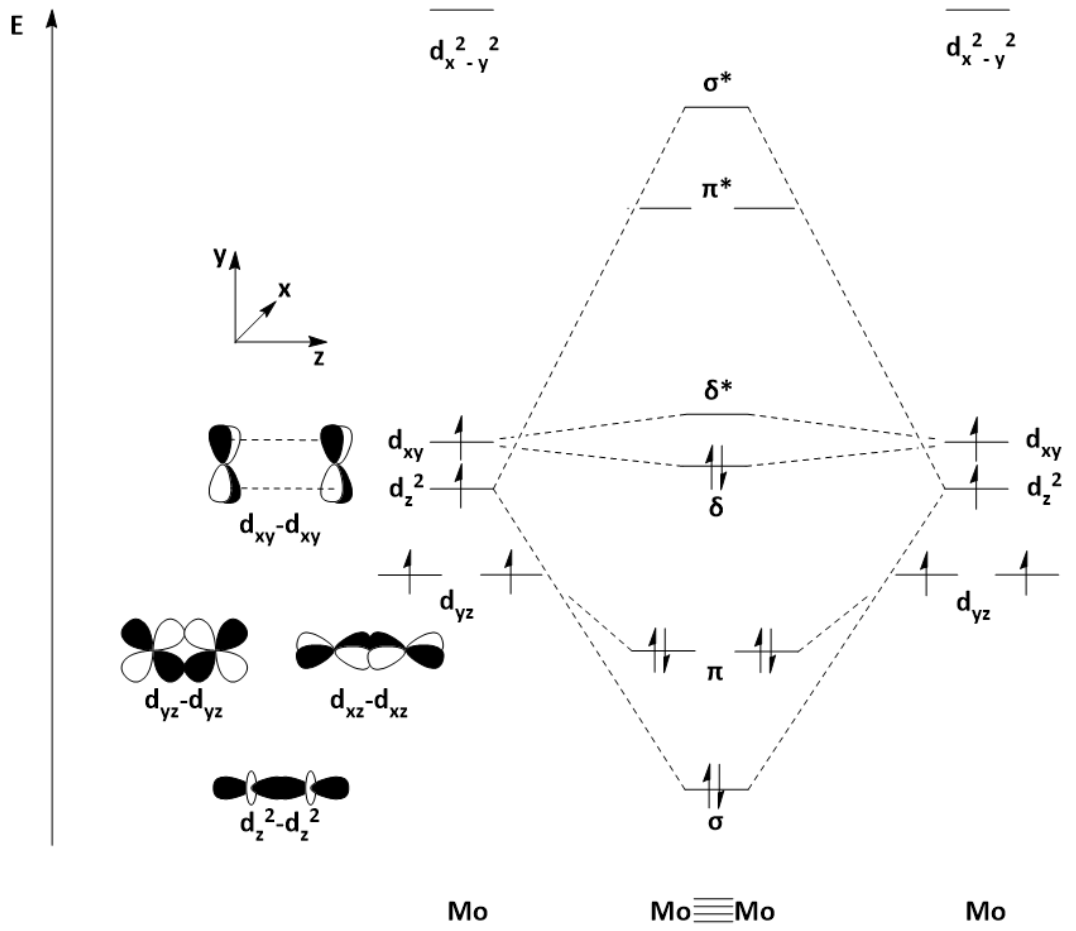

Figure 9 The qualitative MO diagram for Mo_2PWCs. The overlap of specific d orbitals illustrates a bond order of 4 between the two Mo(II) ions and an electronic configuration of $\sigma^2\pi^4\delta^2$.

Ligands can also be coordinated to PWCs axially, usually as σ-donors.[52] For example, the strong Lewis acidic axial sites of Rh_2PWCs have been exploited for catalysis,[53] bio-medical applications,[54] and molecular sensors.[55] Mo_2PWCs are not as Lewis acidic and therefore struggle to compete with Rh_2PWC in these applications. However, research into Mo_2PWCs has been extensive with regards to molecular electronics applications and towards the construction of macromolecules, supramolecules and metal-organic frameworks (MOFs).[56]

Research on Mo_2PWCs as building blocks for the construction of molecular assemblies has been driven by the electronic and structural properties of the paddlewheel motif, which are strongly influenced by the strong orbital overlap between the Mo_2 δ orbital and the ligand π/π* orbitals (Figure 9). This energetically and symmetrically favourable interaction facilitates excellent electronic communication between the Mo_2 unit and the ligands, which is an integral property for the development of molecular wires and molecular electronics.[57] Additionally, their well-defined structure of a Mo_2 core, coordinated by 4 chelating ligands on two perpendicular planes defined by the Mo_2 quadruple bond makes their supramolecular assemblies predictable. Furthermore, structural variation of the organic linker used can lead to the development of molecular assemblies of a variety of shapes to fit technological needs. Mo_2PWCs are redox active, which allows electronic communication between two Mo_2 cores in molecular assemblies to be investigated by cyclic voltammetry. Also, the ^{1}MLCT state is long-lived (τ ≈ 1-20 ps) before converting to the even longer lived triplet state ($^3Mo_2\delta\delta^*$, <100 μs), making them potential candidates for DSSCs.[58]

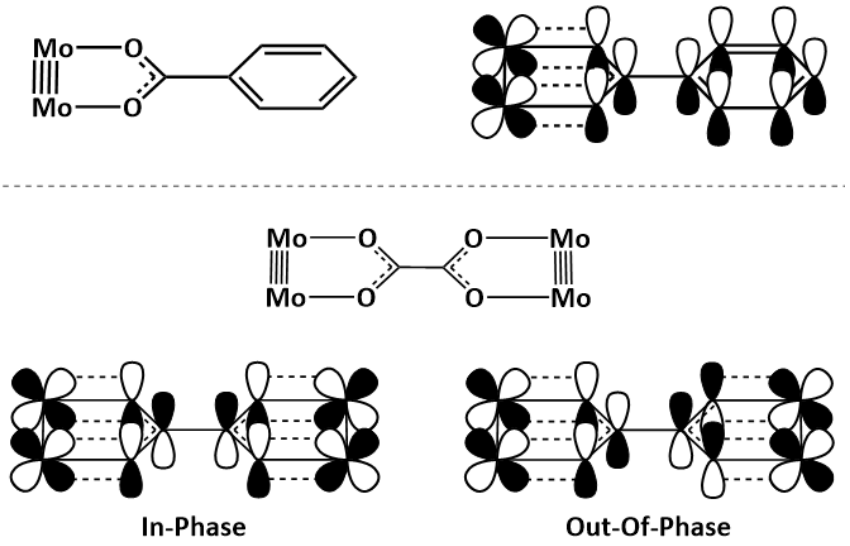

Figure 10 Top: Depiction of Mo_2 δ → π* orbital overlap between metal and ligand. Bottom: depiction of orbital overlap taking place between two Mo_2 cores bridged by an oxalate linker.

Mo_2PWCs Towards Supramolecular Assemblies

In the early 1990s, the Chisholm group was motivated by the idea of oligomeric Mo_2-based molecular wires, which, based on the molecular structure of the linker unit, would adopt two different structural arrangements: perpendicular and parallel (Figure 10).

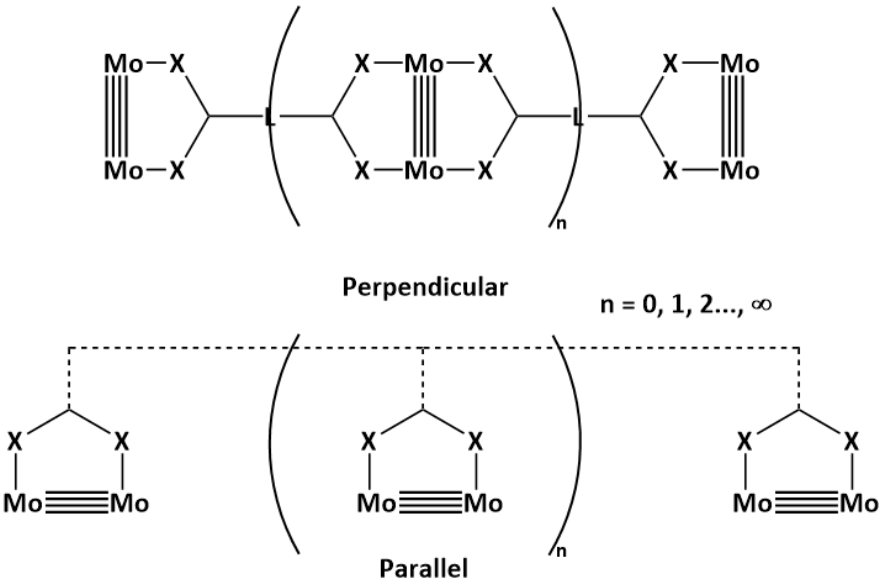

Figure 11 Representation of parallel and perpendicular types of Mo_2 oligomers.

With these structural motifs in mind, a series of compounds (**1-7**, Figure 11) was made using simple starting materials and one of the two methodologies shown in Scheme 1. Method 1 was only used for compounds **1** and **2** since, under those conditions, potential Mo_2 dimers (**3-7**) would decompose in solution *via* a ligand disproportionation reaction. This effect is observed due to the known substitutional lability of carboxylate ligands on Mo_2PWCs. For parallel structural types of Mo_2 oligomers (compounds **5** to **7**, see Figure 11, dashed bonds), coordinated ligands were less likely to undergo substitution with free ligands compared to those for perpendicular structural types, which is

speculated to be due to weak Mo-O interactions between Mo cores and neighbouring, spatially close carboxylate ligands.[59]

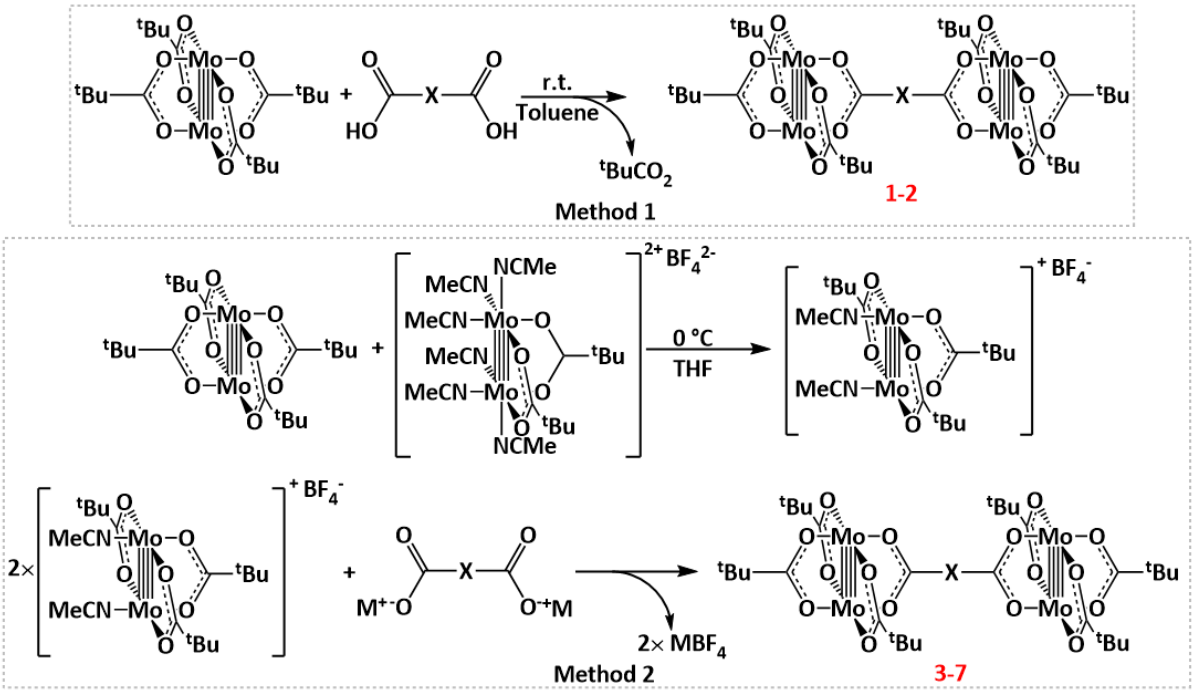

Scheme 1 Reaction pathways towards Mo_2 dimers.

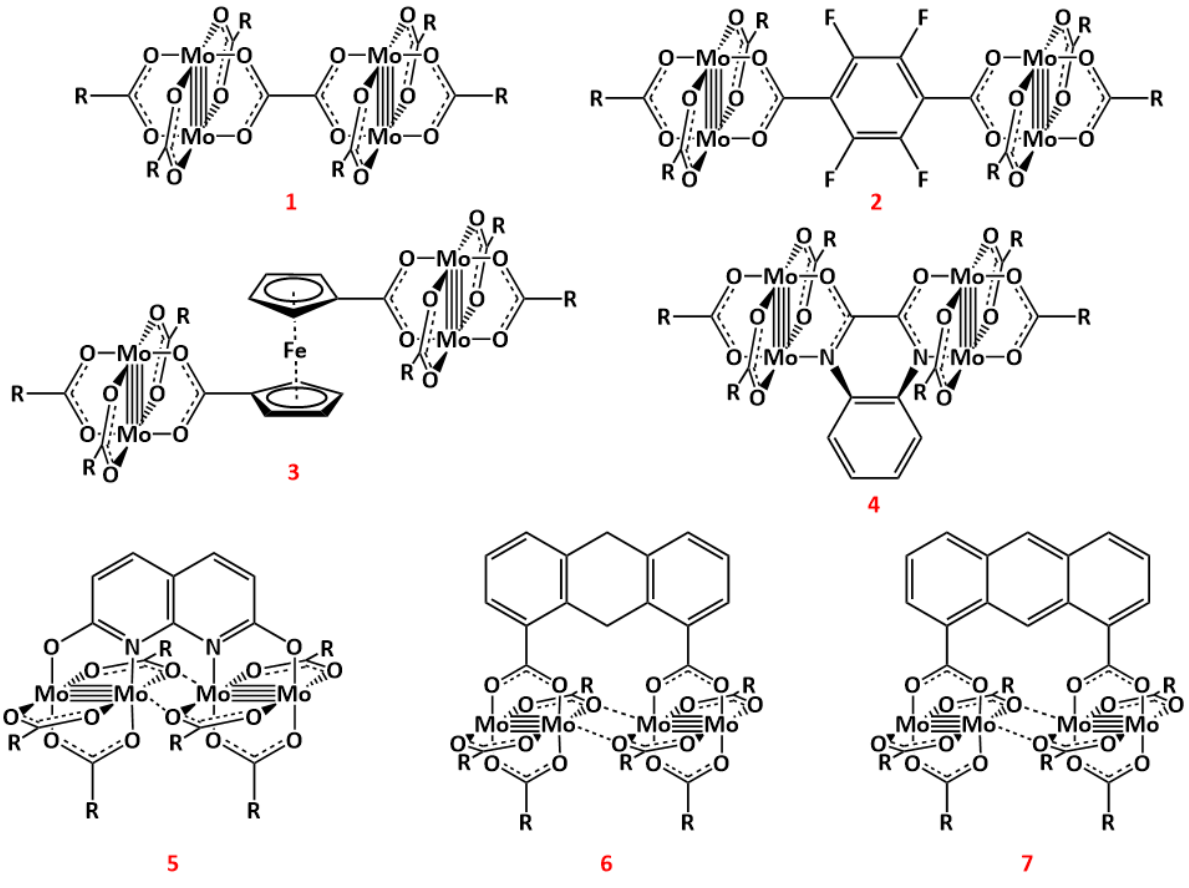

Figure 12 Series of compounds made by Chisholm, 1991.

To improve on the synthesis of this class of compounds and avoid the formation of higher-order oligomers, a previously reported Mo_2 complex, $Mo_2(DAniF)_3Cl_2$, was used as the starting material. Using two equivalents of this new precursor, along with an oxalate or a 2,3,5,6-tetrafluorophthalate as the dicarboxylate organic linkers (Scheme 2) Cotton was able to successfully and cleanly obtain the desired carboxylate-bridged species $(Mo_2(DAniF)_3)_2(\mu\text{-}O_2C\text{-}X\text{-}CO_2)$ (DAniF = di-p-anisyl formamidinate).[60] The electrochemical properties of these complexes are similar to those reported by Chisholm *et al*. using the same set of organic linkers. This investigation therefore highlights the role of the complexes with the formula $Mo_2(DAniF)_xCl_{8-2x}$ (x = 0, 1, 2, 3, 4) as not only viable alternatives to the traditionally investigated $Mo_2(O_2CR)_4$ complexes, but also ones that can be more easily isolated.

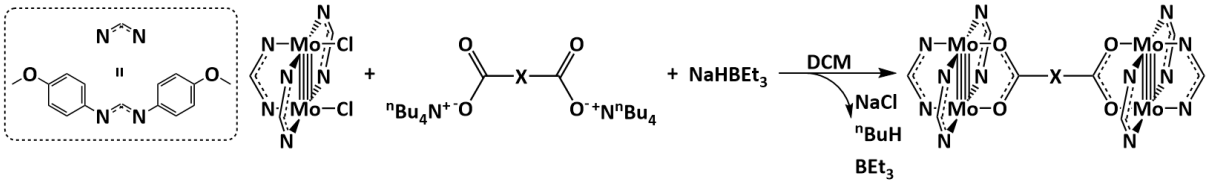

Scheme 2 First reported synthesis of Mo_4 complexes by Cotton et al.

The problem of ligand scrambling was also investigated;[61] In a system containing two homoleptic Mo_2 cores coordinated by different carboxylate ligands, it was hypothesised that ligand scrambling takes place as a result of adventitious carboxylic acid ligands in solution, which allows for the removal of one carboxylate from one Mo_2 core and its placement onto another *via* ligand substitution. To combat this, 2,6-bis(tert-butyl) pyridine was introduced to various reaction systems as a base, with ligand scrambling in one system being mitigated. Encouraged by this observation, $[Mo_2(DArF)_2(CH_3CN)_4]^{2+}[BF_4^-]_2$ (DarF = Diphenyl Formamidinate $[(PhNC(H)NPh)^-]$) was added as a carboxylate trap, in addition to the pyridine base trap, in a system containing $Mo_2(O_2C^tBu)_4$ and $Mo_2(O_2CCF_3)_4$ in CD_3CN. After 12 hours, no sign of ligand exchange was visible by ^1H NMR spectroscopy. Not only did this series of experiments prove that adventitious carboxylate in solution was the cause of ligand scrambling, but also proposed that using an appropriate baseand carboxylate trap can help work around this limitation.

The groups of Cotton and Chisholm collaboratively released a paper detailing a synthetic protocol for the synthesis of mono-, bis- and tris-formamidinate-substituted Mo_2 complexes as their BF_4^- salts with the formula $[Mo_2(DAniF)_{4-n}(CH_3CN)_{2n}][BF_4]_n$.[62] For n = 2, only the *cis*-$[Mo_2(DAniF)_2(CH_3CN)_4][BF_4]_n$ isomer was made as it is the preferred isomer (Figure 12). Dissolving the bis-formamidinate Mo_2 complex in pyridine replaces the CH_3CN ligands with pyridine molecules, causing the resulting complex to slowly isomerise to the preferred *trans*- equivalent. The formamidine ligands are inert, whereas the other ligands (pyridine or CH_3CN) are more labile.

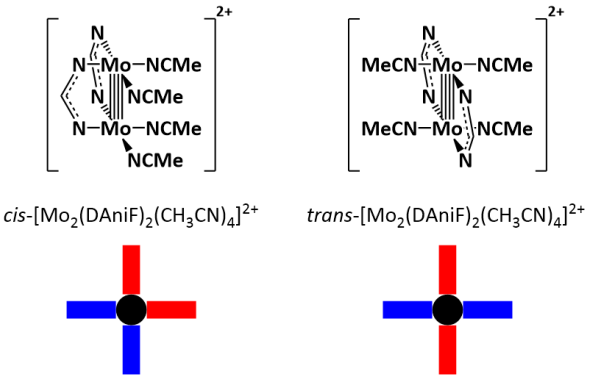

Figure 13 Potential geometric isomers of $[Mo_2(DAniF)_2(CH_3CN)_4]^{2+}$.

All of the aforementioned complexes were made with the expectation that they would serve as useful starting materials for the construction of oligomeric molecular assemblies, and that is exactly what was made possible in a series of follow-up studies by the Cotton group. A "square" molecular array was made by combining *cis*-$[Mo_2(DAniF)_2(CH_3CN)_4][BF_4]_2$ and a dicarboxylate organic linker.[63] Two crystal structures were isolated for the oxalate-bridged Mo_2 tetramer (Scheme 3, compound **8**) as well as for the ferrocene-1,1'-dicarboxylate-bridged Mo_2 tetramer (Scheme 3, compound **10**). The square shape is derived from the fact that the paddlewheel motif positions the bidentate ligands at a 90° angle relative to each other. This allows each Mo_2 core to act as a corner for a square-shaped molecule without straining the organic linker. The choice of organic linker is quite important as it determines the shape and size of the molecular squares. Additionally, since some molecular squares have been shown to stack on top of each other in a crystal lattice, the choice of the organic linker can be influential on the size of the cavities formed at the empty space inside the molecular squares.

A more extensive study on the formation of molecular squares from Mo_2PWCs was released a year later. A series of molecular squares was prepared (Scheme 3)[64] and crystal structures could be characterised for compounds **8-11.** All four of them consist of stacked molecular squares that form cavities of different sizes depending on the structure of the organic linker. Based on the size of the cavities, different solvent molecules can be trapped within them.

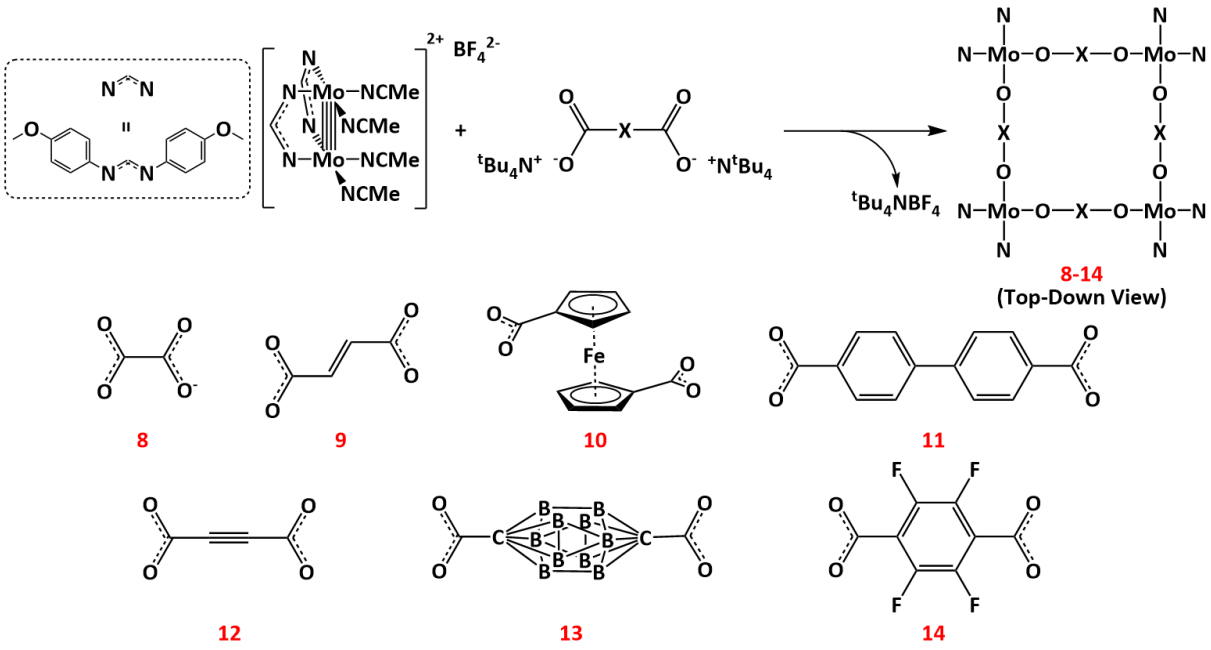

Scheme 3 Molecular squares constructed by Cotton et al.

With the 90° angle imposed by the paddlewheel motif, an additional challenge is imposed when trying to construct molecular assemblies that are not molecular squares. This limitation was addressed by Cotton *et al.* by using an organic linker with a higher degree of conformational freedom, 1,4-dicarboxylatocyclohexane.[65] Three equivalents of the *cis*-$[Mo_2(DAniF)_2(CH_3CN)_4][BF_4]_2$ complex along with three equivalents of the alkylammonium salt of the dicarboxylate gave the molecular triangle trimer (compound **15**, Scheme 4), whose crystal structure was obtained. Under these conditions, it should be possible to also form the molecular square tetramer. Nevertheless, the tetramer does not form, and there is a clear chemoselective preference for the trimer. One factor affecting chemoselectivity is entropy; the reaction pathway towards a molecular triangle trimer has a greater entropic contribution to the reaction system compared to that towards the molecular square tetramer. Moreover, an additional determining factor is proposed which is solvent entropy, as a molecular triangle forms a smaller cavity compared to a molecular square and is therefore less capable of trapping solvent molecules.

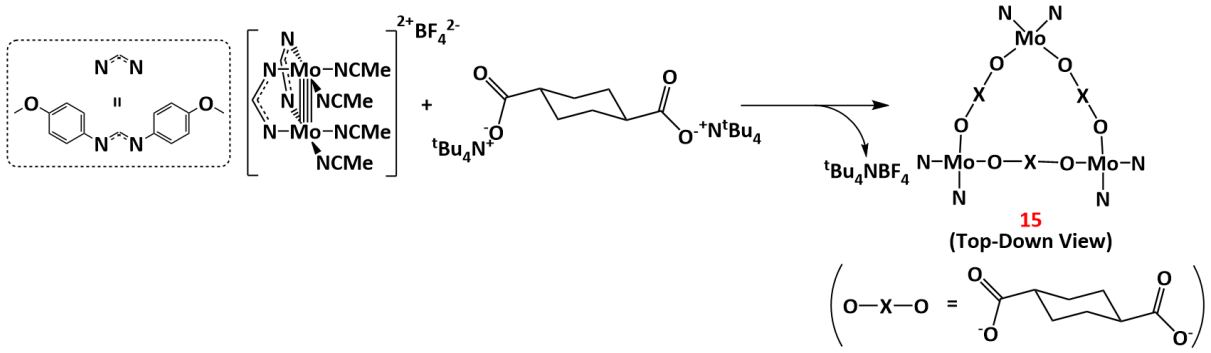

Scheme 4 Molecular triangle constructed by Cotton et al.

In a similar manner, picking the organic linker with the appropriate structure can allow for the synthesis of assemblies where two Mo_2 cores are bridged by two dicarboxylate bridging ligands, effectively forming a molecular loop. A 2001 study by Cotton *et al*. utilises four different dicarboxylate ligands to construct four different molecular loops (Scheme 5, **16-19**).[66] For all four of these organic ligands, their internal angle is too obtuse to allow for the formation of a molecular square. Compounds **16**, **18** and **19** stack directly on top of each other, but compound **17** does not behave the same way as it packs in a different way, with two different types of layers stacking in an alternating fashion.

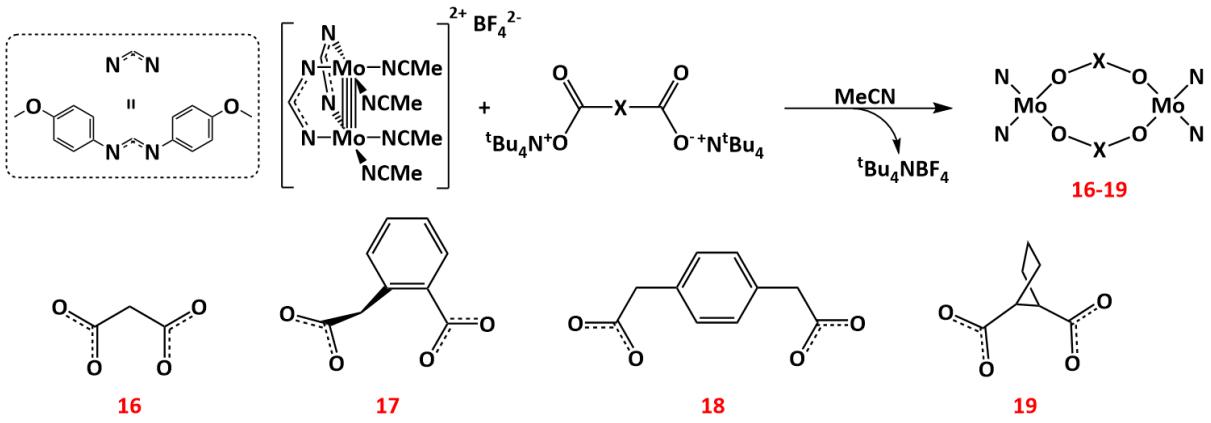

Scheme 5 Synthesis of Mo_4-based molecular loops.

During that same year, Cotton's group further realised the potential of the formamidine-based Mo_2PWCs to construct a 3-dimensional molecular cage shaped like an octahedron, which consists of

six Mo_2 units (Figure 13).[67] These Mo_2 units assume the apical positions of the octahedron cage and are linked together by a 1,3,5-tricarboxylatobenzene linker, whose phenyl rings are positioned at the centre of a face of the octahedron. The degree of symmetry of this molecule is staggering as all aromatic hydrogen atoms in the organic linkers show up in the ^1H NMR spectrum of the compound dissolved in CD_2Cl_2 as a singular peak. This compound was speculated to allow for host-guest chemistry for medium-size molecular entities such as N_2 and noble gases.

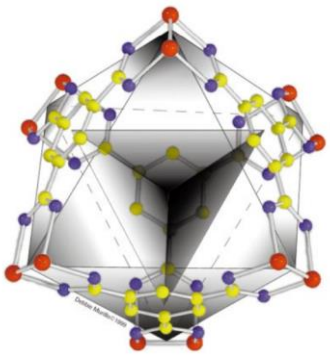

Figure 14 Illustration of the 3-D molecular assembly designed by Cotton *et al*.[67] Figure reproduced with permission from the Royal Society of Chemistry.

All of the above examples serve as evidence of the same concept: by varying the structural features of the organic building unit and by using the appropriate ligand substitution pattern for the Mo_2 node, a large variety of molecular assemblies can be constructed. With that being said, there is more to the usefulness of a Mo_2 complex towards supramolecular assemblies besides acting as an element of a structural template. In the following section, a series of investigations on Mo_2 dimers of dimers will be discussed. The simplicity of these oligomers relative to those covered in the current section allows for a more detailed investigation on their electronic properties, making it possible to further understand the factors affecting through-ligand electronic communication between Mo_2 units.

Dimers of Dimers: A Simple Model for Electronic Communication

Before delving into the literature examples for making Mo_2 dimers of dimers, it is important to discuss some underlying concepts that are pertinent to our understanding of electronic communication between two Mo_2 metal cores. First of all, molecules containing two redox centres that are almost identical besides their oxidation level are known as mixed-valence complexes, with the first study on a mixed-valence complex being conducted by Creutz and Taube.[68] Mixed-valence complexes can have their electron density either entirely localised on one of the two redox centres, or delocalised throughout the molecule, with the degree of delocalisation being varied from molecule to molecule. Electron-transfer processes are typically coupled to specific vibrational modes as a direct consequence of the Franck-Condon principle, which states that processes involving electron movement are too fast for any nuclear rearrangement to take place in the interim. Therefore, the potential hypersurface corresponding to each redox site within a mixed-valence complex is conventionally represented by a hyperbola, with the reorganizational energy required to bring upon a vibration where an intervalence charge transfer is possible being denoted as λ.[69]

Universally, the electronic communication between two redox centres is described by the Robin and Day classification system.[70] A mixed-valence complex can be described using a potential energy diagram which plots the potential energy over an electron-transfer coordinate, which expresses a structural element of the complex that is sensitive to electron-transfer. In a mixed-valence system, if there is no electronic communication present between two redox sites, they will be

considered independent of each other, and their ground states can be described by two separate diabatic hyperbolae. This system would be considered to be a class I system in the Robin and Day regime (Figure 14, left). In a class II system in the Robin and Day regime (Figure 14, centre), some electronic communication is present, but the electron density is still largely localised on one of the two redox centres. With that said, the limited electronic communication of such systems would be enough to allow for a photoinduced promotion of an electron from the ground state to the excited state, followed by relaxation into either ground state. The capacity of the electron to relax into either ground state defines the excitation as an inter-valence charge transfer (IVCT). In a class III system in the Robin and Day regime (Figure 14, right), the two hyperbolae coalesce into a broad energy minimum, which is representative of the two redox sites being structurally identical. This is possible if the electronic coupling in this system, expressed by the electronic coupling parameter (H_{AB}), is sufficiently large so that $2H_{AB} > \lambda$. In this case, excitation of the lone electron occurs between two orbitals which are both delocalised over the two redox centres; this is referred to as a charge resonance transition.

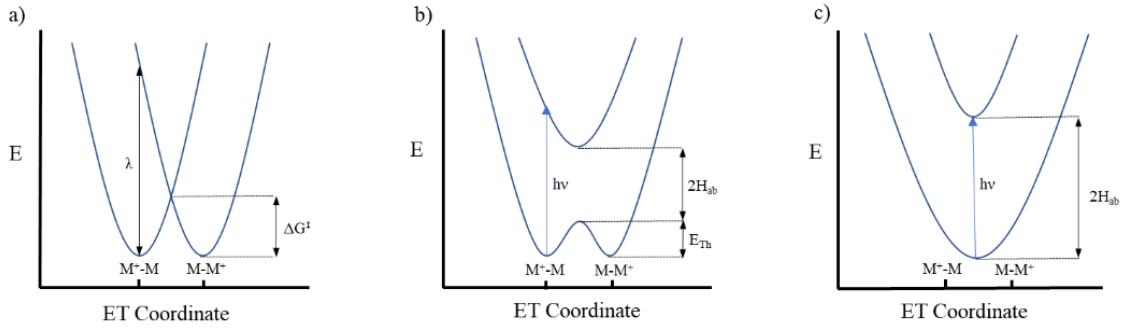

Figure 15 Energy level diagrams for mixed-valence complexes according to the Robin and Day regime: Class I (left), Class II (centre), Class III (right).[71]

Homoleptic Mo_2PWCs coordinated by a single type of ancillary ligand *e.g.* $Mo_2(TiPB)_4$ (TiBP = 2,4,6-triisopropyl benzoate) display a one-electron oxidation peak in the cyclic voltammogram corresponding to the removal of a single electron from the M-M δ-bonding orbital.[72] This oxidation is strongly influenced by the nature of the ligand and can be easily tuned with the addition of electron-donating and withdrawing components, or through variation of the donor atom from O to N to S.[73,74]

When dealing with a system containing two Mo_2 paddlewheel cores linked together by an organic linker, the extent of electronic communication between the two cores can be inferred by their redox properties, which can be investigated by cyclic voltammetry. If complete charge localisation is present (weak or non-existent electronic communication), the one-electron oxidation for both Mo_2 cores will occur at the same half-wave potential ($E_{1/2}$). In a DPV (Differential Pulse Voltammetry) experiment, the two bell-shaped curves describing each process will therefore be overlapped on top of each other and will appear as one curve. If some electronic communication is present between the two Mo_2 cores, a second oxidative process will be observed at a higher potential than the first, and in a DPV experiment, the two bell-shaped curves describing each process will be separated, with the degree of separation ($\Delta E_{1/2}$) often being proportional to the extent of electronic communication.

The comproportionation constant (K_C) is an equilibrium constant which describes the stability of the Mo_2^{5+} mixed-valence state in relation to the fully oxidised Mo_2^{6+} and neutral Mo_2^{4+} species and is illustrated in Figure 18. This value is often related to the extent of electronic communication between two Mo_2 cores because the latter is often a key contributor to that stability. Through cyclic voltammetry, it is facile to determine the K_C value for a mixed-valence complex by measuring the

difference between the first two redox waves of a mixed-valence complex ($\Delta E_{1/2}$ as demonstrated in Figure 15) and applying it in the Nernst equation (Figure 16).[75] For that reason, it will be referenced when discussing cyclic voltammetry data in mixed-valence systems. It is essential to note, however, that the comproportionation constant is not a quantitative indicator of electronic communication and can only be used as a means of comparing the extent of electronic communication between two mixed-valence complexes under identical conditions.[69]

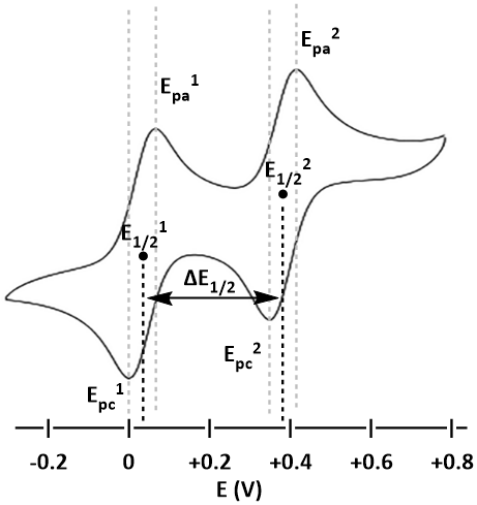

Figure 16 Cyclic voltammogram of an example of a mixed-valence complex.[76] Figure reproduced with permission from the American Chemical Society.

$$Mo_2^{2+} — Mo_2^{2+} + Mo_2^{3+} — Mo_2^{3+} \overset{K_c}{\rightleftharpoons} 2\times Mo_2^{2+} — Mo_2^{3+}$$

$$\Delta E_{1/2} = (RT/F)\ln K_c \Longrightarrow K_C = \exp[(\Delta E_{1/2}F)/(RT)] = \exp(\Delta E_{1/2}/25.69) \text{ at } 298K$$

Figure 17 Relation of K_C vs $\Delta E_{1/2}$.
F: Faraday constant, R: gas constant, T: temperature.

In 2001, the Cotton group published their first extensive study on a series of one-dimensional molecular assemblies (Mo_4 complexes, a.k.a. "dimers of dimers").[77] Starting from the dichloride precursor depicted in Scheme 6, two different methods were used, employing a different reducing agent in each case. One route used $NaHBEt_3$ (Method A) and the other used Zn powder (Method B) (Scheme 6). Method B was employed because certain organic linkers were prone to reduction by the $NaHBEt_3$. The structural features of the organic linker play a direct role in the placement of the two Mo_2 cores; in this case, they are either in-plane (*e.g.* using ligand **20** or **21**) or forming a step (*e.g.* **25**, **31**). The conformational freedom of each linker is important to consider: the distance between two Mo_2 cores may be different when in solution relative to their crystallised form. This is likely the case for compounds **27**, **28**, **29** and **31**. In fact, for compound **31**, ^{1}H NMR studies show a broad signal for the methine protons at the organic linker. This signal is presumed to be broad as a result of the coupling of the methine protons with the adjacent CH_2 protons and would be narrower if the methine protons were in the equatorial position, hinting that compound **31** in solution exists with the carboxylate groups in the equatorial conformation.[77,78] This observation is inconsistent with the crystallographic data, where X-Ray crystallography shows the carboxylate groups in the axial conformation.

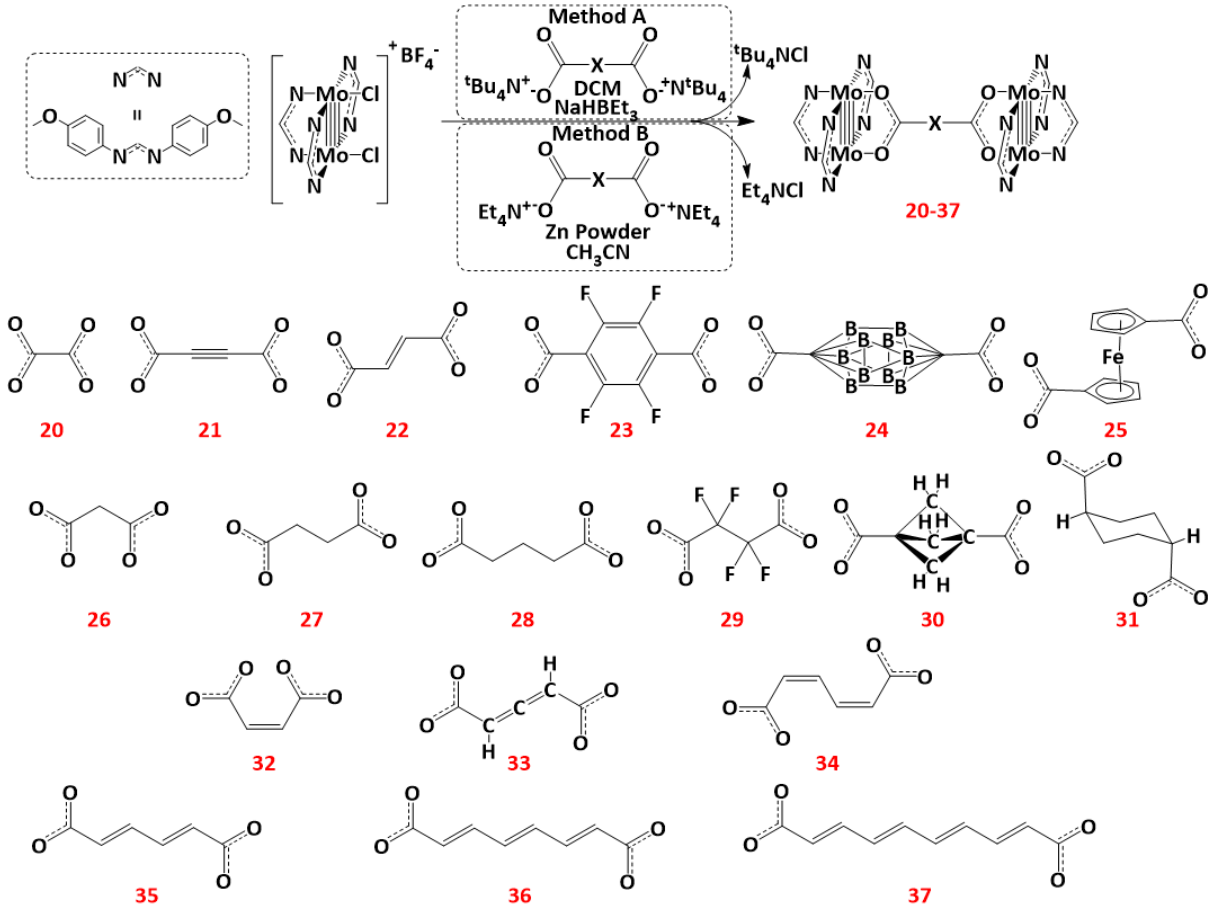

Scheme 6 Synthesis of Mo_2 dimers of dimers by the Cotton group, 2001 and 2003.

Cyclic voltammetry and DPV were used to study the electronic communication between the two Mo_2 cores for each system. In the case of no electronic transmission through the organic linker, the $\Delta E_{1/2}$ value should be inversely correlated with the square of the distance, as a Coulombic effect would be the only interaction in place between the two Mo_2 cores. A plot between the distance squared (d^2, $Å^2$) and $\Delta E_{1/2}$ was produced, with the only deviations to that plot being compounds **20**, **21**, **22** and **31** (Figure 17). Compound **31** shows deviation due to the conformational change observed in solution relative to the conformation in the crystal lattice. Compound **20** shows partial delocalisation attributed to the small length of the organic linker, which explains the deviation in the plot. The deviation for **21** and **22** is postulated to be a result of polarisation of the unsaturated organic linker caused by the different charge of the Mo_2 cores and is enhanced by the shorter length of the organic linker.

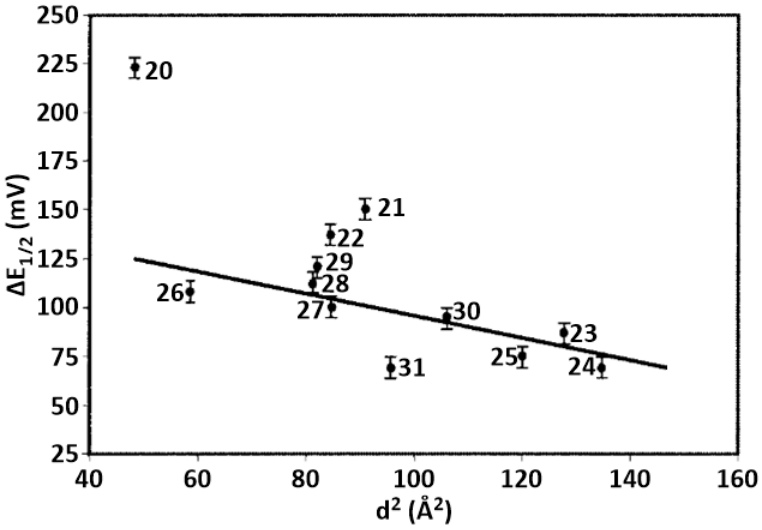

Figure 18 Plot of $\Delta E_{1/2}$ vs d^2 for compounds **20**-**31**. The best fit line includes all compounds except **20**, **21**, **22** and **31**.

A further 2003 study by Cotton *et al*. presented a new set of Mo_4 complexes connected *via* unsaturated organic linkers (**32-37**, Scheme 6).[79] They were all studied through X-Ray crystallography. Out of these complexes, only compound **32** showed significant deviation in planarity, which is expected to also exist in solution. In terms of electrochemistry, the trends are similar to those observed in previous studies: electronic communication is inversely proportional to the distance of the two metal cores and is somewhat enhanced by an established π-system. Compound **33** exhibits poor metal-ligand electronic communication, which is likely owed to the interruption in the π-system caused by the orthogonal set of MOs in the allene group. A relationship between the distance of the two Mo_2 cores with the $\Delta E_{1/2}$ was investigated (Figure 18). It is shown that dimers of dimers connected by an unsaturated organic linker show a higher $\Delta E_{1/2}$ value relative to other saturated dimer of dimers with an equal distance between Mo_2 cores. This highlights the fact that an organic linker containing a π-system is beneficial towards electronic coupling between Mo_2 cores.

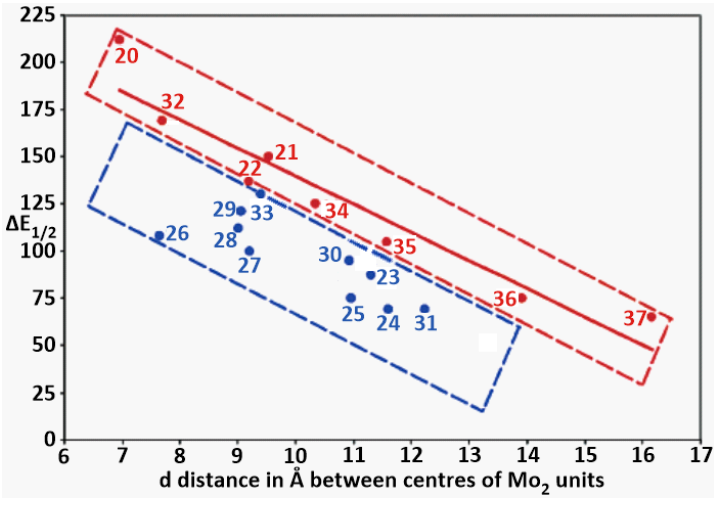

Figure 19 Plot of $\Delta E_{1/2}$ over d for compounds **20**-**37**. The best line fit for compounds **20**, **21**, **22**, **32**, **34**, **35**, **36** and **37**, which contain unsaturated, conjugate linkers, is shown in red. Compounds **23-31** and **33** are shown in blue. The lower values of $\Delta E_{1/2}$ for the compounds in blue relative to the compounds in red with similar distances reflects the poor electronic communication between the two Mo_2 cores for the compounds in blue.[79]

Subsequent investigations in the Cotton group attempted to replicate the success of synthesising these Mo_2 dimers of dimers by using oxamidate anions as organic linkers, hoping to improve electronic communication between the two Mo_2 cores. However, an additional synthetic challenge emerged as the more nucleophilic character of the new organic linkers allowed them to react with the electrophilic acetonitrile ligands that are coordinated to the Mo_2 starting materials, hence hindering the ligand substitution reaction. This type of reactivity between nucleophiles and electrophilic acetonitrile ligands coordinated to transition metal cores has been extensively discussed in prior literature.[80,81] To work around this issue, the group developed a new set of heteroleptic starting materials of the formula $Mo_2(DAniF)_n(OAc)_{4-n}$ (Figure 19).[82] What is particularly notable is that both *cis*- and *trans*- variations of $Mo_2(DAniF)_2(OAc)_2$ were synthesised. The *cis*- product was made by reacting $[Mo_2(DAniF)_2(CH_3CN)_4](BF_4)_2$ with 1.5 equivalents of NaO_2CCH_3 in acetonitrile, whereas the *trans*- product was made from a suspension of $Mo_2(OAc)_4$ and precisely two equivalents of HDAniF in THF. The stoichiometry needs to be highly accurate, as a slight excess beyond the two equivalents of the formamidine will give a statistical mixture of $Mo_2(DAniF)_2(OAc)_2$ and $Mo_2(DAniF)_3(OAc)$. Due to their relative difference in substitutional inertness, formamidinate ligands cannot be easily displaced.

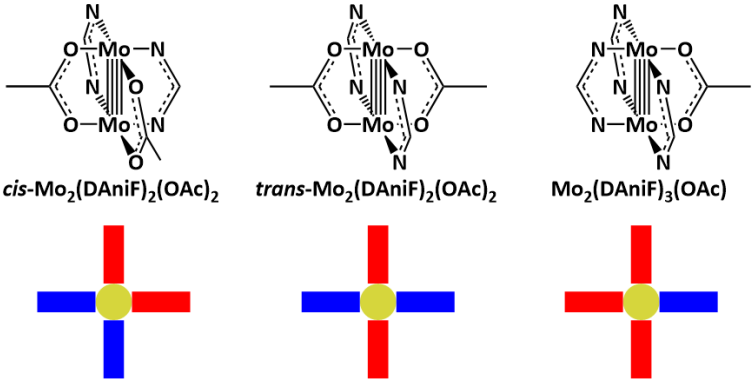

Figure 20 New Mo_2 building blocks for molecular assemblies.
Top-down view along the Mo-Mo axis is provided below, with Mo_2 cores presented using yellow circles, inert ligands (*i.e.* formamidinate) presented using red bars and labile ligands (*i.e.* acetate) presented using blue bars.

With this new set of starting materials, the Cotton group released a study on using dioxamidate organic linkers to form Mo_2 dimers of dimers (Scheme 7, compounds **37-40**).[83] Due to the difference of coordinating atoms in the chelating oxamidate unit, two different isomers are expected for each type of organic linker used. For compounds **37-38**, a twist in the dihedral angle of the organic linker is observed, which is caused by the steric demand put in place by the aryl substituents of the organic linker. Such systems have been observed in prior studies when tetrahedral inorganic linkers were used to link together two Mo_2PWCs (Scheme 7, top).[84,85] As a result, the Mo_2 quadruple bonds for the two redox centres are perpendicular to each other, which disrupts electronic communication *via* the π-system established by the two metal cores and the ligand. This is reflected by the lower $\Delta E_{1/2}$ and K_C values for compounds **37** and **38** relative to **20**, which exhibits planarity throughout the entire

compound and is therefore influenced by some delocalisation through the metal-ligand-metal π-system.

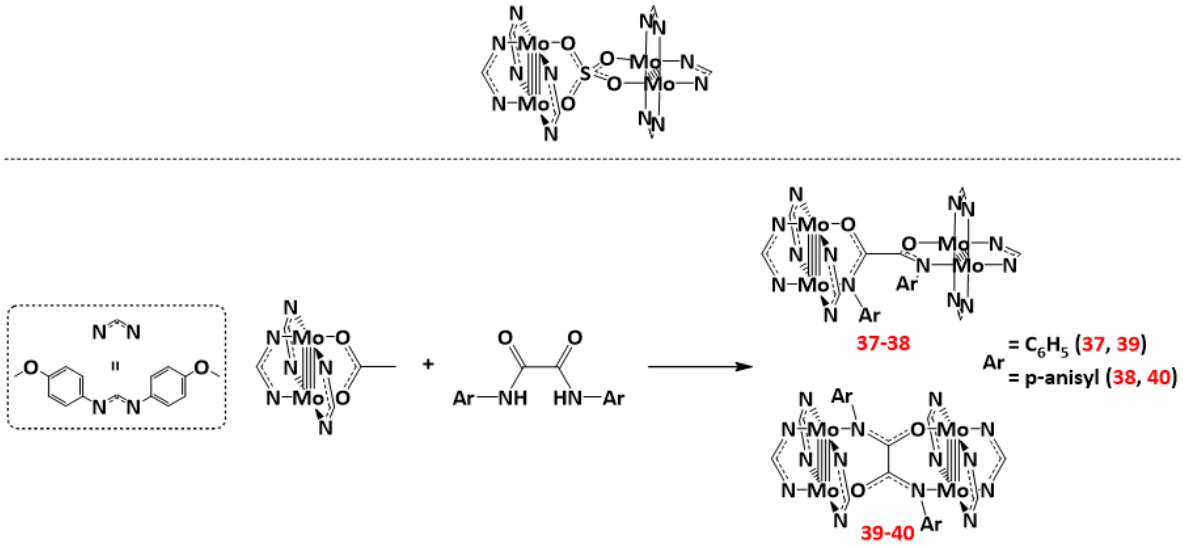

Scheme 7 Top: Pairing of two Mo_2PWCs with tetrahedral inorganic linkers.[84]
Bottom: Dioxamidate-based dimers of dimers by Cotton, 2003.

Compounds **39-40** also show some structural deviation from compound **20**. This time, the C-C bond of the oxamidate linker is parallel to the two Mo-Mo bonds of the Mo_2 cores, forming two 6-membered rings (-Mo-O-C-C-N-Mo-). The overall structure of this molecule is slightly bent and not entirely planar. The electrochemical data for compounds **39** and **40** suggest a remarkable electron delocalisation throughout the entire system, with K_C values reaching up to 1.3×10^9. These two compounds show the greatest extent of delocalisation reported for a molecule containing two redox centres up until 2003. To put this in perspective, a system containing two redox centres is generally considered completely delocalised if the K_C value is above 10^6, a value that is 10^3 times lower than that observed for compounds **39** and **40**. This work demonstrates the importance of selecting the right type of chelating ligands to establish electronic communication between two metal cores connected by an organic linker. Out of compounds **1-38**, the only compounds that display a K_C value above 10^6 are compounds **4** and **5**,[59] both of which use oxamidate ligands as organic linkers.

The disruption of the π-system in compounds **37-38** is caused by the bulk of the aryl substituent. It was therefore demonstrated by the Cotton group that removing the substitution led to a planar dimer of dimers, not just because of the removal of the steric demand, but also by the presence of an additional hydrogen-bonding interaction between the hydrogen atom of one amidate and the oxygen atom of the other amidate, keeping the linker in plane (**41**, Scheme 8).[86] This was also shown for dithiooxamidates (**42**) and electrochemical analysis of this compound showed K_C values of 7.6×10^6, indicating complete electronic delocalisation and class III mixed-valence behaviour. This is a stark contrast to Compound 41 which shows very little delocalisation present ($K_C = 2.8 \times 10^3$).

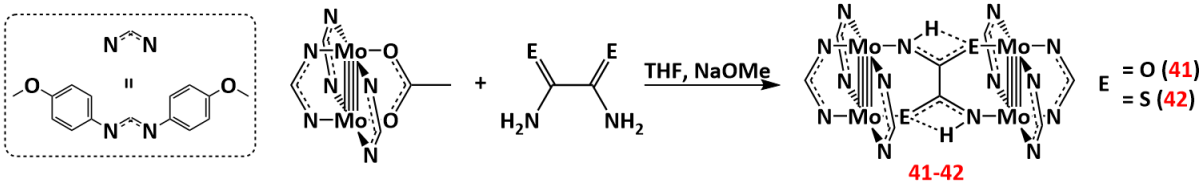

Scheme 8 New dioxamidate and dithiooxamidate dimers of dimers by Cotton, 2007.

A study by the Chisholm group confirmed that SS donor groups in the organic linker improve the communication between two Mo_2 metal cores relative to their OO counterparts for dicarboxylate organic linkers. Practical proof was demonstrated through electrochemical and photophysical analysis of a series of complexes, as well as theoretical proof through DFT calculations of appropriate models.[87] This revelation sparked an interest in the use of organic linkers containing SS donor groups for the development of metal-organic polymers,[88] with one of the first investigations of such systems in Mo_2 dimers of dimers being conducted by the Liu group (Scheme 9).[89] Although electronic coupling for compound **43** was not strong enough for full delocalisation to take place, a marked increase in K_C was observed relative to its terephthalate analogue **45** (Scheme 10), showcasing the impact made by replacing carboxylate linkers with thiolate linkers.

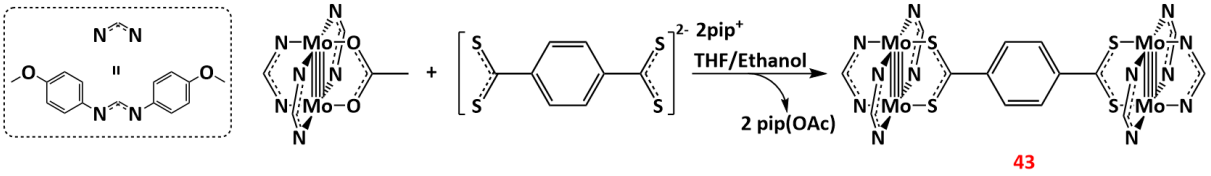

Scheme 9 Mo_2 dimers of dimers linked by tetrathioterephthalate linker, C-Y. Liu, 2009.

Introducing Complexity: Asymmetric Dimers of Dimers

So far, the use of Mo_2 dimers of dimers as models for investigating electronic communication between two redox active centres has been reviewed. By tuning the length, conjugation, functionality and geometrical structure, different organic ligands can either act as insulators or semiconductors. However, every system covered so far besides compound **17** has been symmetric, with each Mo_2 core being structurally indistinguishable from the other. In a pioneering study in 1974, Aviram and Ratner proposed that, for the construction of a molecular rectifier (*i.e.* a diode), it is vital that an asymmetric donor-bridge-acceptor system is constructed, as in such a system, the electronic current will only proceed towards one direction.[90] In recent years, progress has been made on constructing asymmetric Mo_2 dimers of dimers to investigate (among other things) their capacity as molecular rectifiers which will be discussed below.

In 2013, the Liu group published a study investigating the electronic properties of Mo_2 dimers of dimers linked by dicarboxylates, dithiolates and tetrathiolates (compounds **44-46**, Scheme 10).[91] Compound **46** is of particular note, as it constructs a dimer of dimers that lacks the symmetry present in compounds **44** and **45**. This asymmetry was employed with the expectation that a donor-bridge-acceptor system would be made, with the first oxidation occurring selectively at the Mo_2 core coordinated by the carboxylate terminus of the organic linker. Surely enough, the first single-electron oxidation for compound **46** has an $E_{1/2}$ value of 292 mV, which is considerably lower than both that of compound **45** (335 mV) and that of compound **43** (502 mV). This shows that single-electron oxidation occurs selectively at the Mo_2 core coordinated by the carboxylate functionality of the bridging ligand, hinting at the role of the Mo_2 core as an electron donor/acceptor, as well as the role of the organic linker as an "electron transfer bridge". In order to quantify the role that electronic coupling plays in compound **46**, two model compounds, $Mo_2(DAniF)_3(O_2C\text{-}Ph)$ and $Mo_2(DAniF)_3(S_2C\text{-}Ph)$ (Ph = phenyl) were synthesised and had their individual potentials measured. The difference in the potential of the two compounds is 276 mV, which is lower than the $\Delta E_{1/2}$ value of compound **46** (360 mV) by 84 mV. This difference of 84 mV is estimated to account for electronic coupling present in the system. Therefore, despite the fact that compound **46** has a greater $\Delta E_{1/2}$ value relative to compound **45** (360 mV compared to 91 mV respectively), compounds **45** exhibit similar electronic coupling between the two metal cores, since the $\Delta E_{1/2}$ value for compound **46** is heavily influenced by the different nature of the donor atoms in the organic linker.

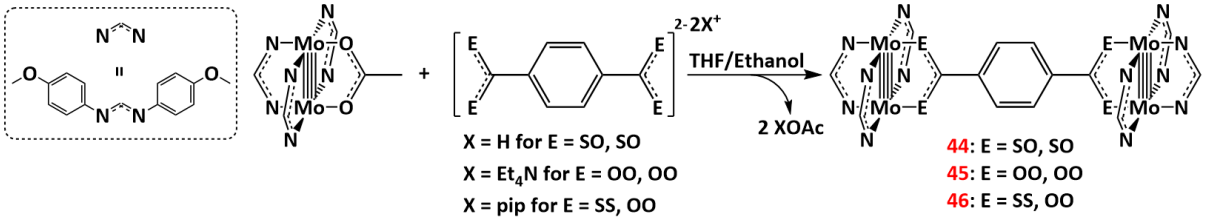

Scheme 10 Mo_2 dimers of dimers reported by C-Y. Liu, 2013.

A further publication focused explicitly on asymmetric dimers of dimers (compounds **47-49**, Scheme 11).[92] A major feature of this study also involves the investigation of the kinetics of electron-transfer throughout the dimers of dimers. These studies were made based on values derived from electrochemistry. These studies confirmed the theoretical expectation that Mo_2 cores can either act as the donors or the acceptors based on their environment, with the NO-coordinated Mo_2 core acting as a donor for compound **47**, but as an acceptor for compound **49**. This could therefore act as precedent for the development of molecular rectifiers using Mo_2PWCs, as the flow of the electrical current can be tuned based on asymmetry.

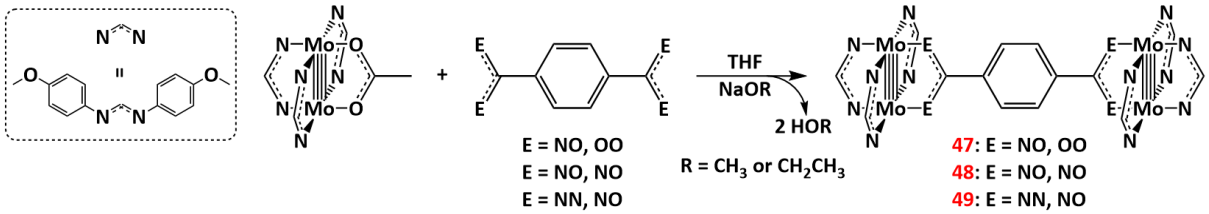

Scheme 11 Synthesis of asymmetric dimers of dimers, C-Y. Liu, 2016.

The above studies showcase the sensitivity of electron-transfer on the (a)symmetry of the bridging ligands compared to their symmetric counterparts, with an emphasis on their potential as molecular rectifiers. Despite the potential for these asymmetric systems in applications towards molecular electronics, there are very few reports on these systems besides the aforementioned publications. The most profound reason for this gap in research is the synthetic challenge of introducing the asymmetry. All of the examples above describing the synthesis of dimers of dimers employ ligand-exchange methods which is a form of self-assembly and, as described earlier, offers little synthetic control. The Liu group has managed to overcome this challenge by introducing asymmetry into the organic linker, which contains the two functionalities that can coordinate to Mo_2PWCs, giving rise to the desired sole product. However, asymmetry could theoretically be introduced by connecting two different Mo_2PWCs, one which would act as a donor and one which would act as an acceptor. The difference in these Mo_2PWCs would be inherent in their ancillary ligands. Indeed, a 2014 study in the Liu group found that the perturbation of substituents with varying functional groups of the formamidinate ligands, even at positions far from the Mo_2 core, can drastically affect the electron density of the Mo_2 centres and, as a result, the electronic communication between two metal centres connected by a ligand.[93] Clearly, there is untapped potential in exploiting the electronic properties of Mo_2 complexes by varying the remote substituents of their ancillary ligands to engineer brand-new, unexplored asymmetric Mo_2 dimers of dimers. The only limitation is synthetic in nature: in a system containing two different Mo_2PWCs and a symmetric organic ligand, there is no thermodynamic driving force towards the asymmetric product, meaning that a statistical mixture of products is generated, whose separation is nontrivial due to their similar properties (Scheme 12). A different strategy is warranted, relying more on directed assembly than self-assembly.

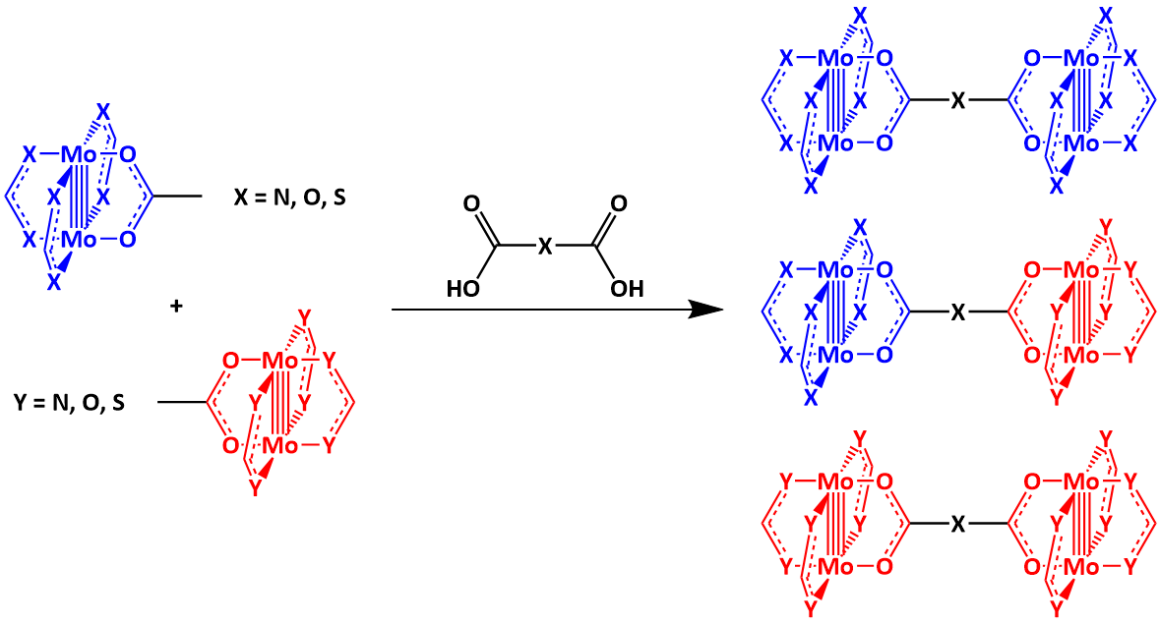

Scheme 12 Formation of an undesirable statistical mixture of isomers.

Reactivity at the Ligand Periphery

Performing reactions at the periphery of transition-metal complexes has been extensively studied as an alternative to ligand substitutions for extending the functionality of ligands coordinated to transition-metal complexes.[94] In recent years, a number of publications have been released which utilise this strategy to add desirable functionality to PWCs (mostly Ru_2 and Rh_2PWCs), however only three papers exist demonstrating this concept for Mo_2PWCs (*vide infra*).

Investigations by the Ren group attempted to add functionality to a diruthenium PWC ($Ru_2^{(ii,iii)}$PWC) by performing the Sonogashira reaction at the periphery of the ligand.[95,96] To do so, an iodide or an alkyne would need to be present, so starting from a $Ru(DmAniF)_3(Cl)(OAc)$ complex (DmAniF = di-m-anisylformamidine), the acetate ligand was replaced with a N,N'-dimethyl-4-iodobenzamidine ligand *via* ligand substitution. Bearing the right functionality, the resulting complex was subjected to Sonogashira conditions and reacted with three different alkynes as shown in Scheme 13. All products (Compounds **50-52**) were produced in high yields. A weakness of this approach was revealed when Ru complexes coordinated by axial butadiynyl ligands were exposed to Sonogashira conditions in a similar context as the axial ligand was dissociated from the Ru_2 core. Despite that, one can work around this issue if peripheral reactivity *via* the Sonogashira reaction is attempted before the axial coordination of the butadiynyl ligands, as it is the Sonogashira conditions that disrupt axial bonding rather than the ligand structure itself. The same strategy was used to perform the copper azide-alkyne cycloaddition (CuAAC) via *click* chemistry on the periphery of terminal alkyne-bearing ligands coordinated to Ru_2PWCs, showing similar success.[97]

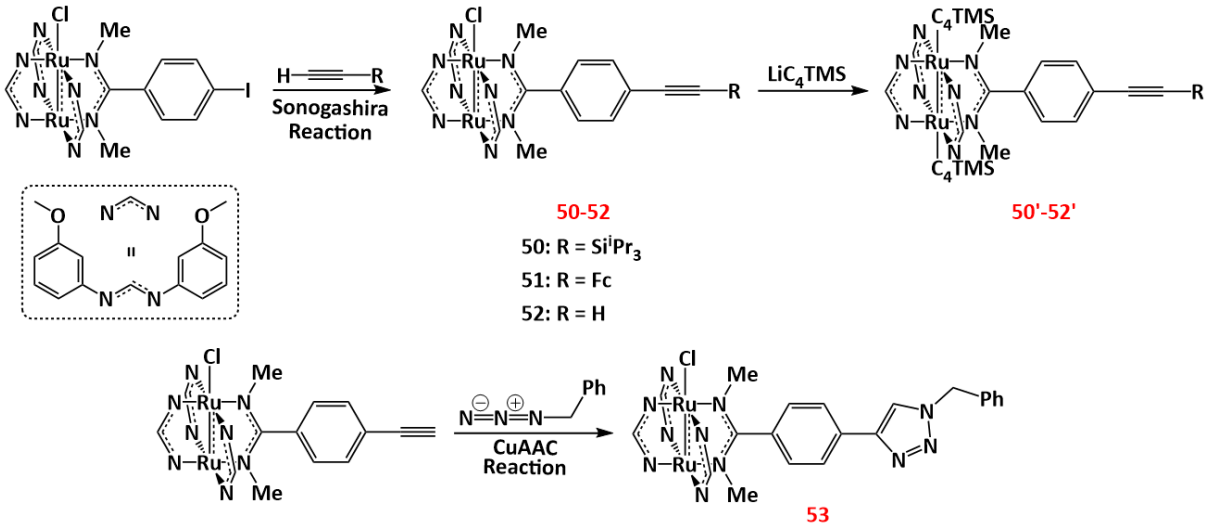

Scheme 13 Sonogashira (top) and CuAAC (bottom) reactions at the ligand periphery of a Ru paddlewheel complex.

Following the attempts at performing the Sonogashira and CuAAC reactions at the ligand periphery of Ru_2PWCs, the Suzuki reaction was also performed on the periphery of coordinated, iodinated formamidinate ligands with an arylboronic acid (Scheme 14).[98] The cross-coupling products were obtained in moderate yields. In a similar vein to previous studies, the Suzuki cross-coupling conditions were employed to an appropriate starting material that also possessed an axially coordinated phenylacetylide ligand. Unlike the axial butadiynyl ligand that dissociated from the complex under Sonogashira conditions in the previous study, the phenylacetylide ligand remained coordinated to the Ru_2 core throughout the Suzuki reaction. It is therefore understood that, although performing reactions at the periphery of a ligand can have adverse effects on other structural elements of a transition-metal complex, some of the reactions do not cause such interferences. This means that, for the utilisation of peripheral reactivity towards the construction of molecular assemblies, it is pertinent that the reaction conditions do not affect the structural framework of the starting materials.

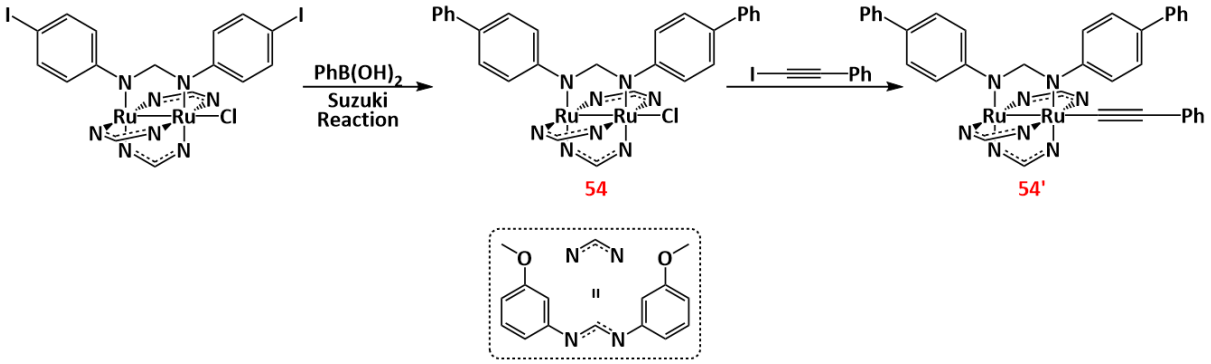

Scheme 14 Suzuki reaction at the ligand periphery of a Ru_2PWC.

With the success of peripheral reactivity on Ru_2PWCs, a precedent was set for similar investigations on Mo_2PWCs. The Sonogashira reaction was also performed on the periphery of Mo_2PWCs by the Chisholm group in 2013 (Scheme 15, top).[99] In this example, two equivalents of 5-ethynylthiophene-2-carboxylate were coordinated to a homoleptic Mo_2PWC in a *trans*- fashion. This precursor underwent two different reactions. Firstly, under Sonogashira conditions, the pi-conjugation of the ligands could be extended by cross-coupling them with phenyl iodide, and secondly,

a new metal centre was appended to the ligand termini by cross-coupling the alkyne to $Au(PPh_3)Cl$. The significance of this study lies in the success of attaching a new metal centre to a ligand coordinated to a redox-active Mo_2PWC, showcasing the potential of building metal-organic oligomers containing more than one metal centre in a controlled manner. Furthermore, it showcases that Mo_2 tetracarboxylates ($Mo_2(O_2CR)_4$) can tolerate the Sonogashira conditions despite the lability of the ligands. Notably, other cross-coupling reactions, such as the Kumada or Negishi coupling, reportedly do not work due to carboxylate ligand scrambling under those conditions. Clearly, this tolerance to the reaction conditions is essential for their use as building blocks towards molecular assemblies.

A follow-up study was reported employing the Heck reaction to add a phenyl group at the periphery of a *meta*- or *para*-vinylbenzoate ligand coordinated to a Mo_2PWC (Scheme 15, bottom).[100] This study is relevant for the incorporation of Mo_2 cores into poly-p-phenylene vinylene (PPV) polymers, a type of heavily investigated conductive organic polymers.[101] The Mo_2PWCs can withstand the Heck reaction to give the desired products, opening up the path for future incorporations of Mo_2 metal cores towards metal-organic assemblies that feature unsaturated C=C bonds in their organic linkers.

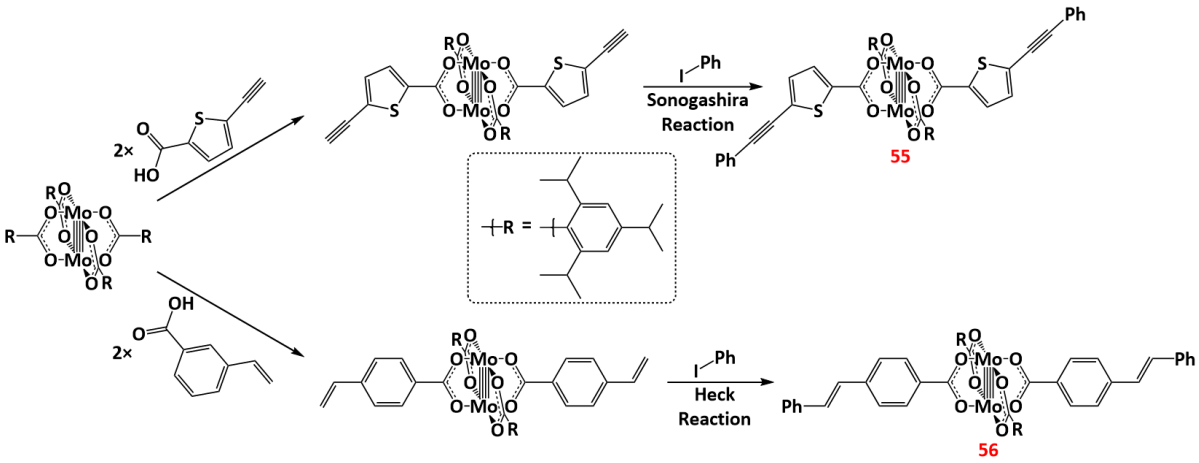

Scheme 15 Sonogashira (top) and Heck (bottom) reactions at the ligand periphery of Mo_2PWCs.

A 2016 study by the Nitschke group incorporated Mo_2PWCs as structural units for the construction of a molecular cube.[102] The edges of this cube are Fe^{II} or Zn^{II} metal centres coordinated by a chelating ligand. The ligands coordinated to the Mo_2 core were aniline-4-carboxylate ligands, the planarity and *para*-amino functionality of which are crucial factors contributing to the formation of the final assembly. By combining 6 equivalents of Mo_2PWCs, 8 equivalents of zinc or iron triflate, and 24 equivalents of 2-formylpyridine in a one-pot procedure, large molecular cages could be obtained. The 2-formylpyridine ligands underwent imine condensation with the amine groups located at the periphery of the Mo_2PWCs to give the resulting imines, which can coordinate to the zinc/iron metal centres and form the cages through self-assembly (Scheme 16). This study provides a fascinating display of how self-assembly can be coupled with directed assembly to form well-defined molecular structures. Additionally, the modification of the organic linker with fluorine substitution was proven to modify the dynamic behaviour of the ligand, as well as the electronic properties of the Mo_2 coordination sites, hinting at the potential of engineering such cages for various aforementioned applications.

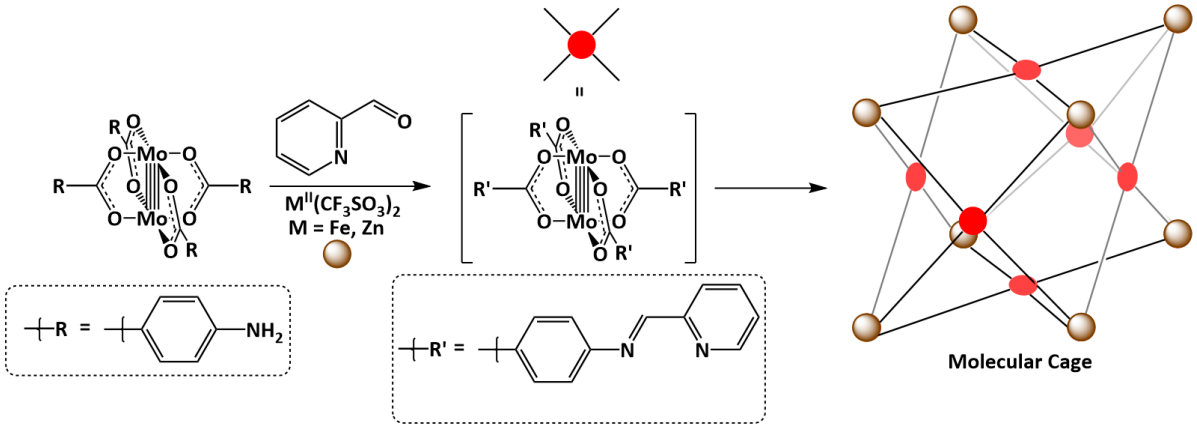

Scheme *16* Construction of a bimetallic molecular cage using Mo_2PWCs and Fe/Zn
The Mo_2 cores are presented as red circles. The Fe or Zn centres are presented as brown spheres. Black lines express the ligands connected to the Mo_2PWCs, which in the cage structure also coordinate to the Fe or Zn centre *via* the chelating terminus.

These examples demonstrate the potential for using reactions on the ligand periphery to generate large molecular assemblies of Mo_2PWCs. Indeed, as long as the right functionality is added to one or more of the ligands coordinated to a Mo_2PWC, and the reaction conditions are relatively mild, they can, in principle, be incorporated into any molecule bearing the appropriate functionality.

Mo_2 dimers of dimers have been synthesised in the past with many examples of note (*vide supra*), and yet, so few of these are asymmetric due to synthetic limitations. Complications arising from the lack of a thermodynamic driving force during the ligand-exchange self-assembly processes, lead to a statistical mixture of products. As an approach, acting through directed assembly, reactivity at the ligand periphery can, in theory, circumvent these limitations by forcefully linking two different Mo_2PWCs *via* covalent bonding at two positions marked by an appropriate functionality. The Investigation of this approach will be the subject of the present work.

Project Aims and Objectives

The introduction of asymmetry in molecular assemblies is not a trivial matter. There is literature precedent set for using directed assembly as an alternative approach to building molecular assemblies over the extensively used self-assembly method. Despite that, very little work has presented directed assembly as a way of constructing asymmetric molecular assemblies. Performing reactions at the ligand periphery has been established as a potentially simple way of extending the functionality of a ligand after it has been coordinated to a metal centre. More specifically, the Sonogashira reaction is capable of forming C-C bonds under mild reaction conditions with high selectivity, making it an ideal means of constructing molecular assemblies *via* directed assembly. As a primary objective, this project therefore aims to synthesise an asymmetric Mo_2 dimer of dimers by performing the Sonogashira reaction at the ligand periphery (Scheme 17). Accomplishing this would unlock a new synthetic avenue towards the mostly unexplored asymmetric molecular assemblies based on Mo_2PWCs, paving the way for the investigation of their use as molecular diodes.

The first step to achieving this ultimate objective involves preparing suitable synthons that can undergo the Sonogashira reaction. Work by Cotton's group utilised the substitutional inertness of formamidinate ligands, particularly $DAniF^-$, to prepare building blocks of the formula $Mo_2(DAniF)_x(OAc)_{4-x}$ (x = 1, 2, 3, 4), which can undergo ligand substitution in a predictable manner to construct molecular assemblies of various geometries.[82] The compound with the formula $Mo_2(DAniF)_3(OAc)$ has been used to build one-dimensional molecular arrays.[83,86,89] By using this compound as the starting material, the substitutionally labile acetate ligand can be replaced with another carboxylate ligand containing a terminal alkyne or an iodide to prepare suitable synthons for the Sonogashira reaction. This will constitute the first objective of this work. Next, as a proof of concept, the synthons will undergo the Sonogashira reaction with simple organic molecules of the appropriate functionality. The success of this attempt will prove that this type of molecule can tolerate the Sonogashira conditions, therefore expanding the functionality in a highly selective manner. Once this has been achieved, the Sonogashira reaction will be used to construct a symmetric Mo_2 dimer of dimers, using two Mo_2PWCs that are coordinated by a carboxylate moiety of a different, suitable functionality, but are otherwise identical. This will be followed by the same reaction, this time using two Mo_2PWCs that differ in both the functionality at the terminus of the carboxylate ligand and in the nature of the formamidinate ancillary ligands coordinated to each Mo_2 core. The expected product of that reaction would be an asymmetric Mo_2 dimer of dimers that cannot be constructed through self-assembly methods, unlocking a new synthetic avenue towards a novel type of asymmetric Mo_2 dimers of dimers.

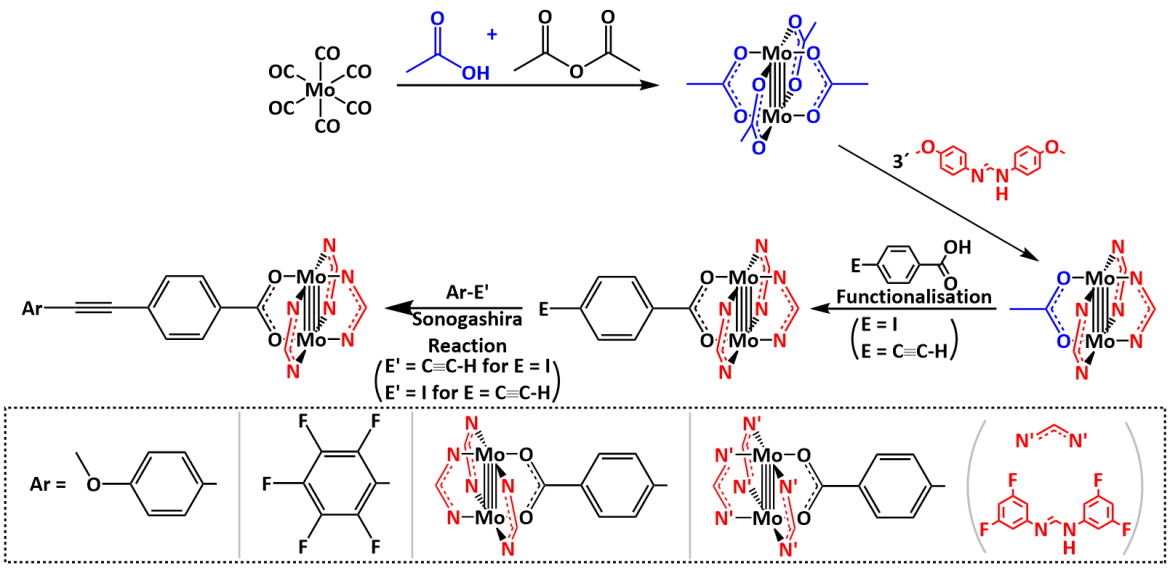

Scheme 17 Overall outline of this work.

Novel molecules will be characterised by various 1D and 2D NMR spectroscopic techniques as well as MALDI-MS and IR spectroscopy. Each novel molecule will be investigated by cyclic voltammetry (CV) and differential pulse voltammetry (DPV) to understand the redox properties of each molecule as well as the electronic communication exhibited by Mo_2 dimers of dimers. UV-Vis spectroscopy will also be used to both characterise novel compounds and provide information on their photophysical properties. Finally, theoretical calculations based on Density Functional Theory (DFT) on model compounds will help rationalise the observations made by the aforementioned analytical techniques.

Results and Discussion

Synthesis of Starting Materials

To perform the Sonogashira reaction at the periphery of Mo_2PWCs, the first step was to synthesise suitable starting materials. The key feature of such compounds is a reactive functionality, which will either be a terminal alkyne or an aryl halide (typically iodide). When constructing molecular assemblies based on Mo_2 complexes, two synthons dominate the literature: dimolybdenum tetracarboxylates,[59,72] and dimolybdenum complexes coordinated by substitutionally inert formamidinate ligands.[82] Since the early 2000s, the most commonly used dimolybdenum tetracarboxylate synthon is $Mo_2(TiPB)_4$ (TiPB = 2,4,6-triisopropybenzoate) due to the excellent solubility of the resulting complex and ability of the bulky TiPB ligand to sterically protect the axial site of the Mo-Mo bond from unwanted axial coordination.[72] There is literature precedent that Mo_2PWCs bearing TiPB ancillary ligands can undergo the Sonogashira reaction to expand ligand functionality,[99] however, there is currently no such precedent for Mo_2PWCs with formamidinate ancillary ligands. For that reason, Mo_2PWCs with formamidinate ancillary ligands were chosen as the type of starting material used in this work, with $Mo_2(DAniF)_3(OAc)$ (**58**) being the first synthetic target. The synthesis of this compound presupposes the synthesis of $Mo_2(OAc)_4$ (**57**), a common starting material made by the thermolysis of $Mo(CO)_6$ in acetic acid and acetic anhydride (Scheme 18).[103]

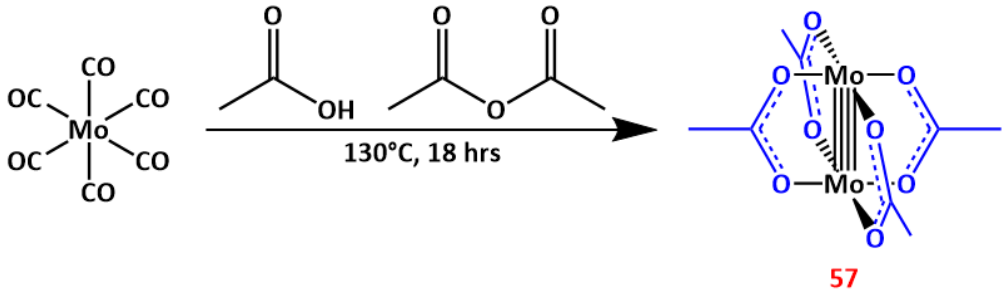

Scheme 18 Thermolysis of $Mo(CO)_6$ towards $Mo_2(OAc)_4$ (**57**).

The synthesis of compound **58** follows the procedure described earlier by Cotton and co-workers.[82] The acetate ligands in compound **57** can readily undergo ligand substitution in the presence of formamidine ligands under mildly basic conditions. Therefore, in a reaction system containing a molar quantity of compound **57** along with "n" molar equivalents of HDAniF and equivalent amounts of a suitable base (such as NaOMe or NaOEt), ligand substitution takes place to form $Mo_2(DAniF)_n(OAc)_{4-n}$ (where n = 1, 2, 3, 4). Formamidinate ligands are substitutionally inert when bound to a dimolybdenum paddlewheel complex, therefore effectively "blocking" the coordination site that they occupy. Conversely, acetate ligands that remain on the Mo_2PWC can readily be replaced by another ligand under mild substitution conditions. This variation in lability allows for the selective design of building blocks that can be used towards supramolecular assemblies.

With the aforementioned strategy in mind, compound **58** was synthesised under air-free conditions in a reaction mixture of compound **57** and exactly 3 equivalents of di-p-anisyl formamidine (HDAniF) and NaOMe (0.5 M in MeOH) each (Scheme 19). The product was characterised by ^{1}H NMR spectroscopy and MALDI-TOF mass spectrometry. The ^{1}H NMR Spectrum is displayed in Figure 20. The key feature of this compound is the asymmetry resulting from its 3:1 ligand ratio. Each proton belonging to the formamidinate ligand exhibits two signals with an intensity ratio of 2:1, which express the protons for formamidinate ligands *cis*- to the carboxylate and *trans*- to the carboxylate respectively. An upfield shift is observed for the protons belonging to the formamidinate ligand *trans*- to the carboxylate ligand relative to the other two that are *cis*- to the carboxylate ligand.

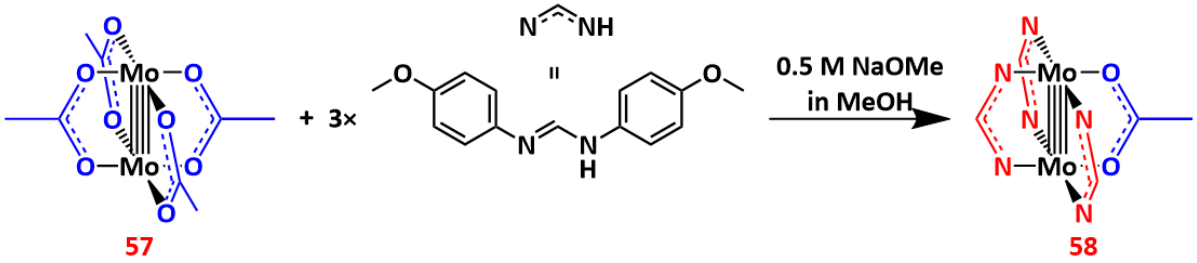

Scheme 19 Reaction scheme for the synthesis of compound **58**.

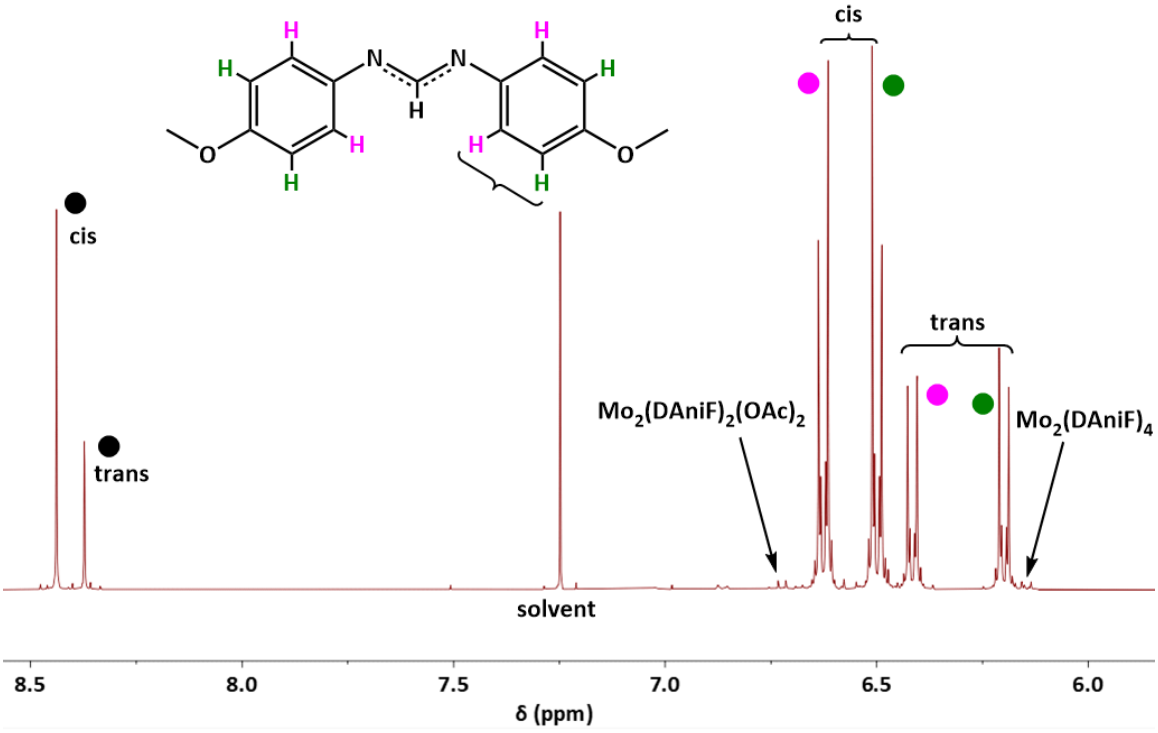

Figure 21 ^{1}H NMR spectrum of compound **58** at the aromatic region.

It is vital that for this product to be obtained in high purity, the stoichiometric quantities of the starting materials are precise. Even slight deviations from the ideal reaction conditions can lead to the formation of $Mo_2(DAniF)_4$ (or even $Mo_2(DAniF)_2(OAc)_2$) being formed in variable quantities (Scheme 20). It was possible to determine the presence of side products by analysis of the ^{1}H NMR spectrum as shown in Figure 20. Due to their reactivity towards atmospheric oxygen, purification with benchtop techniques can be quite challenging. Furthermore, the very similar solubility of impurities and the final product makes it difficult to employ methods such as recrystallisation and solvent extraction. Additionally, flash column chromatography is not an option even if done under anaerobic conditions due to the reactivity of Mo_2PWCs with the stationary phase (silica or alumina). For these reasons, it is vital for the obtained product to be as pure as possible.

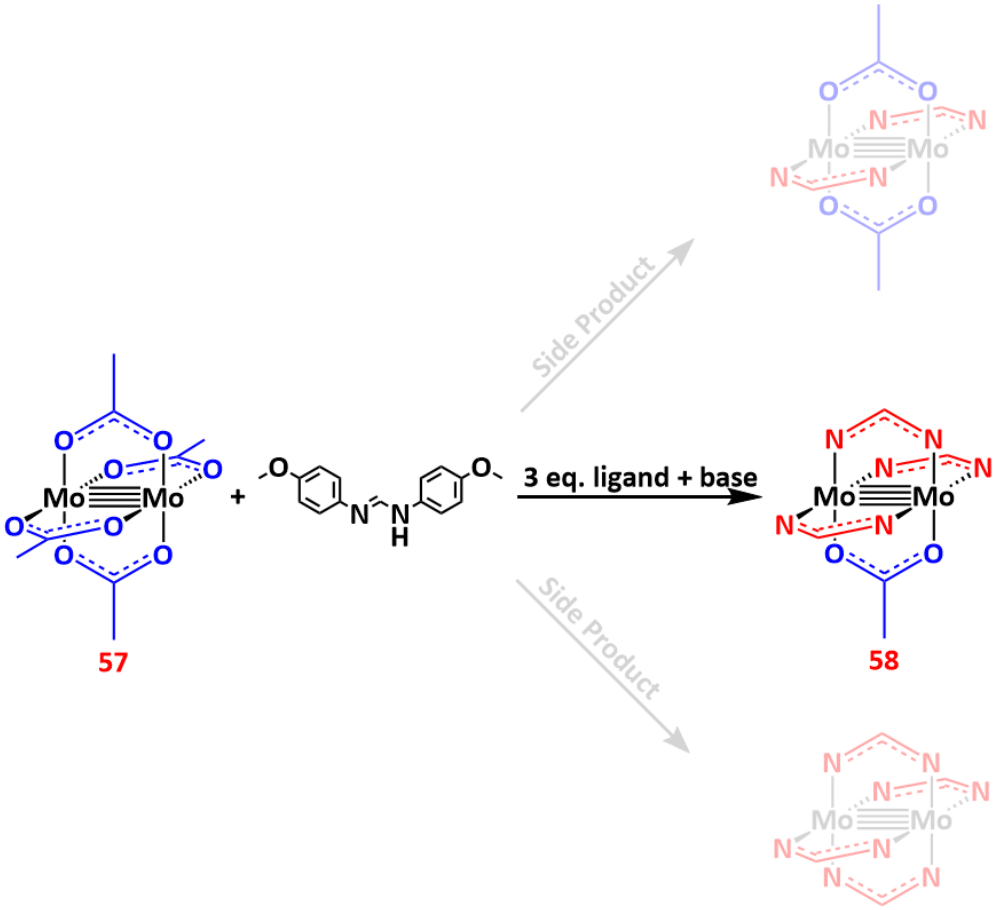

Scheme 20 Representation of the synthesis of compound **58** and side products.

With the three kinetically inert formamidinate ligands placed on the Mo_2PWC, the remaining acetate ligand can be replaced by another carboxylate of suitable functionality to give a single product (Scheme 21). Compound **59a** bears a terminal alkyne functionality, whereas compound **59b** bears an aryl iodide functionality, two functional groups that can take part in a Sonogashira reaction. Initial attempts to synthesise compound **59a** using typical ligand substitution conditions (1 equivalent of carboxylate, 1 equivalent of base, r.t.) were not ideal, as the presence of starting material **58** was evident by ^{1}H NMR spectroscopy. To optimise the reaction conditions, a number of conditions were screened. Increasing the temperature and adding more equivalents of base did not change the conversion but improvements were observed with increased stoichiometry of the carboxylate. Eventually, it was found that adding 5 equivalents of carboxylate (and base) pushed the reaction to completion. The synthesis of compound **59b** requires similar conditions. For both compounds **59a** and **59b**, ^{1}H NMR spectroscopy shows the appearance of two additional overlapped doublets of doublets, each corresponding to protons from the added phenylene group (Figures 40 and 41). The ^{1}H NMR spectrum of compound **59a** also shows an additional peak at 3.17 ppm corresponding to the terminal alkyne proton.

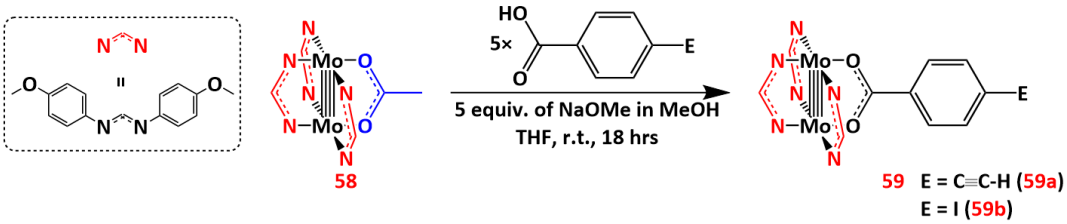

Scheme 21 Reaction scheme for the synthesis of compounds **59a** and **59b**.

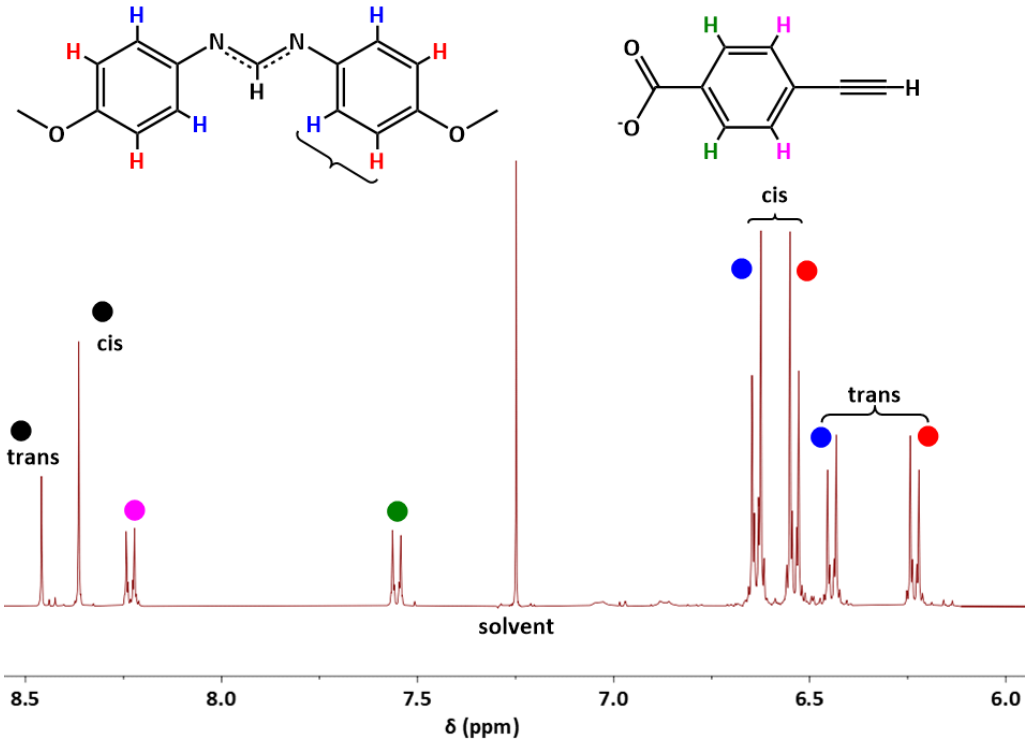

Figure 22 ^{1}H NMR spectrum of compound **59a** at the aromatic region.

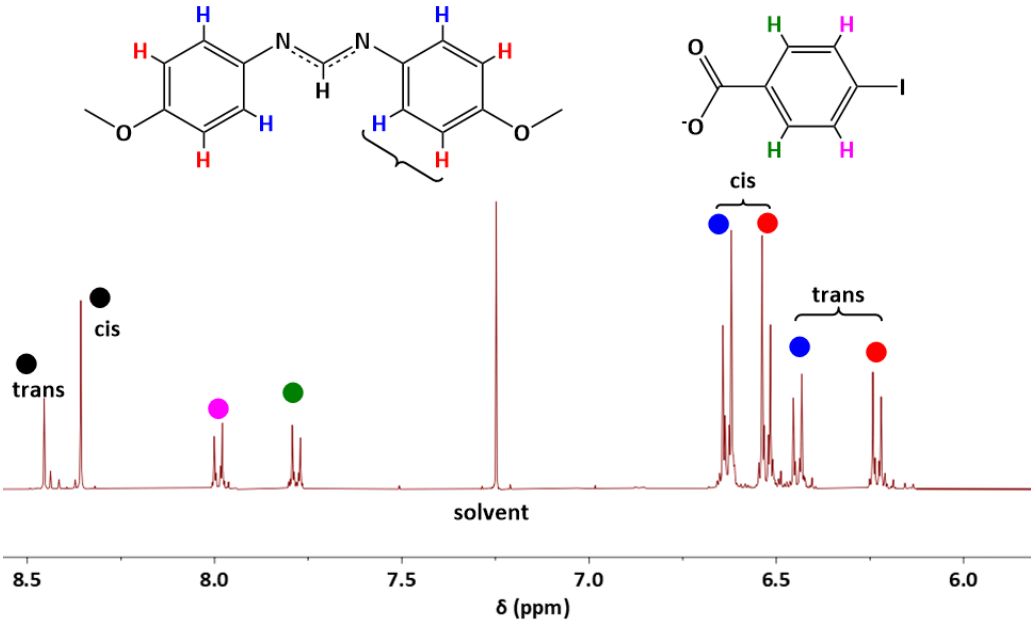

Figure 23 ^{1}H NMR spectrum of compound **59b** at the aromatic region.

Proof of Concept: Expanding the functionality of Mo_2PWCs by Reactions on the Periphery

After the synthesis of the functionalised starting materials for the Sonogashira reaction, a few reactions were undertaken with easily accessible reagents as a proof of concept. The reaction towards the synthesis of compound **60b** was attempted first, using compound **59b** as a starting material, and pairing it with 4-ethynylanisole in a cross-coupling reaction (Scheme 22). Standard Sonogashira conditions were applied based on a literature example.[104] Results from ^{1}H NMR spectroscopy showed a change in the position of the two doublet peaks corresponding to the protons closer to the carboxylate group, indicating that the starting material had been consumed (Figure 23, top and middle spectra). A new set of peaks also appeared, which would be expected to belong to the phenyl protons from the cross-coupled phenyl ring. However, the peaks were not the expected doublets but multiplets that were indicative of two doublets in close proximity with one another (Figure 23, middle).

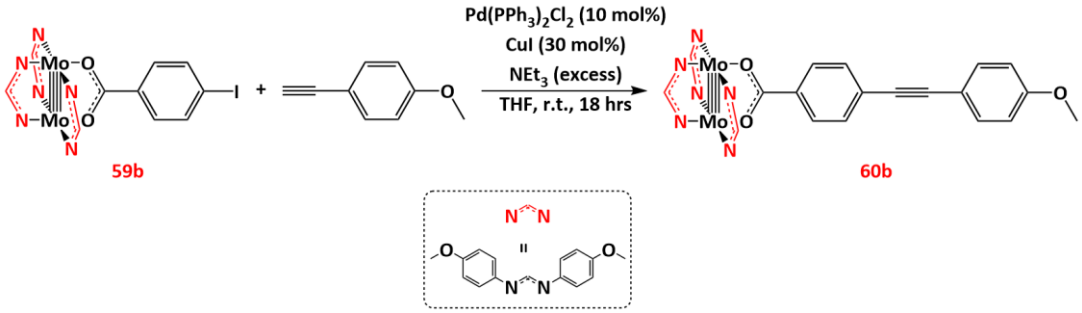

Scheme 22 Reaction scheme for the synthesis of compound **60b**.

The second set of doublets was speculated to have arisen from a common side reaction that often accompanies the Sonogashira reaction: the Glaser homo-coupling.[105] This side reaction requires a terminal alkyne, a copper catalyst, and an oxidising agent (such as O_2 found in air) and consumes two equivalents of the alkyne to generate a homo-coupled product diyne. The most effective way to suppress the formation of these diynes is through the strict exclusion of oxygen from the reaction mixture. Mass spectrometry was employed in an attempt to detect the product of Glaser homocoupling, but MALDI-MS, ESI-MS and APCI-MS did not show signs of any side product.

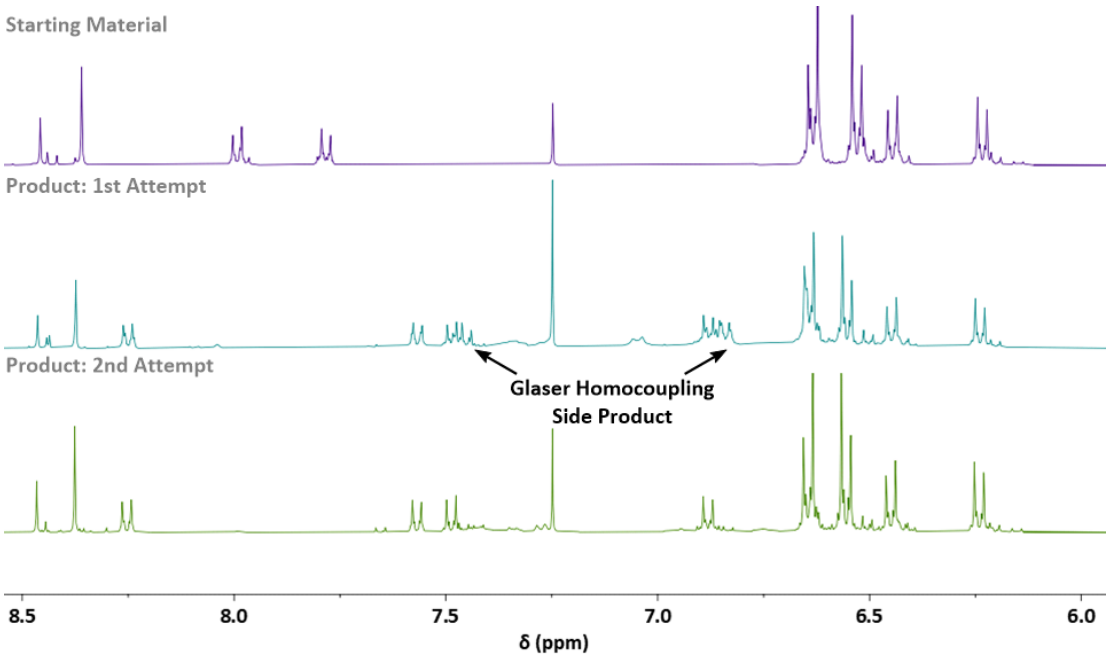

Figure 24 ^{1}H NMR spectra of compound **60b** at the aromatic region.
Top spectrum: Starting material (compound **59b**).
Middle spectrum: First attempt.
Bottom spectrum: Second attempt.

A second attempt at Sonogashira cross coupling was made by reacting compound **59a** with iodopentafluorobenzene following identical conditions (Scheme 23). In the ^{1}H NMR spectrum of compound **60a**, the singlet at 3.17 ppm, corresponding to the proton on the terminal alkyne of compound **59a** integrated to fewer protons (0.03 vs 1), but was still present, hinting at an incomplete conversion (Figure 24). The set of doublets corresponding to the protons closer to the carboxylate group for compound **59a** are also present in compound **60a**, but with significantly reduced integration (Figure 24). Close to the set of doublets belonging to the starting material is that belonging to the product positioned at a slightly lower chemical shift. Another set of doublets is also seen integrating to a lower number of protons (0.33 vs 1), speculated to be the product of Glaser homocoupling. In this attempt, MALDI-MS reveals the presence of an ion with a m/z ratio closely resembling the protonated product of Glaser homocoupling (2205.34 m/z found relative to calculated 2205.86 m/z value).

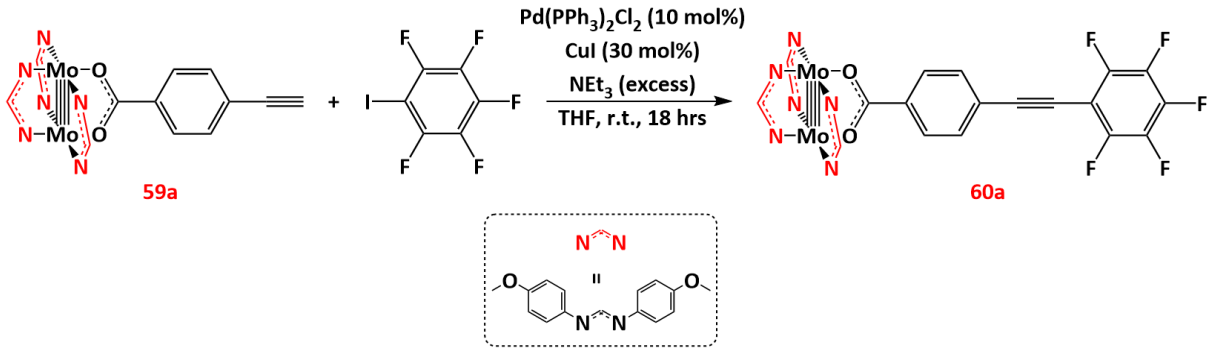

Scheme 23 Reaction scheme for the synthesis of compound **60a**.

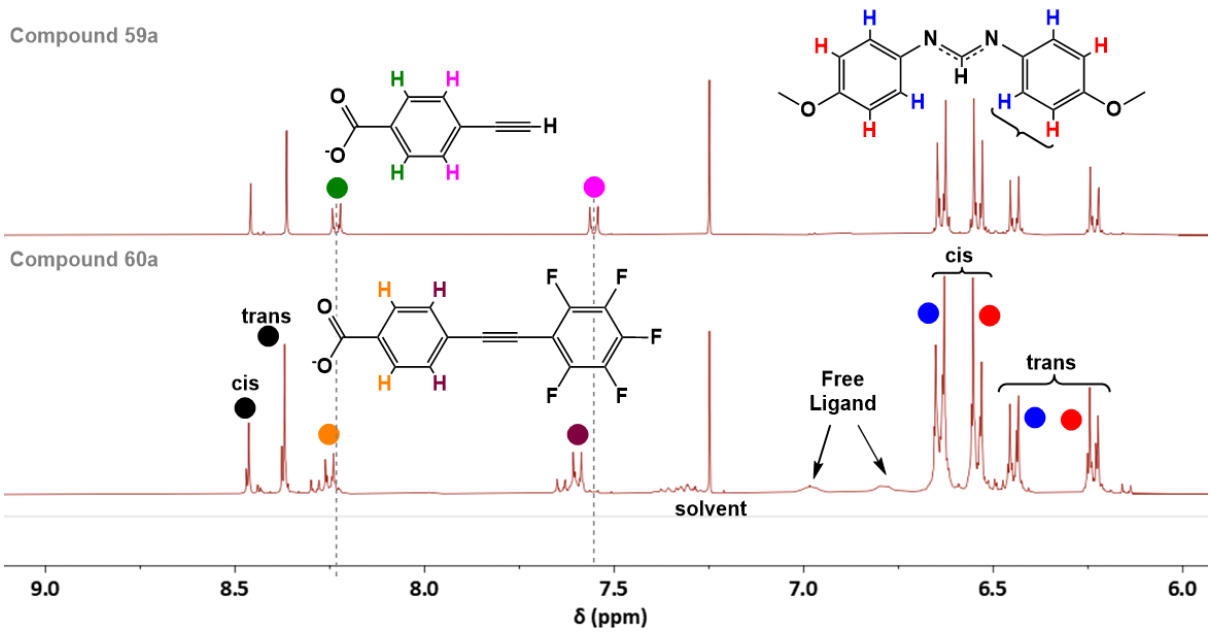

Figure 25 ^{1}H NMR spectrum of compound **60a** at the aromatic region (bottom), compared to the aromatic region of compound **59a** (top).

To tackle the issue of Glaser homocoupling, the reaction towards **60b** was repeated. This time, more rigorous measures were taken at removing traces of oxygen from the solvents and reagents used, but otherwise, the reaction conditions were identical. Pleasingly, the repeated experiment generated a product, the ^{1}H NMR spectrum of which shows a significant decrease in the integration of the extra pair of doublets (Figure 24, bottom). A second attempt was made for the synthesis of compound **60a**, but the ^{1}H NMR results were near identical, with both impurities still present. Attempts to make modifications to the reaction conditions (different catalyst, lower catalyst loading) did not yield satisfactory results as the conversion was significantly lower. Further investigation for this iteration of Sonogashira Cross Coupling was discontinued.

Sonogashira Reaction Towards Mo_2 Dimers of Dimers

Having managed to attach an organic fragment onto the periphery of an Mo_2PWC, the next step for this project was investigating whether two Mo_2PWCs could be coupled together under Sonogashira conditions. Compound **61** was synthesised by combining one equivalent each of compounds **59a** and **59b** (Scheme 24). The reaction conditions were otherwise identical to those for the synthesis of compounds **60a** and **60b**. The synthesis was successful, as confirmed by ^{1}H NMR (Figure 25) and MALDI-MS.

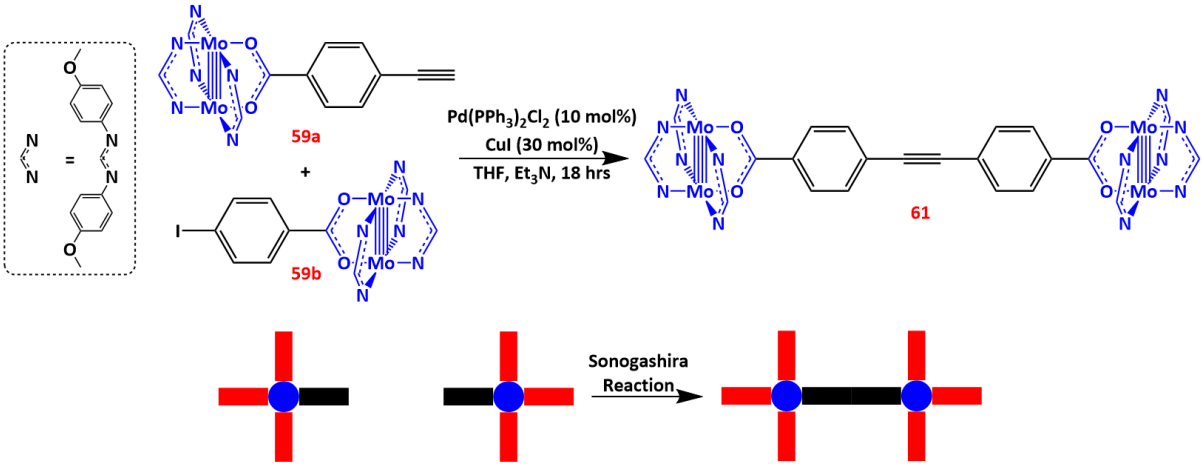

Scheme 24 Reaction scheme for the synthesis of compound **61**.

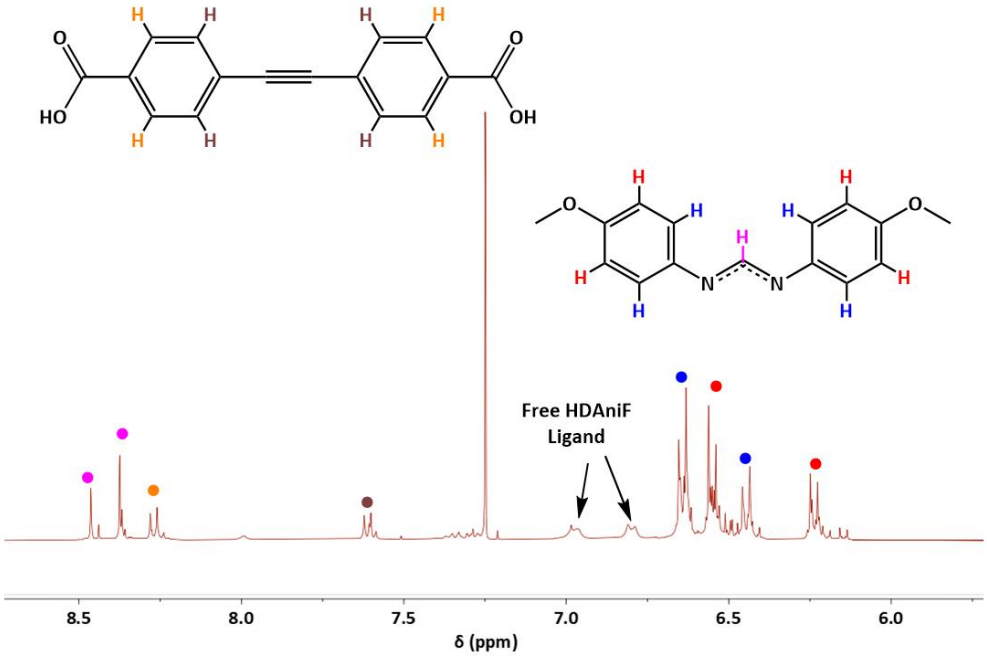

Figure 26 ^{1}H NMR spectrum of compound **61** at the aromatic region. Unassigned peaks belong to $Mo_2(DAniF)_4$ impurities.

Not only was the synthesis of compound **61** an important proof-of-concept for this project, it also represents the first time a dimer of Mo_2PWCs has been achieved by employing reactivity on the ligand periphery and is a significant milestone towards the construction of multicomponent arrays of Mo_2PWCs. To realise the full potential of cross-coupling reactions at the periphery of Mo_2PWCs, the next step would be to synthesise an asymmetric dimer of Mo_2PWCs where each Mo_2 unit is ligated with a different set of ancillary ligands.

Synthesis and Characterisation of a New Coupling Partner

Modifying the ligand properties of Mo_2PWCs can influence the electronic character of Mo_2 cores, even if the modification is located far away from the Mo_2 core.[93] Work within the Wilkinson group has revealed that the addition of fluorine substituents on the aromatic ring of the formamidine ligands drastically changes the oxidation potential of the Mo_2 core, with one particular instance enabling an Mo_2PWC to resist decomposition in air for days.[73] Indeed, considering the reactivity of

Mo_2PWCs towards atmospheric oxygen, with most compounds decomposing within minutes of being exposed into air, a Mo_2PWC that resists decomposition is easier to handle and is more likely to find use in the construction of novel materials. The homoleptic complex $Mo_2(3,5\text{-DFArF})_4$ (DFArF = 3,5-difluorophenyl formamidinate), which contains formamidine ligands with two fluorine atoms in the *meta*- positions of each aromatic ring, was synthesised by Imogen Squire, an MChem student in the Wilkinson group. This homoleptic complex has been shown to have the highest oxidation potential over a series of fluorinated analogues, increasing the likelihood that it resists decomposition.[73] These fluorinated formamidine ligands were used to synthesise the novel heteroleptic complex $Mo_2(3,5\text{-DFArF})_3(OAc)$ (**58'**) (Scheme 25), whose substitution pattern is analogous to compound **58**, and was characterised by ^{1}H NMR spectroscopy (Figure 26) and MALDI-MS.

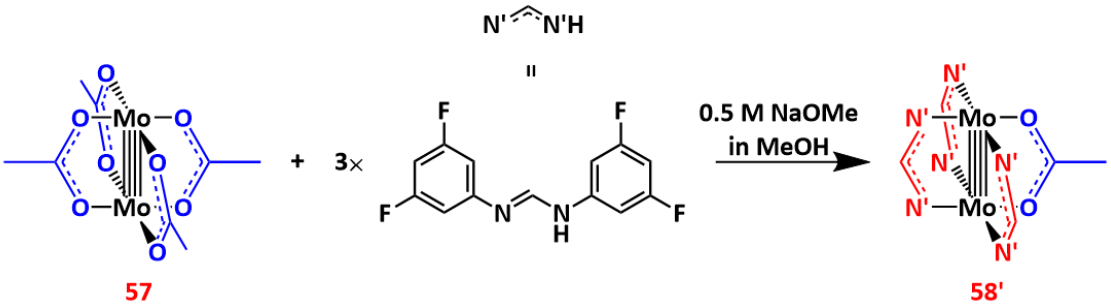

Scheme 25 Reaction scheme for the synthesis of compound **58'**.

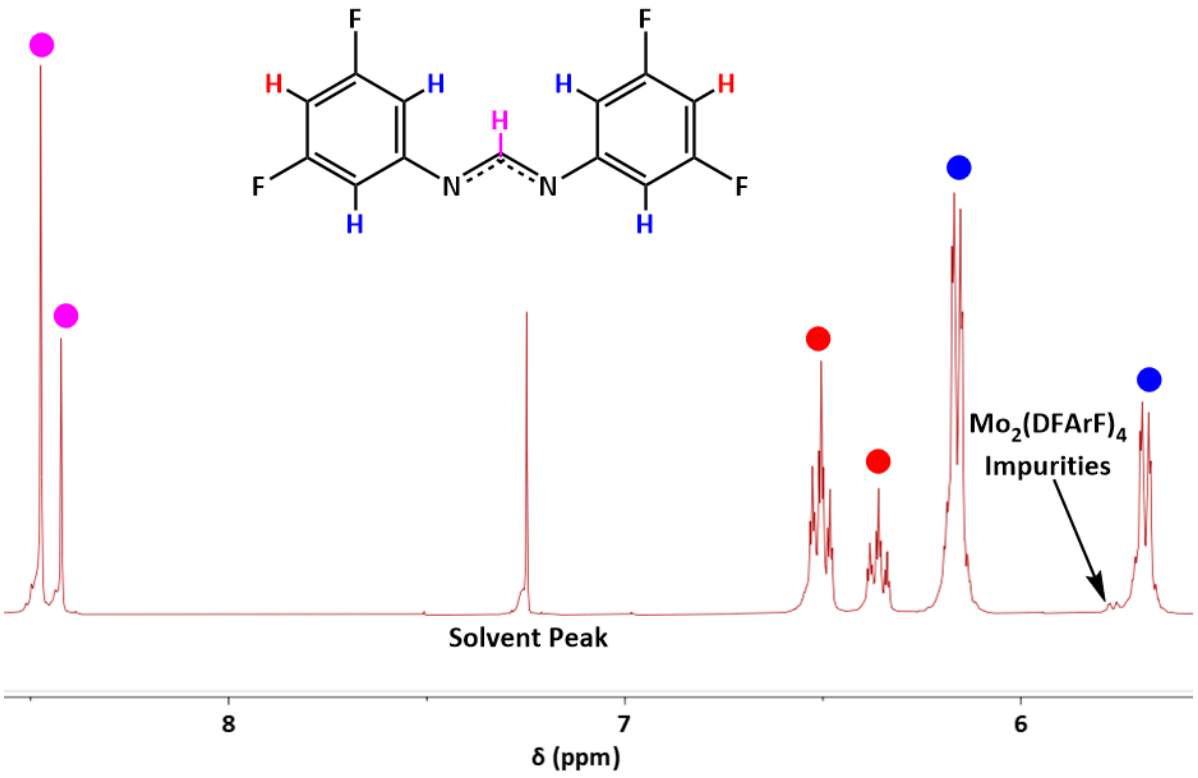

Figure 27 ^{1}H NMR spectrum of compound **58'** at the aromatic region.

To measure the ability of this complex to resist decomposition, a series of NMR experiments was undertaken (Figure 28). For the first experiment, a flask containing compound **58'** was exposed to air and changes in the ^{1}H and ^{19}F NMR spectra were monitored over time. After 114 hours, although there was a small change in the colour (from canary yellow to dark yellow, Figure 27), the peaks in the ^{1}H and ^{19}F NMR spectra corresponding to the compound remained unchanged. Further experiments

involved the compound's capacity to resist decomposition in air whilst in solution. Chloroform-d, taken straight from the bottle without further purification, was used to dissolve compound **58'** under ambient conditions and measurements of the solution were taken over time. After 24 hrs, the peaks corresponding to the product were unchanged and there were still considerable quantities of compound **58'** in the solution, even after 96 hours. This is a stark contrast to compound **58**, which completely decomposes within 4 hours. Clearly, Mo_2PWCs containing the fluorinated formamidine ligands are more resistant to oxidation relative to their non-fluorinated counterparts, even in complexes bearing labile acetate ligands.

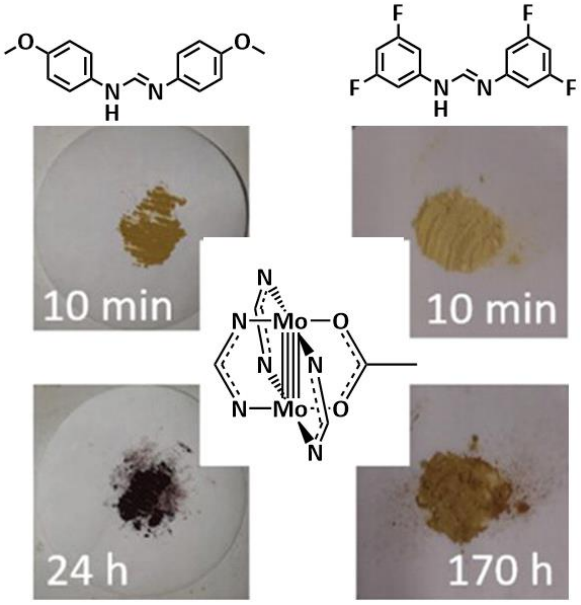

Figure 28 Visual representation of decomposition resistance for compound **58**'.

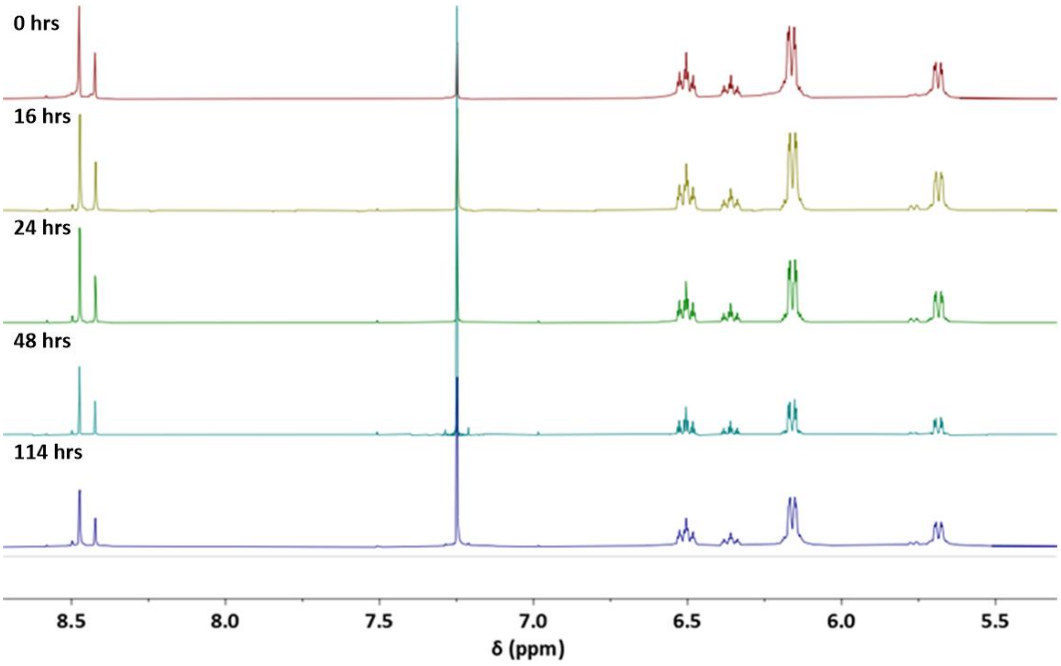

Figure 29 ^{1}H NMR analysis of compound **58**' over time.

The reaction conditions employed to convert compound **58** to compounds **59a** and **59b** should be able to be replicated for compound **58'** to give the functionalised building blocks **59'a** and **59'b** (Scheme 26). Compound **59'b** was isolated and characterised by ^{1}H NMR and MALDI-MS. The synthesis of compound **59'a** was not pursued due to time constraints.

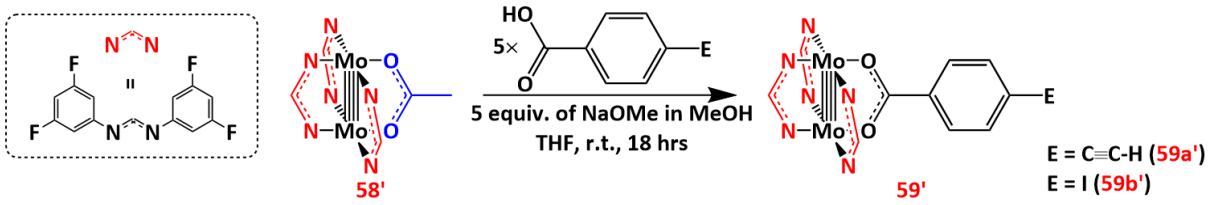

Scheme 26 Reaction scheme for the synthesis of **59a'** and **59b'**.

Compounds **59a** and **59'b** were added to a reaction vessel and the Sonogashira conditions employed for the synthesis of compound **61** were replicated (Scheme 27). The end goal of that synthetic endeavour was to yield an Mo_2 dimer of dimers possessing two redox cores with different ligand environments, connected together by a highly conjugated organic linker (compound **62**). A solid was isolated and analysed by ^{1}H NMR spectroscopy and MALDI-MS. Unfortunately, the ^{1}H NMR spectrum for compound **62** is not as straightforward as for compound **61**, likely due to the asymmetric nature of the molecule, coupled with the potential formation of impurities such as the homo-coupled diyne. What is most interesting is the result coming from the MALDI-MS spectrum. Besides the presence of an intense peak at 1213 m/z indicative of $Mo_2(DAniF)_4$ (a carry-through from the synthesis of compound **58** which is very difficult to remove), another peak at 2179 m/z, corresponding to compound **61** is also present at a significant intensity. The peak corresponding to compound **62** at 2216 m/z is also present but with low intensity.

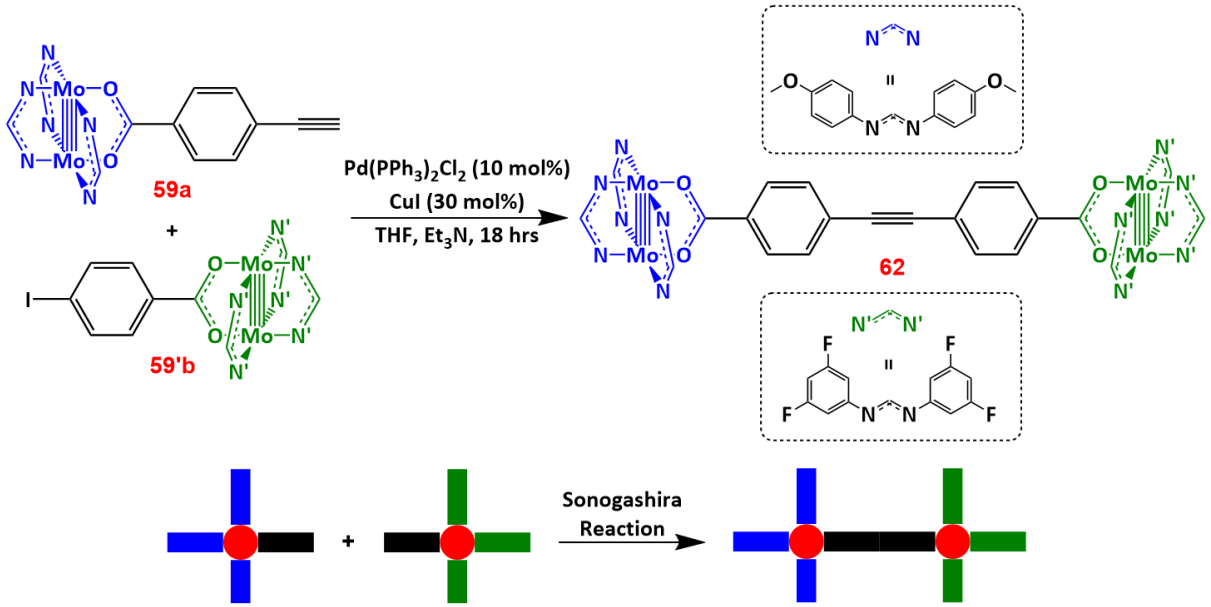

Scheme 27 Reaction scheme for the synthesis of compound **62**.

This observation was suspected to be attributed to ligand scrambling, which has been investigated in Mo_2PWCs in the past.[61,106] As the two complexes entered in solution, the carboxylate ligands have similar kinetic lability. In other words, the activation barrier for replacing each carboxylate

ligand with another ligand (or with each other) is quite similar. This can cause a switch in the functionality of the two different Mo_2 cores inserted in the system, which would explain the possibility of forming compound **61**. To test this hypothesis, a ^{1}H NMR experiment was prepared where the two reactants (compounds **59a** and **59'b**) were dissolved in $CDCl_3$ in an NMR tube and, shortly after, subjected to ^{1}H NMR spectroscopy. The results of the experiment are depicted in Figure 29. Within the 7-8.5 ppm region, elements attributed to the ^{1}H NMR spectra of all possible combinations of Mo_2PWCs with three formamidinate ligands and one carboxylate ligand (compounds **59a**, **59b**, **59a'** and **59b'**) are visible in the ^{1}H NMR sample investigated. This unequivocally shows that ligand scrambling takes place while in solution, as some peaks are displayed in the ^{1}H NMR sample for compounds that could only be present under these circumstances.

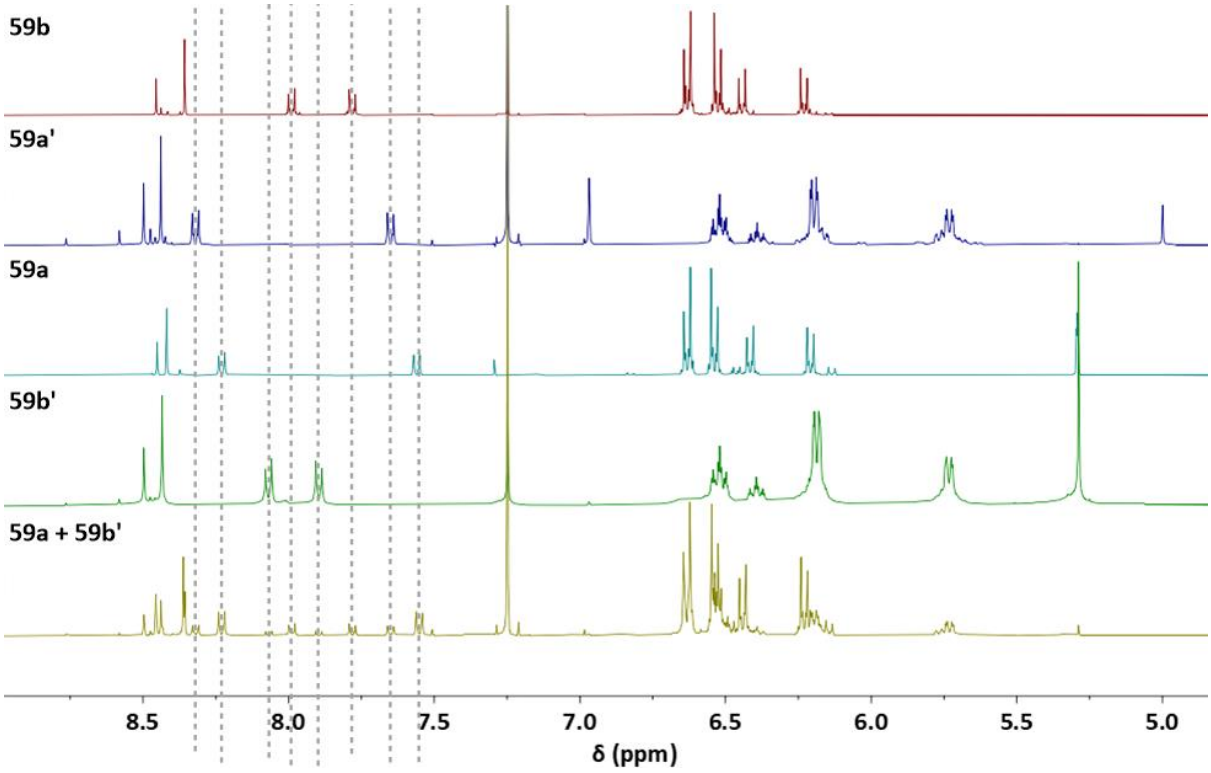

Figure 30 ^{1}H NMR experiment to check for ligand scrambling.

Unfortunately, further synthetic experiments have not been performed past this point due to time restrictions. However, this series of synthetic experiments shows great potential. The Sonogashira reaction clearly works at the periphery of Mo_2 complexes and can successfully form an Mo_2 dimer of dimers through this strategy. Synthetic challenges are still present when trying to couple together two Mo_2PWCs bearing different ancillary ligands, but unlike those posed for the coupling of two Mo_2PWCs by ligand coordination, there are ways to work around them. The Chisholm group has extensively studied the mechanism involved in ligand "scrambling" and, in one particular study, found that adventitious carboxylic acid present in solution can contribute to ligand scrambling.[61] That same study demonstrates that ligand scrambling can be mitigated or indeed eliminated entirely by using a base and a carboxylate anion scavenger. Indeed, 2,6-tert-buyl pyridine can effectively act as a base to prevent ligand dissociation, and $[Mo_2(DArF)_2(CH_3CN)_4]^{2+}[BF_4]^{2-}$ can be added to capture any free carboxylates that may end up in solution regardless. The combination of small quantities of the two reagents in a solution of CD_3CN containing two homoleptic Mo_2 tetracarboxylate complexes showed no signs of ligand scrambling, which is otherwise present when either of the reagents is not used. It is possible that taking such additional measures could prevent ligand scrambling in the reaction mixture

containing **59a** and **59b'**, as the functional groups of the two reactants would likely not interact with the added reagents. However, the carboxylate anion scavenger used in the study by the Chisholm group would not be easy to separate from the compounds investigated in this work, meaning that, to prevent ligand scrambling between compounds **59a** and **59b'**, a different carboxylate anion scavenger would need to be trialled.

Another way to limit ligand scrambling would be to run the Sonogashira reactions in a solvent that has a lower affinity to axial coordination on Mo_2PWCs. Research within the Wilkinson group has found that THF can potentially catalyse ligand dissociation. This was proven by conducting ^{1}H NMR studies on various NMR samples containing $Mo_2(TiPB)_4$ in $CDCl_3$ and other minor solvent impurities (Figure 30). In the presence of small amounts of THF, the integration of the peak corresponding to free carboxylate (HTiPB) ligand relative to that corresponding to $Mo_2(TiPB)_4$ increases compared to the same sample without the presence of THF. When small amounts of 2-MeTHF is added instead of THF, the relative integration of the two peaks remains unchanged. This series of experiments has not been tested for Mo_2PWCs bearing formamidinate ligands due to time constraints.

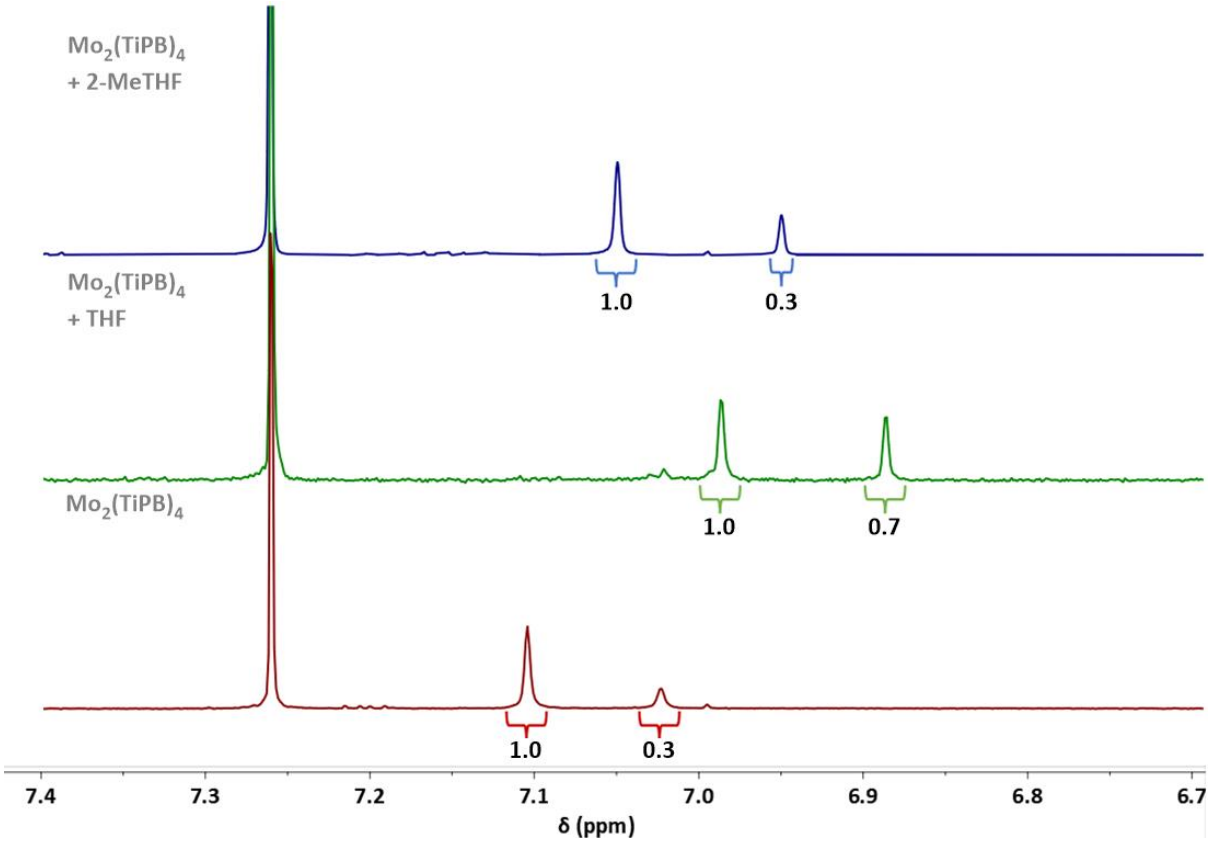

Figure 31 ^{1}H NMR analysis of $Mo_2(TiPB)_4$ in $CDCl_3$ with varying solvent impurities. Data obtained by MRes student Benedict Thompson.[71]

Perhaps a simpler solution to the problem of ligand scrambling would be to use more substitutionally inert ligands for peripheral reactivity. Amidinate ligands are drastically more inert compared to their carboxylate counterparts and have been used for that purpose in studies regarding reaction at the periphery of rhodium PWCs.[95–97] Imposing the right functionality to amidine complexes and coordinating them to $Mo_2(DAniF)_3(L)$ (where L = labile ligand) should be achievable, which would constitute them as appropriate synthons for the dimers of dimers *via* the Sonogashira reaction at the ligand periphery.

Purification Attempt *via* Size Exclusion Chromatography

For most of the reactions investigated, there has been a recurring problem with regards to the purification of all Mo_2PWCs synthesised that used $Mo_2(DAniF)_3(OAc)$ or $Mo_2(DFArF)_3(OAc)$ as a precursor. For the synthesis of the two precursors, a precisely stoichiometric amount of three equivalents of formamidinate ligand and base to one equivalent of $Mo_2(OAc)_4$ is required to minimise the formation of *trans*-$Mo_2(DAniF)_2(OAc)_2$ and $Mo_2(DAniF)_4$ side products. Attempts to synthesise this compound by the Wilkinson group have shown that the formation of side products to a small extent is inevitable. Indeed, in more than one instance, attempts to synthesise the isolated $Mo_2(DAniF)_3(OAc)$ has shown signs of both homoleptic and heteroleptic impurities showing up, hinting that, at these reaction conditions, complete isolation of $Mo_2(DAniF)_3(OAc)$ is incredibly challenging (Figure 31). The heteroleptic impurity contains two labile acetate groups that can form further side products while the homoleptic impurity is substitutionally inert and unreactive under Sonogashira conditions. Even if the presence of impurities is only in minor quantities, further reactivity of the synthesised complexes only increases the amount of impurity present relative to the desired product. This has led to peaks in ^{1}H NMR and MALDI-MS spectra displaying these impurities, and elemental analysis showing increasing deviations from the calculated values with increasing reaction steps taking place (see Experimental).

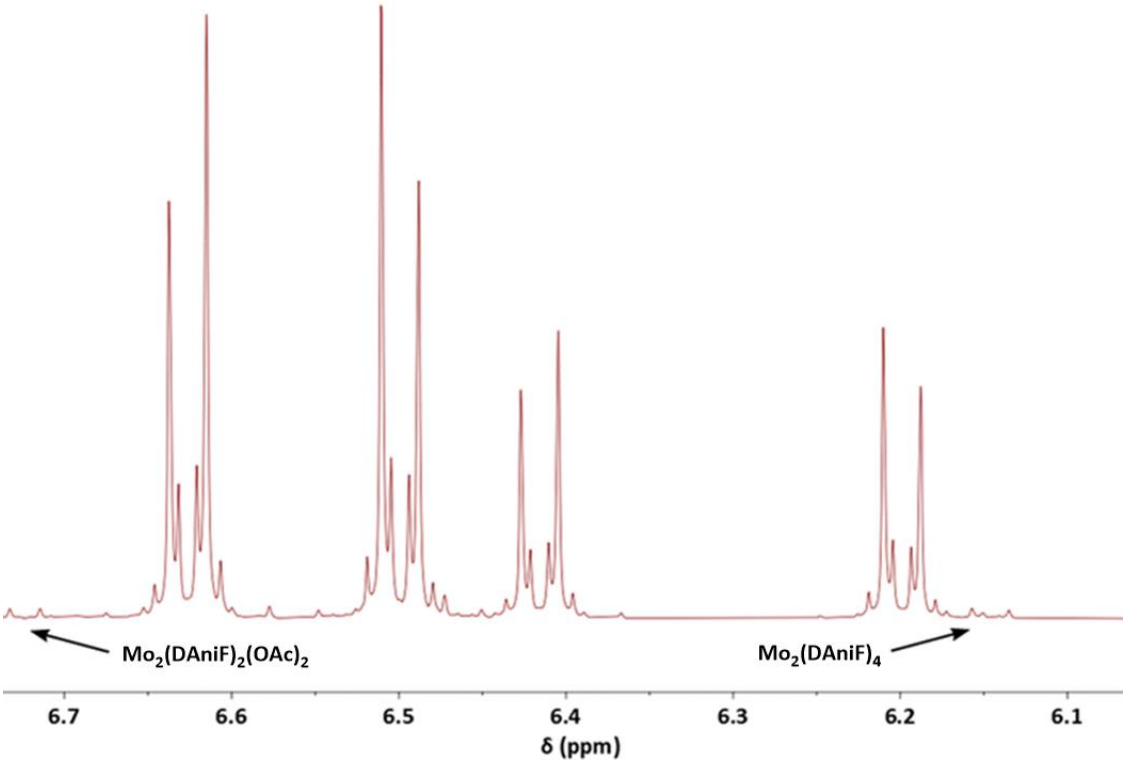

Figure 32 ^{1}H NMR spectrum of a particularly good sample of $Mo_2(DAniF)_3(OAc)$ (**58**) showing peaks corresponding to both potential side products.

The molecules synthesised in this project are all air-sensitive and bear very similar properties, so their separation is not trivial. The labile acetate ligands are easily substituted by coordinating functionalities in silica and alumina, so standard chromatography is often unfeasible as a method of purification. Additionally, the similar solubility of compounds in the series $Mo_2(DAniF)_n(OAc)_{4-n}$ makes recrystallisation impractical. However, size-exclusion chromatography (if performed under inert conditions) may offer a viable method for purification as the gel used in the stationary phase should be inert with respect to the Mo_2PWCs. Diffusion-ordered spectroscopy (DOSY) NMR experiments were performed on a sample containing both compounds in $CDCl_3$. The diffusion coefficient obtained from

the spectrum can be used to provide information on the relative size of each compound through Equation 1 and hence, their capacity to be separated based on their size. The relative size is expressed by the hydrodynamic radius, which describes the radius of the solvation sphere of a compound.

$$R_H = a = \frac{k_B T}{6\pi\eta D}$$

Equation 1 Relationship between the Stokes radius and the diffusion coefficient of a compound. k_B = Boltzmann's constant (1.38×10^{-23} m^2 kg s^{-2} K^{-1}), T = temperature, assumed 298 K, η = dynamic viscosity of the NMR solvent ($CDCl_3$), D = diffusion coefficient.

The diffusion coefficients of each compound were obtained from two sets of peaks in the aromatic region (6-7 ppm) corresponding to each compound. The results obtained for the hydrodynamic radius and the Stokes volume are shown in Table 1. The relatively large difference in the hydrodynamic radius hints that it may be possible to separate the two compounds through size-exclusion chromatography, using a gel filtration resin containing pores that are large enough to trap the $Mo_2(DAniF)_4$ impurity, but not large enough to trap compound **61**. This procedure was performed inside a glove box, supplied with inert nitrogen gas. Sephadex G-20 gel filtration resin was used as the stationary phase, whereas THF was used as the mobile phase. The objective was that effective separation would be achieved when the smaller molecule (for example, the homoleptic $Mo_2(DAniF)_4$ impurity) would be trapped inside the pores of the resin, whereas the larger molecule, which is the coupled Mo_2 dimer product, would pass through the resin without being delayed.

Table 1 Hydrodynamic radius of compound **61** and $Mo_2(DAniF)_4$.

	Compound **61**	$Mo_2(DAniF)_4$
Diffusion Coefficient ($\times 10^{-10}$ m^2/s)	3.8	5.0
Hydrodynamic Radius (nm)	1.02	0.78
Hydrodynamic Volume (nm^3)	2.04	1.55

A small amount of the same sample used for the DOSY experiment was loaded onto a column packed with the Sephadex resin in THF. No separation was observed on the basis of colour, which would be expected for a successful separation given the intense colours of both compounds within the sample. 8 fractions were collected into small test tubes and were each investigated using MALDI-TOF mass spectrometry. Unfortunately, all fractions collected contained both compounds. This shows that size exclusion chromatography under the conditions applied is not capable of separating the two compounds. The intensity of the peak corresponding to compound **61** decreases relative to the impurity as more fractions are collected. This means that there is a possibility that some of the $Mo_2(DAniF)_4$ impurity gets trapped in the gel filtration resin. In that case, perhaps repeating the experiment using a larger column that contains more resin in which the impurity can be trapped would lead to the isolation of the product. This has not been attempted due to time constraints.

Analysis of Photophysical and Electrochemical Properties

To gain a better understanding of the electrochemical and photophysical properties of the Mo_2PWCs synthesised in this project, a series of analytical techniques were applied for these molecules. UV-Vis spectroscopy was used to detect the wavelength, hence the energy, at which electronic transitions occur. This is reflected both by the structure of the ligands coordinated at the Mo_2PWC as well as by the colour exhibited by these complexes. The redox potential of these complexes also varies with the nature of the coordinating ligands and is investigated by electrochemical techniques such as cyclic voltammetry (CV) and differential pulse voltammetry (DPV).

Computational studies employing density functional theory (DFT) calculations were made to further interrogate the electronic structure of the compounds and complement the experimental results.

DFT Calculations

DFT calculations were performed by Dr Luke Wilkinson on a series of model complexes that closely resemble compounds **58**-**61** (and are denoted as the compound number in square brackets *e.g.* **[58]**). To reduce computational throughput, the formamidine ancillary ligands in each complex were replaced by the simpler N,N'-dimethylformamidinate ligand. To model the asymmetry of compound **62**, the full ligand set would have to be calculated but unfortunately this was too computationally expensive to perform and so the results for compound **62** are not included herein. The calculations were performed using the Gaussian 16 suite with the B3LYP functional and the def2_SVP basis set. Table 2 displays the data obtained for relevant molecular orbitals corresponding to the model compounds of interest, and Figures 58, 59, 60 and 62 visualise the data as molecular orbital energy level diagrams, providing further context with an illustration of each molecular orbital. While these data correspond only to models of the compounds synthesised in this work, the contribution of the formamidinate ancillary ligands is expected to be minimal. Herein, these data are analysed to support the observed electrochemical and photophysical properties of the synthesised molecules.

Table 2 DFT values obtained for the energy of molecular orbitals of model compounds **[58]**-**[61]**. All values are represented in eV.

Orbital	[58]	[59a]	[59b]	[60a]	[60b]	[61]
LUMO+3	0.26	-0.24	-0.42	-0.23	-0.76	-0.49
LUMO+2	0.26	-0.29	-0.57	-0.37	-1.19	-0.49
LUMO+1	-0.42	-0.55	-1.01	-0.50	-1.37	-0.82
LUMO	-0.50	-1.49	-1.32	-1.56	-2.45	-1.76
HOMO	-4.01	-3.86	-3.89	-3.79	-4.08	-3.75
HOMO-1	-5.23	-5.04	-5.07	-4.99	-5.23	-3.83
HOMO-2	-5.52	-5.33	-5.36	-5.28	-5.53	-4.98
HOMO-3	-5.78	-5.69	-5.73	-5.53	-5.92	-4.98

Of the model compounds investigated, **[58]** displays the greatest HOMO-LUMO gap (Figure 32). The reason for this is because the HOMO and LUMO orbitals are the Mo_2-based δ and the Mo_2-based δ^* orbital respectively, whereas for compounds **[59a]**-**[61]** the more conjugated carboxylate ligand leads to a low energy ligand π* orbital which lies lower than the Mo_2 δ* such that it becomes the LUMO. Consequently, the HOMO-LUMO transition for all model compounds, besides that of compound **[58]**, occurs between the Mo_2-δ orbital and the ligand-based π* orbital. This means that, for compounds **59**-**61**, tuning the electronic properties of the ligand (either by varying the substituents or by varying the length of the π-system) will directly affect the HOMO-LUMO gap, which will be

represented visually by a change in colour and spectroscopically by absorbing visible light at longer wavelengths in the UV-Vis spectrum (*vide infra*).

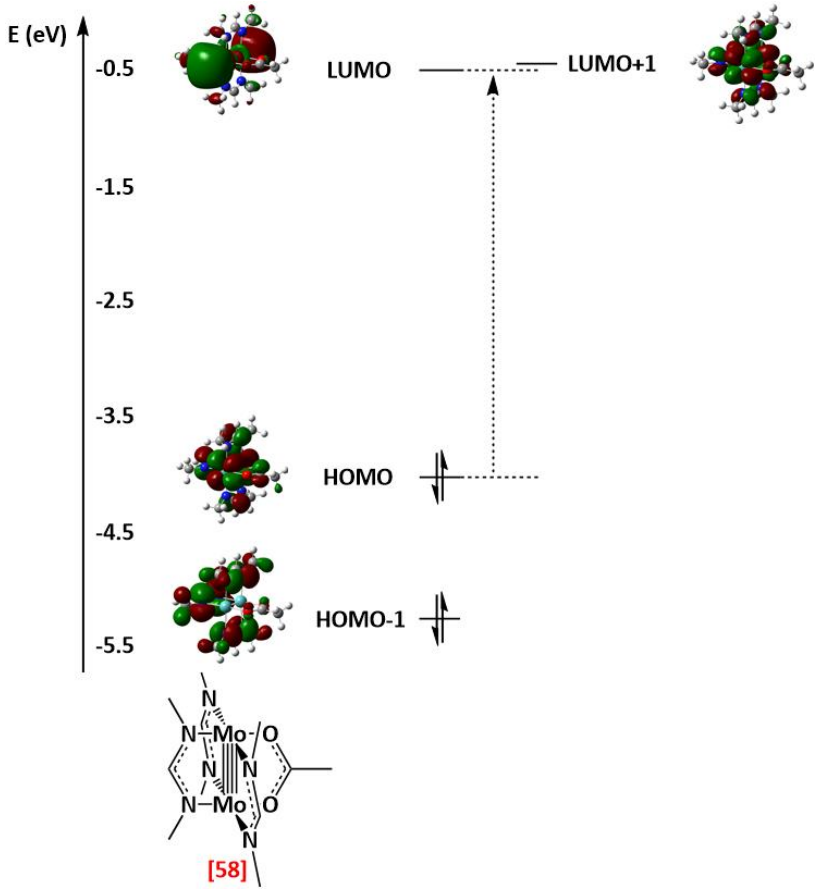

Figure 33 MO diagram of model compound [**58**], derived from DFT calculations.

Compounds **59a** and **59b** are electronically similar in nature, which is why the molecular orbital diagrams for the model compounds **[59a]** and **[59b]** bear similar characteristics (Figure 33). A key difference is the greater conjugation for compound **[59a]** compared to compound **[59b]**, which slightly narrows the HOMO-LUMO gap. Compounds **[60a]** and **[60b]** display HOMO and LUMO orbitals of similar nature (Figure 34). However, the electron-withdrawing effect of the five fluorine substituents on **[60a]** slightly stabilises its HOMO compared to **[60b]** and stabilises the LUMO considerably.

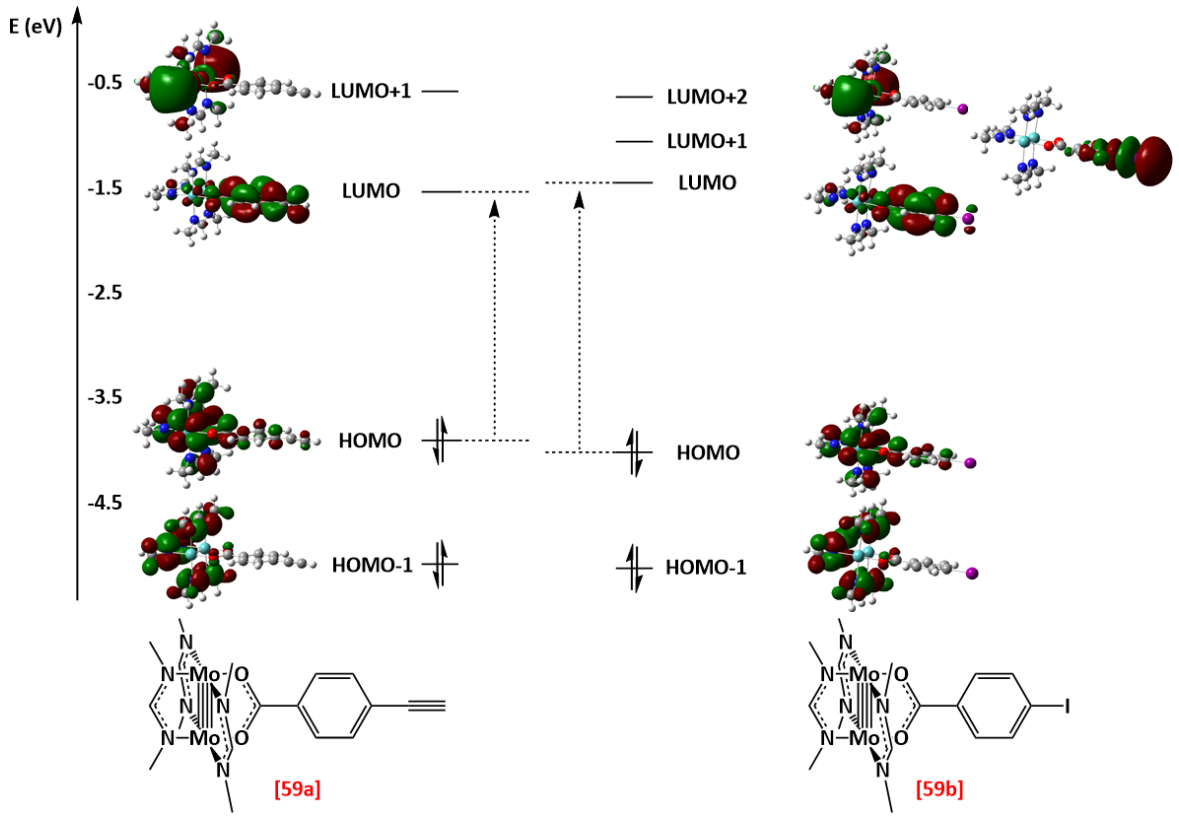

Figure 34 MO diagram of model compounds **[59a]** (left) and **[59b]** (right), derived from DFT calculations.

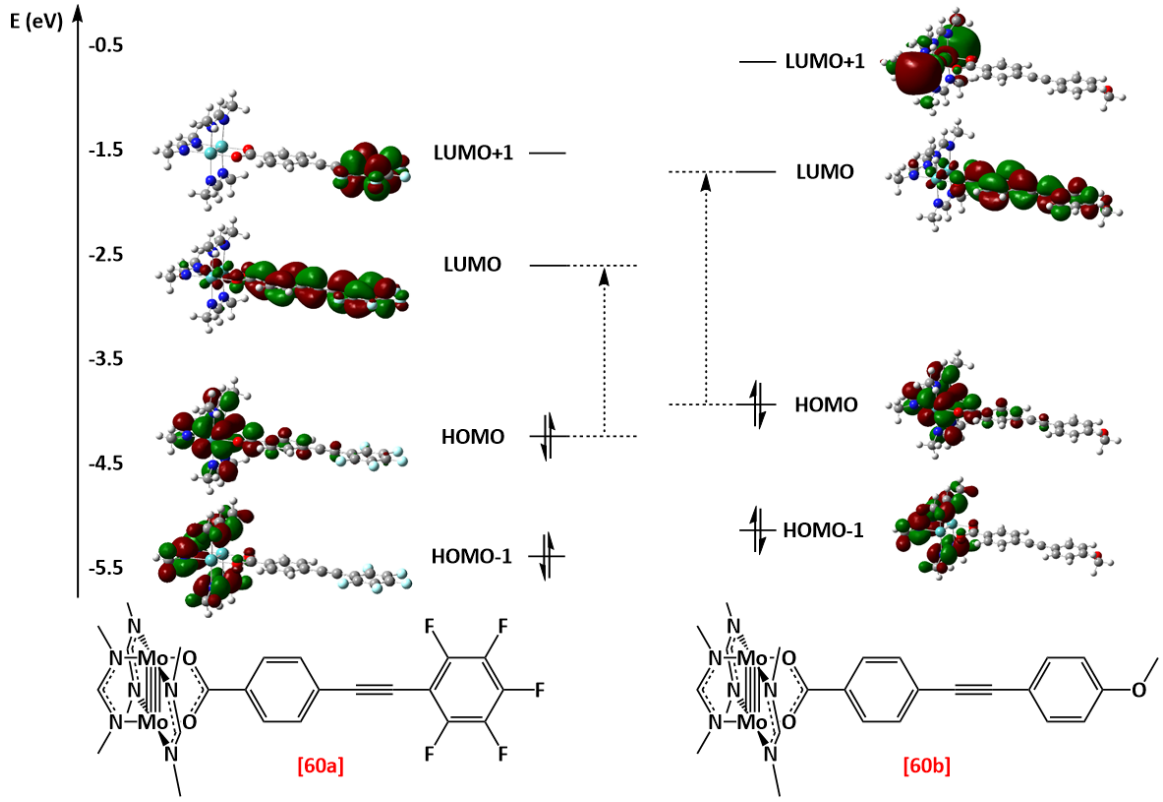

Figure 35 MO diagram of model compounds **[60a]** (left) and **[60b]** (right), derived from DFT calculations.

The molecular orbital calculations for **[61]** show some interesting properties (Figure 36). In dimers of dimers, the HOMO and HOMO-1 molecular orbitals are often largely metal-based.[75] One of those molecular orbitals consists of an in-phase combination of M_2 δ-orbitals, while the other molecular orbital consists of an out-of-phase combination of M_2 δ-orbitals (Figure 35). The former describes the overlap of filled M_2 δ orbitals with empty ligand π* orbitals, whereas the latter describes the overlap of filled M_2 δ orbitals with filled ligand π orbitals. For mixed-valence complexes where through-ligand electronic communication is achieved, the degeneracy of these two molecular orbitals is lifted. As a result, the separation of the two energy levels of the two molecular orbitals is related to the extent of electronic communication between the two metal cores.[51] According to the calculations, **[61]** is anticipated to have the molecular orbital corresponding to an in-phase combination of Mo_2 δ orbitals at a higher energy compared to the out-of-phase counterpart. However, the extent of destabilisation is minimal, as the energy gap between the HOMO and HOMO-1 is a mere 0.07 eV. This is expected, as the distance between the two metal cores is too large for electronic communication to be achieved.

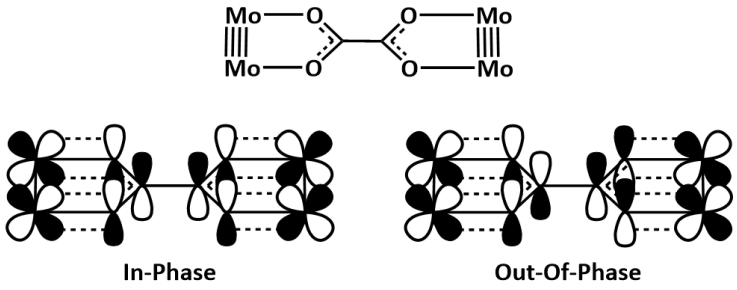

Figure 36 Schematic representation of the two highest occupied molecular orbitals in a molecule consisting of two Mo_2 cores bridged by an oxalate anion. Compound **61** involves solely an extension of the π-system displayed above, with the orbital interactions being otherwise identical.

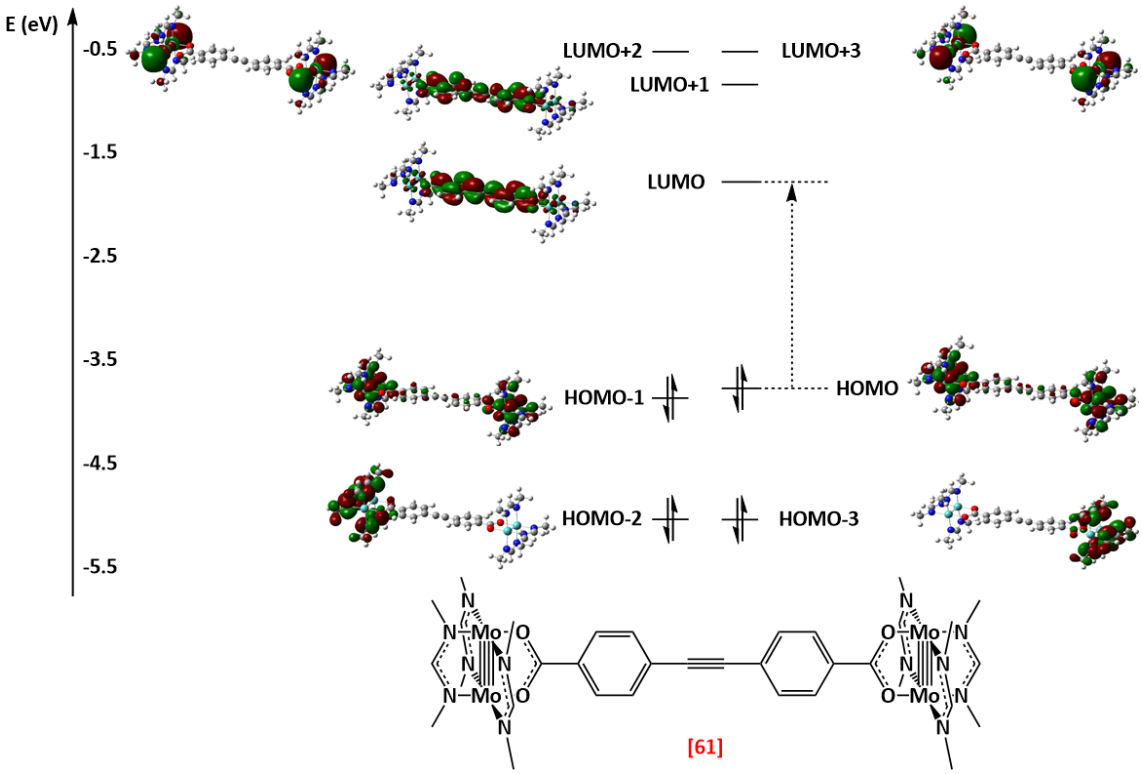

Figure 36 MO diagram of model compound **[61]**, Derived from DFT calculations.

UV-Vis Spectroscopy

The types of complexes studied in this work display two types of absorptions in the UV-Vis spectrum. The first absorption is a high-energy π → π* absorption, often seen in the ultraviolet region of the spectrum. The second absorption is a band stemming from the Mo_2 δ → Mo_2 δ* transition (or from the Mo_2 δ → ligand π* transition if the orbital overlap of the Mo_2 δ-orbital and the ligand π* orbital is strong enough) and is often seen in the visible region of the spectrum. Both transitions are varied based on the electronic properties of the ligands used. Compounds **58'**, **59a**, **59b**, **60a**, **60b** and **61** were dissolved in THF to make solutions of similar concentrations. The solutions were made under inert conditions (glove box), with inert atmosphere maintained whilst the measurements were taken through the use of a cuvette sealed with a Youngs tap. The data are presented in Table 3.

Table 3 Data summary of results from UV-Vis spectroscopy.

Compound	Conc. (× 10^{-5} M)	Abs1	Abs2	λ1 (nm)	λ2 (nm)	ε1	ε2
58'	2.85E-05	2.565	0.129	284	372	89994	4526
59a	2.72E-05	1.942	0.127	277	460	71393	4668
59b	2.91E-05	1.921	0.123	277	443	66125	4233
60b	2.89E-05	3.114	0.251	278	469	107570	8670
60a	2.76E-05	2.451	0.191	283	513	88862	6924
61	2.75E-05	2.598	0.236	282	501	94382	8573

All of the compounds investigated are intensely coloured, with the colour exhibited changing based on the absorption band that is lower in energy, which is dependent on the electronic properties of the ligands coordinated to the Mo_2 core. Compound **58** and **58'** display the same intense yellow colour. The only difference between the two compounds is the substitution pattern at the periphery of the formamidine ligands. The lower-energy bands for these two compounds, which define their optical properties as light is absorbed in the visible region of the UV-Vis spectrum, are dependent on the energy difference between the HOMO δ orbital and the LUMO δ* orbital. The effects of the substituents on the aromatic rings of the formamidine ligands affect the δ and δ* orbitals in the same way, meaning that the energy difference between the two energy levels is the same for both compounds. This overall lack of influence towards the HOMO-LUMO gap by remote substituents has been previously documented for homoleptic Mo_2PWCs within the literature and from research within the Wilkinson group on homoleptic, fluorinated Mo_2PWCs (Figure 37).[73,107] These electronic effects explain the similarity in the colour of the two compounds.

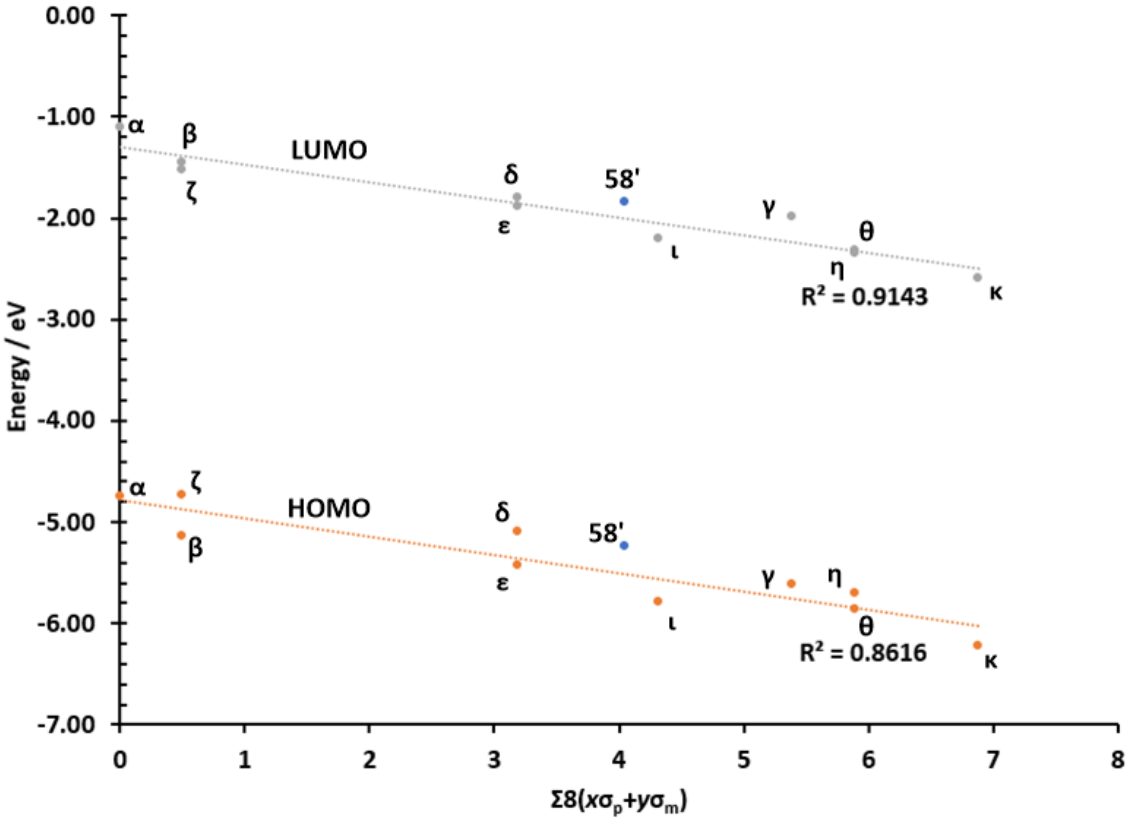

Figure 37 Least-squares regression plot demonstrating the relationship between calculated frontier molecular orbital energy levels and Hammett constants for homoleptic Mo_2PWCs (labelled α-κ) bearing different fluorine substituents on the periphery of formamidinate ligands and for the heteroleptic Mo_2PWC **58'**. Very little variation is shown in the HOMO-LUMO gap, with all compounds exhibiting an intense yellow colour. R^2 values were determined without accounting for compound **58'**.[73]

Significant changes are observed in the optical properties of the transition-metal complexes when highly conjugated ligands are coordinated onto the metal cores. Compounds **59a** and **59b** exhibit intense red and orange colours respectively in accordance with the absorption wavelength of their UV-Vis spectra (Figure 37). Extended ligand conjugation decreases the energy level of the ligand-based π* molecular orbital and, as mentioned, if the energy level of this orbital is lower than that of the metal-based δ* orbital, the HOMO-LUMO transition is now Mo_2 δ → ligand π*. Accordingly, compound **59a** shows greater conjugation relative to **59b** owed to the inclusion of an alkyne functionality, extending the π-system, and lowering the energy level of the LUMO. The HOMO is also somewhat stabilised. This decreases the energy gap between the HOMO and LUMO, lowering the energy (and increasing the wavelength) of the Mo_2 δ → ligand π* transition and causing the compound to display a strong red colour compared to the orange colour displayed by compound **59b**.

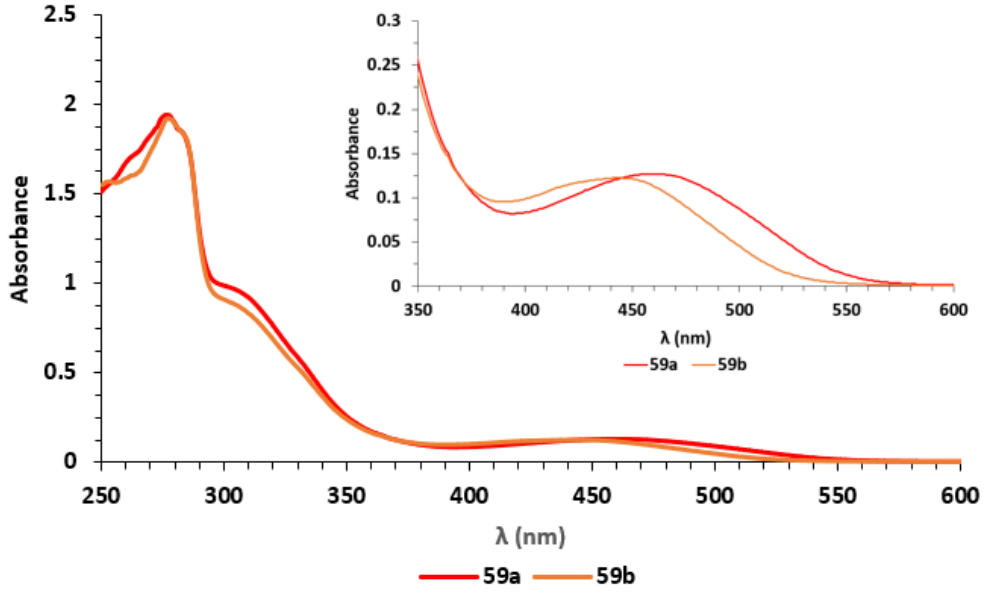

Figure 38 Comparison of UV-Vis spectra for compounds **59a** and **59b**.

As envisioned by the DFT models discussed previously, the HOMO-LUMO transition continues to be between the Mo_2 δ and the ligand π* for the products of the Sonogashira reaction (**[60a-61]**). For this series of compounds, the influence of the substituents on the periphery of the highly conjugated ligands is also evident (Figure 38). Compound **60b** shows the highest-energy MLCT transition of the three Sonogashira products, likely because the electron-donating nature of the methoxy group located at the ligand terminus raises the energy level of the π* orbital, causing the transition to be of a larger energy compared to a hypothetical unsubstituted analogue. Compound **60a**, on the other hand, possesses 5 electron-withdrawing fluorine substituents on the ligand terminus, which should lower the energy of the π* orbital, contributing to a lower-energy MLCT transition. Indeed, this compound displays the transition of the highest wavelength compared to the other compounds investigated. Compound **61** is found to have an MLCT transition with an energy lying between compounds **60a** and **60b**, being closer to the energy of compound **60a**. It is speculated that there are two reasons for this. Firstly, the extended π-system between the Mo_2 metal cores and the ligand is larger for compound **61** compared to that for compounds **60a** and **60b**. As a result, the extent to which the energy level of the ligand-based π* molecular orbital is lowered by is greater. Secondly, the fluorine substituents also play a role in stabilising the HOMO, albeit less significant than that in stabilising the LUMO. This effect is absent for compound **61**, leading to the HOMO of that compound being higher relative to compound **60a**, hence bringing the HOMO-LUMO gap for compound **61** closer to that for compound **60a**.

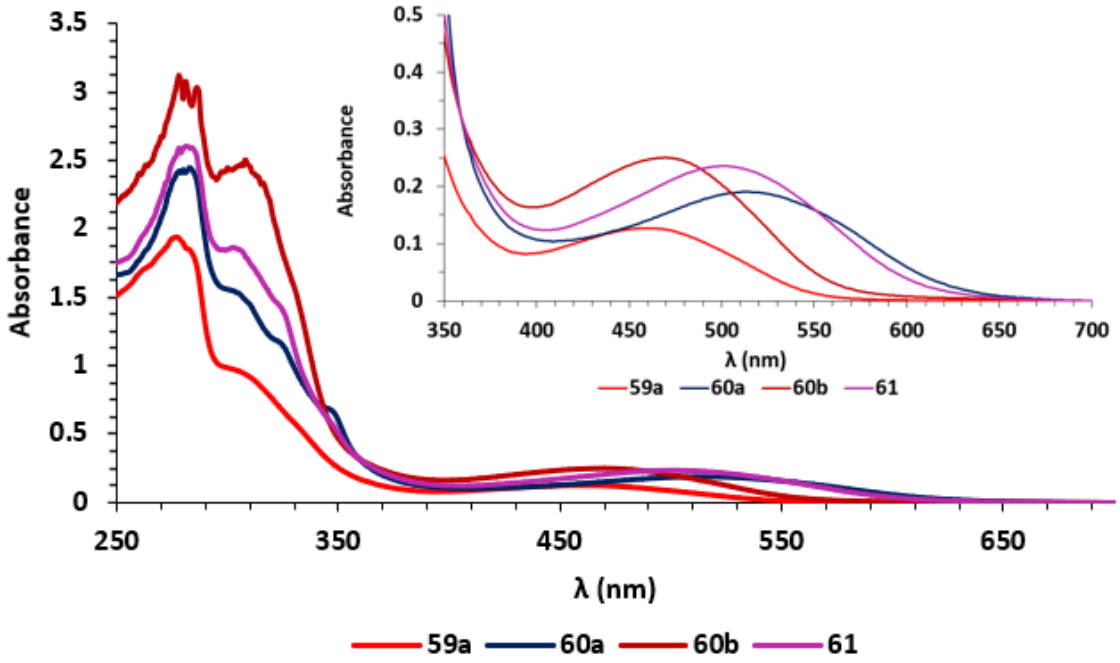

Figure 39 Comparison of UV-Vis spectra for compounds **60a**, **60b** and **61**.

Comparing the experimental data obtained through UV-Vis spectroscopy with the theoretical data obtained for the model compounds *via* DFT, the HOMO-LUMO gap trends between the model compounds are in complete agreement with the energy of the MLCT transitions observed experimentally. The larger the HOMO-LUMO gap, the higher the energy of the MLCT transition.

Electrochemistry

To gain a deeper understanding of the redox properties of the synthesised complexes, they were subjected to cyclic voltammetry (CV) and differential pulse voltammetry (DPV) experiments. Table 4 summarises the relevant results.

Table 4 Cyclic voltammetry data collected for compounds **58**, **59a**, **59b**, **60a**, **60b** and **61**. Measurements taken in 0.1 M $(n\text{-}Bu)_4N^+[PF_6]^-$ solutions in DCM vs Fc/Fc^+ (see experimental for more details).

	E_1 (mV)	E_2 (mV)	$E_{1/2}$ (mV)	$\Delta E_{1/2}$ (mV)	I_{pa}/I_{pc}
58	-340	-430	-385	89	0.98
59a	-279	-409	-344	130	1.23
59b	-208	-302	-255	94	1.10
60a	-315	-403	-359	88	1.10
60b	-280	-418	-349	139	1.06
61	-305	-407	-356	102	0.93

The chemical reversibility of each complex was determined by measuring the values for I_{pa} and I_{pc} and obtaining a ratio. These values correspond to the shortest distance between the current peaks and the extrapolated baseline relevant to each process (Figure 39). For a chemically reversible redox process, the ratio of I_{pa}/I_{pc} would be very close to 1. That is not the case for any of the compounds investigated. This demonstrates partial chemical irreversibility, which may be a result of partial decomposition of oxidised species as they react with adventitious water or oxygen in the electrochemical cell.

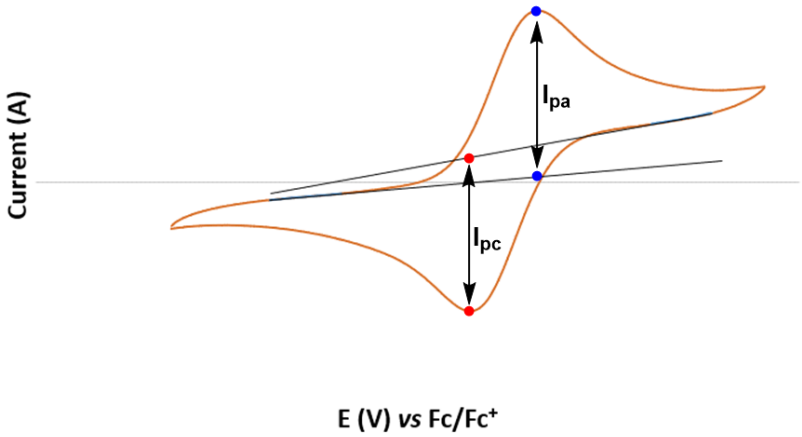

Figure 40 Cyclic voltammogram of compound **58** showing how I_{pa} and I_{pc} were determined from the distance between redox peaks and extrapolated baselines.

Each compound was scanned multiple times at varying scan rates (Figure 40). The variation of scan rates is applied in order to estimate the electrochemical reversibility of the system. This property describes the electron-transfer kinetics between the sample and the electrode. In an ideal "Nernstian" system (one that follows the Nernst equation), electron-transfer takes place without any barriers, with oxidation and reduction peaks showing no change in potential as scan rates vary. However, if electron-transfer is "sluggish", an increase in scan rates will cause the two peaks to drift apart, increasing the ΔE value.[108] The compounds investigated showed either reversible or quasi-reversible behaviour, with the latter case showing only minor deviations of ΔE.

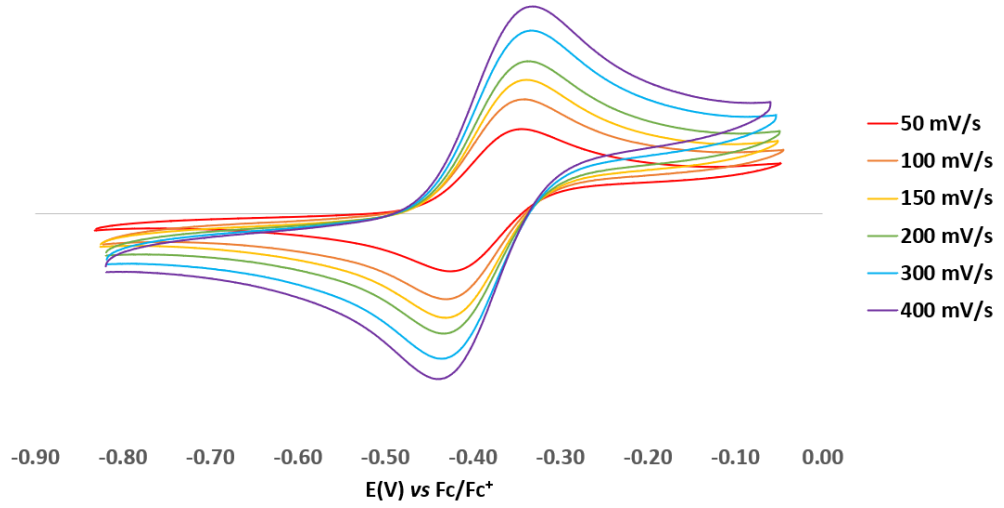

Figure 40 The cyclic voltammogram of compound **58** with varying scan rates, exhibiting electrochemically reversible behaviour.

Accurate measurements of cyclic voltammetry require that the analyte is homogeneous with the solvent system and therefore freely diffusing into it. To ensure that this is the case for all compounds investigated, a series of plots was made relating the square root of the scan rate to the current intensity of oxidation or reduction peaks (an example is shown in Figure 41). For a homogeneous system (where no adsorption of the analyte onto the electrode surface is observed), this relationship should be linear according to the Randles-Sevcik equation (equation 2). Experimentally, all systems investigated display a strictly linear relationship between the square root

of scan rate and the current intensity, with the R^2 value of all plots being higher than 0.99, proving that all redox processes measured took place in a homogeneous system.

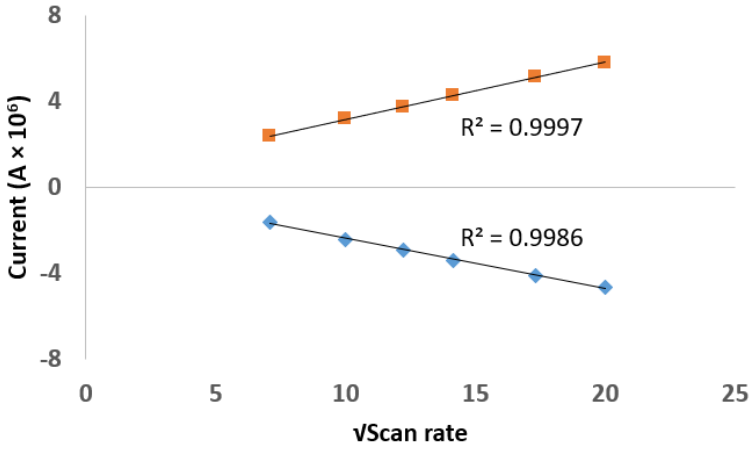

Figure 41 Linear fit between current of oxidation/reduction peaks relative to the square root of the scan rate for compound **58**.

$$i_p = 0.446nFAC^0\left(\frac{nF\upsilon D_o}{RT}\right)^{1/2}$$

Equation 2 Randles-Sevcik Equation.
i_p = current maximum (Amp), n = number of electrons taking part in the redox process, F = Faraday constant (C/mol), A = electrode area (cm^2), C = concentration (mol/mL), v = scan rate (V/s), D = diffusion coefficient (cm^2/s), R = gas constant (J/(mol×K)), T = temperature (K).

As mentioned, the electrochemistry of mixed-valence complexes often reflects the extent at which the two metal cores exhibit through-bond electronic communication. Compound **61** shows only one reversible redox peak that corresponds to the removal of an electron from the Mo_2 δ orbital (Figure 42). This means that the two Mo_2 units are oxidised at the same time, meaning that there is no mixed valency present. This is further corroborated by the theoretical values of the energy levels of the HOMO and HOMO-1 derived from model compound **[61]**. The destabilisation of the HOMO and HOMO-1 for mixed-valence complexes is directly linked to the electronic communication between the two metal cores and, for model compound **[61]**, that destabilisation is very small (0.07 eV). This lack of electronic communication is expected, as the spacing between the two metal cores, which is proportional to the length of the organic linker, is relatively large for any electronic communication to be present.

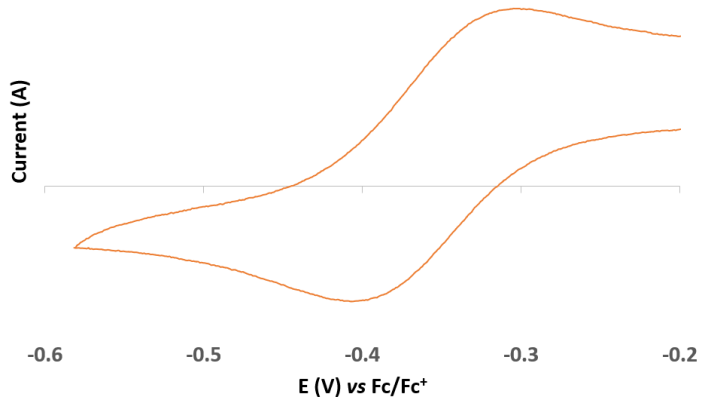

Figure 42 Redox peak corresponding to the first oxidation/reduction wave of compound **61**.

As discussed previously, the first oxidation of a Mo_2PWC involves the removal of an electron from the δ-orbital. The energy required to remove that electron is directly related to the first oxidation potential. This means that, the lower the energy level of the HOMO for a given compound, the higher its oxidation potential will be, as removing an electron from a molecular orbital requires more energy if it is more stable. On that note, it should be possible to relate the theoretical calculations for the energy of the HOMO for the model compounds determined in the prior DFT study to the experimental results for $E_{1/2}$ obtained by cyclic voltammetry for the compounds that the models correspond to.

However, when comparing the values obtained for the energy of the HOMO of the model compounds **[58**-**61]** to the $E_{1/2}$ values of compounds **[58-61]** respectively, a large discrepancy between the two data sets is observed. The root cause of this discrepancy likely stems from the fact that DFT has estimated the energy of molecular orbitals corresponding to models of the compounds, rather than the compounds themselves. Therefore, any influence from the DAniF ancillary ligands would not be evident in the DFT calculations. Indeed, the DFT models suggest that the influence of the ancillary ligands towards the HOMO is greater than that of the conjugated carboxylate ligands. This discrepancy is not observed when comparing the theoretical data obtained from the model compounds with the experimental UV-Vis data for the actual compounds because the UV-Vis transitions are dependent on the relative energy levels of both the HOMO and the LUMO, and since for all compounds besides **2** the LUMO is largely based on the nature of the conjugated carboxylate ligand, which the theoretical models account for, the experimental data corresponding to the HOMO-LUMO gap will be in accordance with the data obtained for the theoretical model compounds.

Conclusion and Future Work

Mo_2PWCs have received tremendous attention over the last few decades as ideal synthons towards molecular assemblies due to their fascinating photophysical and electrochemical properties. This project has managed to make a promising first step towards unlocking a new synthetic avenue towards constructing Mo_2-based molecular assemblies through performing reactions at the ligand periphery of a Mo_2PWC. The starting materials **59a**, **59b** and **59b'** have been successfully made and used to synthesise compounds **60a**, **60b** and **61** through the Sonogashira reaction. Provided that air-free conditions are rigorously maintained through the course of the reactions, the Sonogashira reaction has proven to succeed in a highly selective manner. The synthesis of asymmetric dimer of dimers **62** was attempted, which is a compound that is not accessible as pure material through any other known synthetic approach. Unfortunately, ligand scrambling between the starting materials **59a** and **59b'** takes place while the compounds are dissolved in THF, leading to the formation of large quantities of undesirable side product that cannot be separated from compound **62**, which seems to appear in much smaller quantities. Despite the unsuccessful attempt to isolate compound **62**, ligand scrambling, the reason behind the formation of side products, is unrelated to the Sonogashira reaction mechanism. Consequently, if ligand scrambling is mitigated, with potential solutions being proposed in the main text, performing reactions at the ligand periphery will prove to be a valuable tool in constructing a novel type of asymmetric Mo_2 dimer of dimers, with the asymmetry being owed to the variation in the ancillary ligands that modify the electronic environment of each Mo_2 core. Therefore, future work will aim towards reducing the extent to which ligand scrambling takes place in an attempt to isolate compound **62**.

Should the prevention of ligand scrambling be achieved, the investigation of one-dimensional molecular assemblies should be extended to more diverse asymmetric molecular arrays. For example, ligands bearing different chelating atoms, such as partially or fully thiolated analogues of the carboxylic acids used may show enhanced electronic communication through the organic linker, as has been shown by extensive studies from the Liu group.[89,91] Therefore, if two SS- or SO-chelating ligands, each bearing either a terminal iodo- or alkyne functionality, are coordinated separately to $Mo_2(DAniF)_3(OAc)$, the resulting two Mo_2PWCs would be able to be linked together to form a Mo_2 dimer of dimers which should exhibit greater electron delocalisation through the organic linker compared to their dicarboxylate-linked analogues (Scheme 28).

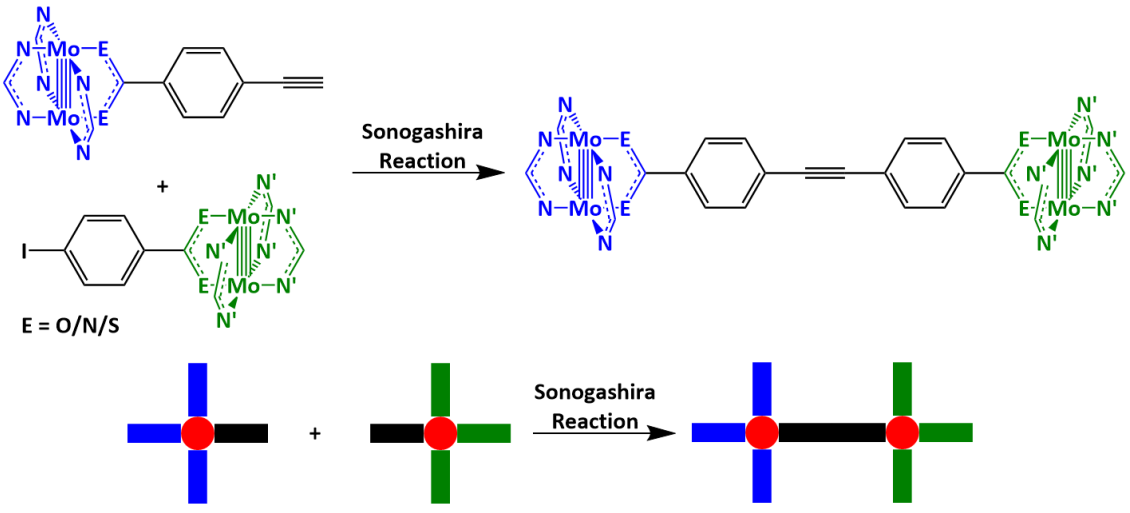

Scheme 28 Sonogashira reaction towards asymmetric Mo_2 dimers of dimers with different coordinating atoms in the organic linker.

One-dimensional molecular assemblies can be expanded to contain more than two Mo_2 cores. By using $Mo_2(TiPB)_4$ as a starting material, it is possible to synthesise a Mo_2PWC containing two of the same carboxylate ligand coordinated to a Mo_2PWC in a *trans*- fashion. Work within the Wilkinson group has successfully synthesised compound **63** (Scheme 29) containing two 4-ethynylbenzoate ligands coordinated to a Mo_2PWC, while being *trans*- to each other. If this compound undergoes the Sonogashira reaction with compounds **59b** and **59b'** and no ligand scrambling takes place, it is postulated that a Mo_2 trimer of dimers will be formed as the product (Scheme 29). With the asymmetry present through the variation of the ancillary ligands, this molecular array is expected to have the properties of a donor-bridge-acceptor system, with an additional redox centre in the middle of the organic bridge.

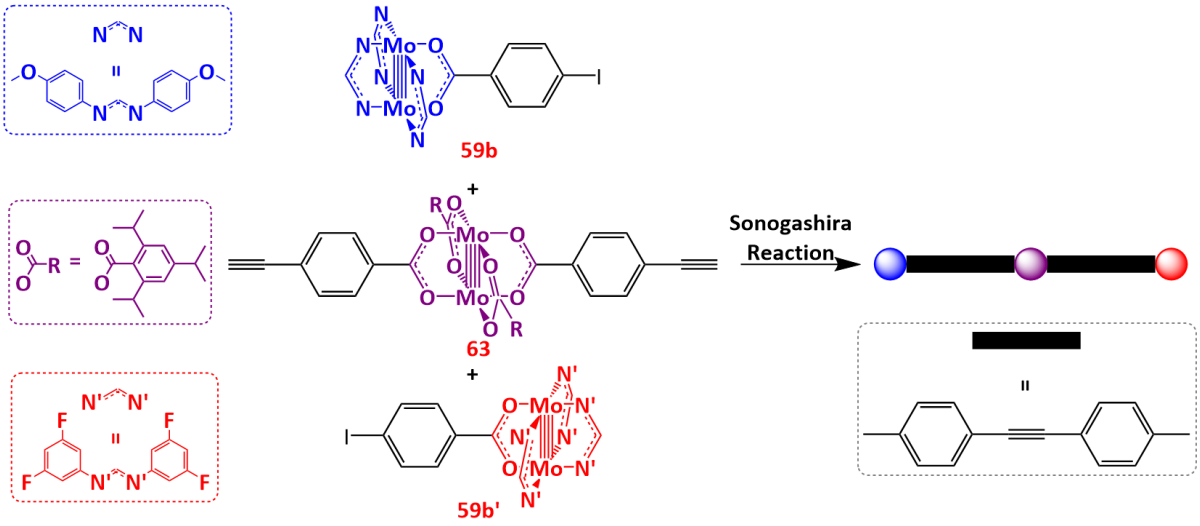

Scheme 29 Sonogashira reaction towards asymmetric Mo_2 trimers of dimers.

The use of reactivity at the periphery of ligands coordinated to Mo_2PWCs should not be limited to one-dimensional molecular arrays. Indeed, the degree of control exhibited by peripheral reactivity allows for a number of possibilities. By using *cis*-$Mo_2(DAniF)_2(OAc)_2$ as a synthon to make two new compounds containing either a terminal alkyne or an iodide within their chelating ligands (Scheme 30, top), it should be possible to employ the Sonogashira reaction to construct a molecular square, with each Mo_2 core serving as the corners within the structural framework (Scheme 30, bottom). If the Sonogashira reaction could successfully be used to synthesise compound **61**, there should not be a limiting factor for constructing molecular squares using two Mo_2PWCs that only vary in the functionality of the carboxylate linkers. As these molecular squares are expected to have a greater hydrodynamic radius relative to compound **61**, it is also more likely that performing size exclusion chromatography for these compounds would be effective at isolating them from other impurities of a smaller size.

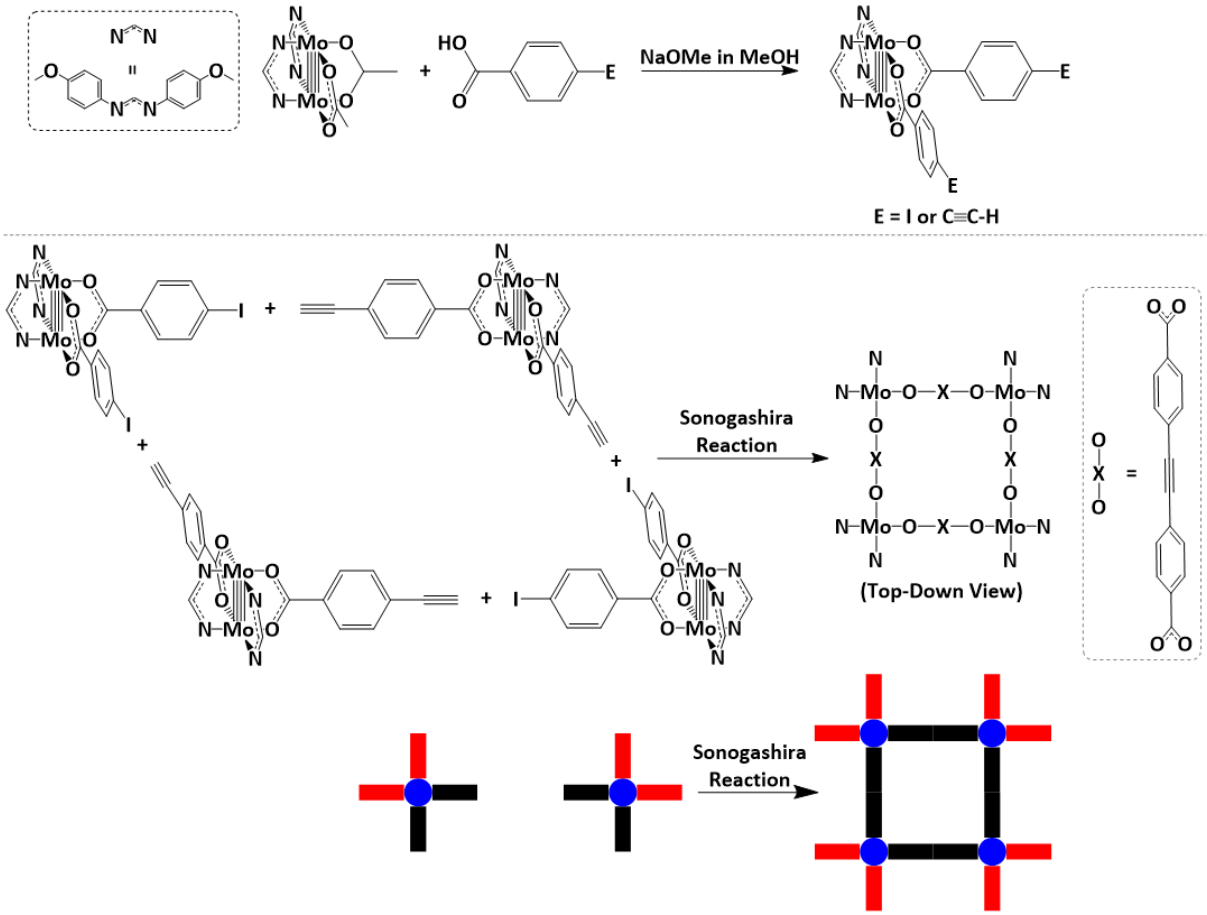

Scheme 30 The Sonogashira reaction at the ligand periphery to construct molecular squares.
Top: Synthesis of starting materials.
Bottom: Sonogashira reaction towards molecular squares.

The above suggestions are only the tip of the iceberg regarding the potential behind directed assembly through the use of reactions at the ligand periphery. The construction of symmetric molecular assemblies should be possible through this methodology without the formation of significant side products but, admittedly, this is also possible through conventional methods based on self-assembly. Introducing asymmetry into these systems is not possible as long as ligand dissociation takes place while the starting materials are in solution. Some potential ways to work around this issue have been presented, with investigations towards their viability being the subject of future work.

Experimental

Justification for Impurities in Elemental Analysis

As discussed in the main text, the synthesis of compound **58** comes with the challenge of preventing the formation of side products such as $Mo_2(DAniF)_2(OAc)_2$ and $Mo_2(DAniF)_4$. In particular, the latter impurity is unreactive under both standard ligand substitution reaction conditions and Sonogashira cross-coupling reaction conditions. As a result, increasing the reaction steps also increases the relative quantity of these impurities, therefore increasing the relative deviation of the experimental CHN elemental analysis data from the calculated values (experimental data for compounds **59a**, **59b**, **59a'** and **59b'** show mild deviations from the calculated values, whereas for compounds **60a**, **60b**, **61** and **62**, the deviations are much more significant).

Materials and Methods

Unless otherwise stated, all reagents were purchased from commercial sources and used without further purification. N,N'-di-(3,5-difluoroanisyl) formamidine was synthesised by MChem student Imogen Squire in a procedure similar to **HDAniF**. Anhydrous THF, DCM and hexane were obtained from an Innovative Technology Inc. PureSolv® solvent purification system. Anhydrous ethanol was dried over magnesium and iodine in a solvent still overnight and distilled. $CDCl_3$ used for NMR analysis was dried over CaH_2 overnight and distilled *via* vacuum transfer on a Schlenk line. For all compounds besides **HDAniF** and **1**, all solvents and reagents were degassed prior to use (either by sparging or by freeze-pump-thaw degassing). ^1H NMR, $^{13}C\{^1H\}$ NMR and ^{19}F NMR spectra were recorded on a JEOL ECX400 or JEOL ECS400 spectrometer, operating at 400 MHz, 100 MHz and 376 MHz respectively. All spectral data were acquired at 298 K. Chemical shifts (δ) are quoted in parts per million (ppm), with the residual solvent peaks; δ_H 7.26 and δ_C 77.16 for $CDCl_3$ being used as a reference. Coupling constants (*J*) are reported in Hertz (Hz) to the nearest 0.5 Hz. The multiplicity abbreviations are: s singlet, d doublet, dd doublet of doublets, t triplet, tt triplet of triplets. Signal assignment was achieved by analysis of COSY, HSQC and HMBC experiments where required. Infrared (IR) spectra were recorded in the solid state on a Shimazdu IRPrestige-21 spectrometer with an Specac ATR Golden Gate stage. Mass-spectra (low and high-resolution) were obtained by the University of York Mass Spectrometry Service, using electrospray ionisation (ESI) on a Bruker Daltonics, Micro-TOF spectrometer or matrix-assisted laser desorption/ionisation (MALDI) on a solariX XR FTMS 9.4T Spectrometer. Electrochemical measurements including cyclic voltammetry and differential pulse voltammetry were collected in solutions of 0.1M n-$Bu_4N(PF_6)$ in dried and deoxygenated DCM under an atmosphere of argon, saturated with the same solvent. Measurements were taken with a platinum working electrode, and Pt wire counter and *pseudo*-reference electrodes. The voltammograms were recorded using a Gamry Reference 3000 potentiostat. Potentials were reported relative to Fc/Fc^+, with decamethyl ferrocene or ferrocene added as an internal reference. UV-Vis spectra were recorded using Jasco V-560 UV/Vis spectrophotometer with a Young's tap adapted quartz cuvette, in dried and deoxygenated THF.

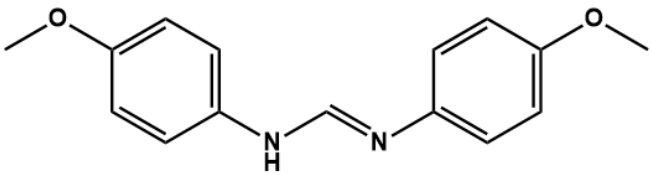

Synthesis of $C_{15}H_{16}N_2O_2$ (HDAniF): *p*-anisidine (10 g, 81.2 mmol) was dissolved in triethyl orthoformate (7 mL, 42 mmol). The solution was set to reflux (140 °C, 18 hrs). Residual ethanol was removed by evaporation (140 °C, 10 mins). The solution was cooled to r.t. to form a light purple solid. The solid was recrystallised from warm toluene and petroleum ether (40-60 °C). Recrystallisation was repeated

until a colourless solid was obtained (4.49 g, 19.453 mmol, 47.9%). **^{1}H NMR** (400 MHz, $CDCl_3$) δ (ppm): 8.02 (1H, s, NC(*H*)N), 7.00 (4H, d, $^3J_{H,H}$ = 6.4 Hz, N-C=C*H*), 6.84 (4H, d, $^3J_{H,H}$ = 8 Hz, O-C=C*H*), 3.78 (6H, s); ***m/z*** (ESI-TOF) Calc. [M^+] $C_{15}H_{16}N_2O_2$ 256.307. Found [M-H^+] 257.13. **Elemental Anal.** Calc. for $C_{15}H_{16}N_2O_2$: C 70.22; H 6.24; N 10.92. Found: C 70.07, H 6.07, N 10.79.

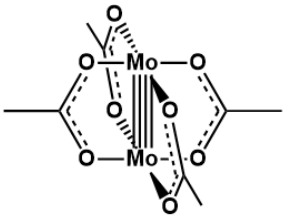

Synthesis of $Mo_2(OAc)_4$ (57): A 2-necked round-bottom flask (RBF) equipped with an air-condenser was placed under an inert atmosphere. To the RBF, acetic acid (80 mL) and acetic anhydride (20 mL) were added. The liquid mixture was sparged with N_2 (10 mins) and was stirred under inert conditions at reflux (120 °C) for 1 hr. The flask was then allowed to cool to r.t.. Molybdenum hexacarbonyl (5.013 g, 19.0 mmol) was added. The colour of the mixture turned gradually from colourless, to yellow, to almost black. The solution was left to reflux overnight (120 °C, 18 hrs) under N_2. The reaction was allowed to cool to r.t. without stirring and left to stand until crystals were clearly visible. The solid was filtered in air and washed with ethanol (2×20 mL) and diethyl ether (20 mL) to give yellow crystals of $Mo_2(OAc)_4$ (1.133 g, 2.6 mmol, 27.9%). **Elemental Anal.** Calc. for $C_8H_{12}O_8Mo_2$: C 22.44; H 2.82; N 0. Found: C 22.40, H 2.71, N 0; **FT-ATR** $\nu_{max.}$ (neat) 1491, 1436, 1405, 1352, 1042, 1031, 934, 673, 628.

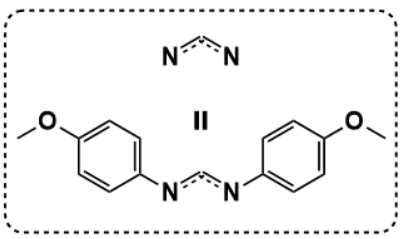

***Cis*- to carboxylate**

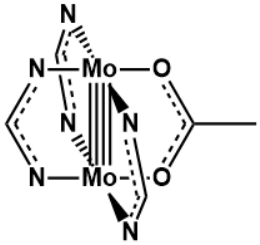

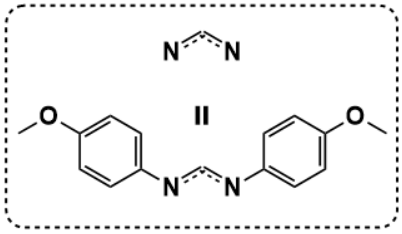

***Trans*- to carboxylate**

Synthesis of $Mo_2C_{47}H_{48}N_6O_8$ (58): Under inert conditions, to a suspension of $Mo_2(OAc)_4$ (**57**) (0.4997 g, 1.17 mmol) and N,N'-di-p-anisyl-formamidine (0.8984 g, 3.51 mmol) in THF (20 mL), a solution of sodium methoxide in methanol (0.5 M, 7 mL) was added. The resulting solution turned red and, progressively, dark brown. The solution was stirred overnight (r.t., 18 hrs) under N_2. A yellow precipitate formed in a dark-brown solution. The solvent was removed *in vacuo* and the remaining solid washed with ethanol (2×22 mL) and hexane (10 mL), maintaining inert conditions. Trace amounts of solvent were removed *in vacuo*. The crude yellow fine solid was retrieved (0.9403 g, 0.92 mmol, 79.18%); **^{1}H NMR** (400 MHz, $CDCl_3$) δ (ppm): 8.44 (1H, s, NC(*H*)N), 8.37 (1H, s, NC(*H*)N), 6.62 (2H, d, $^3J_{H,H}$ 9 Hz, N-C=C-*H*), 6.50 (2H, d, $^3J_{H,H}$ = 9 Hz, O-C=C-*H*), 6.42 (2H, d, $^3J_{H,H}$ = 9 Hz, N-C=C-*H*), 6.20 (2H, d, $^3J_{H,H}$ = 9 Hz, O-C=C-*H*), 3.71 (6H, s, C=C-O-CH_3), 3.64 (6H, s, C=C-O-CH_3), 2.59 (3H, s, O_2C-CH_3); **^{13}C{^{1}H} NMR** (100 MHz; $CDCl_3$) δ_C (ppm): 179.2 (*C*O_2), 155.9 (N-*C*(H)-N), 154.9 (N-*C*(H)-N), 143.3 (C=*C*-N), 143.0 (C=*C*-N), 123 (O-C=*C*H), 122.7 (O-C=*C*H), 114.6 (N-C=*C*H), 114.3 (N-C=*C*-H), 55.8 (*C*H_3), 25.7 (O*C*H_3), 23.9 (O*C*H_3); ***m/z*** (MALDI TOF) Calc. [M^+] $Mo_2C_{47}H_{48}N_6O_8$ 1016.8. Found [M-H^+] 1017.2; **Elemental Anal.** Calc for $C_8H_{12}O_8Mo_2$: C 55.63; H 5.07; N 8.43. Found: C 55.47, H 4.76, N 8.27.

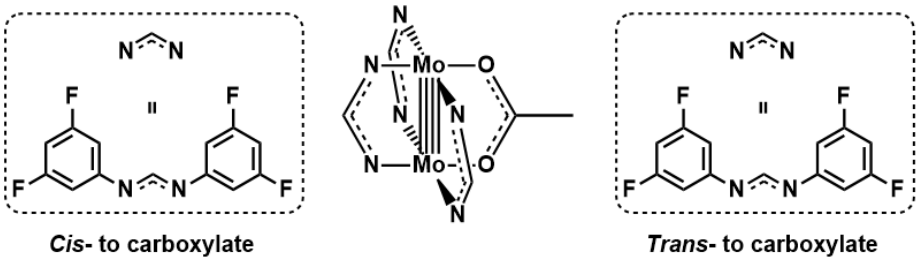

Synthesis of $Mo_2C_{47}H_{48}N_6O_8$ (58'): Under inert conditions, to a suspension of $Mo_2(OAc)_4$ (**57**) (0.4997 g, 1.17 mmol) and N,N'-di-(3,5-difluoroanisyl) formamidine (0.8984 g, 3.51 mmol) in THF (20 mL), a solution of sodium methoxide in methanol (0.5 M, 7 mL) was added. The resulting solution turned orange and, progressively, light brown. The solution was stirred overnight (r.t., 18 hrs) under N_2. A yellow precipitate formed in a brown solution. The solvent was removed *in vacuo* and the remaining solid washed with ethanol (2×22 mL) and hexane (10 mL), maintaining inert conditions. Trace amounts of solvent were removed *in vacuo*. The crude yellow fine solid was retrieved (0.8080g, 0.767 mmol, 65.7%); **^{1}H NMR** (400 MHz, $CDCl_3$) δ (ppm) 8.47 (1 H, s, NC(*H*)N), 8.42 (2H, s, NC(*H*)N), 6.50 (4H, tt, $^4J_{H,H}$ = 2 Hz, $^3J_{H,F}$ = 9 Hz, FC=C(*H*)-CF), 6.36 (2H, tt, $^4J_{H,H}$ = 2 Hz, $^3J_{H,F}$ = 9 Hz, FC=C(*H*)-CF), 6.16 (8H, dd, $^4J_{H,H}$ = 2 Hz, $^3J_{H,F}$ = 9 Hz, N-C=C-*H*), 5.69 (4H, dd, $^3J_{H,F}$ = 9 Hz, N-C=C-*H*), 2.72 (3H, s, O*CH*$_3$); **^{13}C{^{1}H} NMR** (100 MHz; $(CD_3)_2CO$) δ (ppm) 205.3 (*C*O_2), 181.5 (O-*C*H_3) 162.2 (CF), 160 (N*C*(H)N), 158.9 (N*C*(H)N), 152.4 (C=*C*-N), 106.1 (*C*=C-N), 105.9 (*C*=C-N), 99.3 (FC=*C*(H)-CF), 98.9 (FC=*C*(H)-CF), 22.9 (O*C*H$_3$); **^{19}F NMR** (376 MHz, $(CD_3)_2CO$) δ (ppm) -107.8 (t, ^3J = 8 Hz), -108.2 (t, ^3J = 9 Hz); ***m/z*** (MALDI TOF) Calc. [M^+] $Mo_2C_{47}H_{48}N_6O_8$ 1052.57. Found [M-H^+] 1053; **Elemental Anal.** Calc. for $Mo_2C_{47}H_{48}N_6O_8$: C 46.79; H 2.3; N 7.98. Found: C 47.44; H 1.88; N 7.4; **FT-ATR** $\nu_{max.}$ (neat) 1619, 1591, 1540, 1479, 1458, 1438, 1317, 1156, 1136, 1120, 1036, 991, 952, 844, 775, 679, 614.

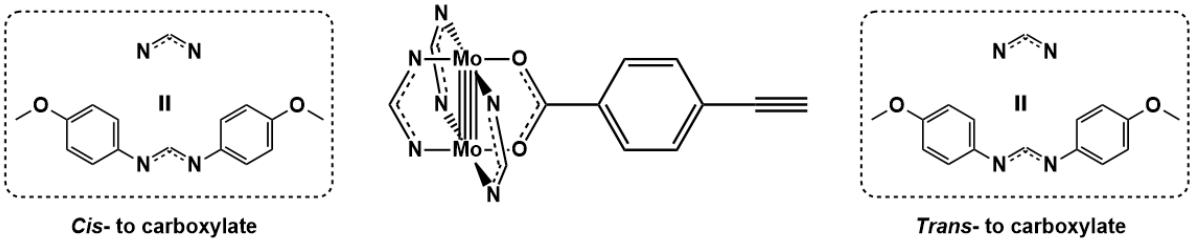

Synthesis of $Mo_2C_{54}H_{50}N_6O_8$ (59a): 4-ethynylbenzoic acid (0.3235 g, 2.2 mmol) was added to a Schlenk flask and dried *in vacuo*. Under inert conditions, Mo(DAniF)$_3$(OAc) (**58**) (0.4500 g, 0.44 mmol) was added to the Schlenk flask. THF (20 mL) was added to the solid mixture before adding sodium methoxide in methanol (0.5 M, 4.2 mL). The solution was stirred (r.t., 18 hrs). THF was removed *in vacuo*. The resulting red solid was filtered under inert conditions and washed with ethanol (2×20 mL,) and hexane (10 mL,). The resulting red solid was dried *in vacuo* and obtained (0.2610 g, 53.5%); **^{1}H NMR** (400 MHz, $CDCl_3$) δ (ppm) 8.46 (1H, s, N-C(*H*)-N), 8.37 (2H, s, N-C(*H*)-N), 8.23 (1H, d, $^3J_{H,H}$ = 9 Hz, O_2C=C*H*), 7.55 (2H, d, $^3J_{H,H}$ = 8 Hz, HC≡C-C=C*H*), 6.64 (8H, d, $^3J_{H,H}$ = 9 Hz, N-C=C*H*), 6.54 (8H, d, $^3J_{H,H}$ = 9 Hz, N-C=C*H*), 6.45 (4H, d, $^3J_{H,H}$ = 9 Hz, O-C=C*H*), 6.24 (2H, d, $^3J_{H,H}$ = 9 Hz, O-C=C*H*), 3.71 (6H, s, O*CH*$_3$), 3.65 (3H, s, O*CH*$_3$), 3.17 (1H, s, C≡C-*H*); **^{13}C{^{1}H} NMR** (100 MHz; $CDCl_3$) δ (ppm): 172.2 (O_2C), 156.5 (N-C(*H*)-N), 156 (N-C(*H*)-N), 132.8 (C≡C-*C*=CH), 131.9 (HC≡C-*C*H), 130.3 (O_2C-C=*C*H), 124.44 (HC≡*C*-C=*C*H), 123 (O-C=*C*H), 122.9 (O-C=*C*H), 114.5 (N-C=*C*H), 114.4 (N-C=*C*H), 83.3 (HC≡*C*-C*)* 55.8 (O*C*H$_3$); ***m/z*** (MALDI TOF) Calc. [M^+] $Mo_2C_{54}H_{50}N_6O_8$ 1102.89. Found [M-H^+] 1103.17; **Elemental Anal.** Calc. for $C_8H_{12}O_8Mo_2$: C 58.81; H 4.57; N 7.62. Found: C 58.49, H 4.62, N 8.32; **FT-ATR** $\nu_{max.}$ (neat) 1585, 1538, 1503, 1428, 1391, 1303, 1242, 1217, 1207, 1181, 1171, 1105, 1040, 850, 828, 787, 765, 695, 646, 618.

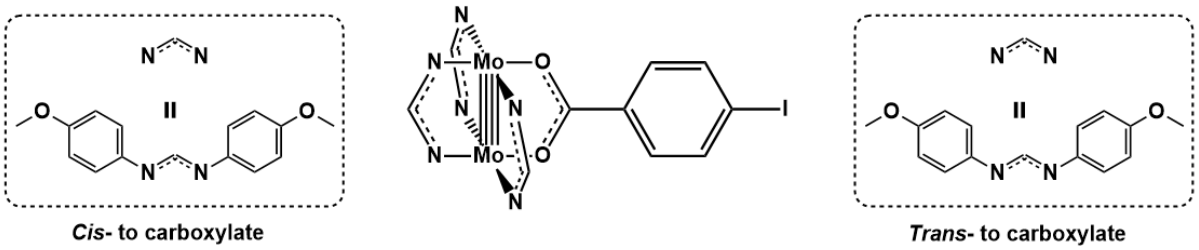

Synthesis of $Mo_2C_{52}H_{49}N_6O_8I$ (59b): 4-iodobenzoic acid (0.2192 g, 0.88 mmol) was added to a Schlenk flask which was then evacuated. Under inert conditions, $Mo(DAniF)_3(OAc)$ (**58**) (0.3652 g, 0.37 mmol) was added to the Schlenk flask. THF (35 mL) was added to the solid mixture before adding sodium methoxide in methanol (0.5 M, 1.8 mL). The solution was stirred (60 °C, 18 hrs). THF was removed *in vacuo*. The resulting red solid was washed with ethanol (2×20 mL) and hexane (10 mL). The resulting orange solid was dried *in vacuo* and obtained (0.2693 g, 62.2%) **^{1}H NMR** (400 MHz, $CDCl_3$) δ (ppm): 8.46 (1H, s, N-C(*H*)-N), 8.36 (1H, s, N-C(*H*)-N), 7.99 (2H, d, $^3J_{H,H}$ = 8 Hz, I-C=C*H*), 7.79 (2H, d, $^3J_{H,H}$ = 8 Hz, O_2C-C=C*H*), 6.63 (2H, d, $^3J_{H,H}$ = 9 Hz, N-C=C*H*), 6.53 (2H, d, $^3J_{H,H}$ = 9 Hz, O-C=C*H*), 6.44 (2H, d, $^3J_{H,H}$ = 9 Hz, N-C=C*H*), 6.23 (2H, d, $^3J_{H,H}$ = 9 Hz, O-C=C*H*), 3.71 (6H, s, OCH_3) 3.65 (3H, s, OCH_3); **^{13}C{^{1}H} NMR** (100 MHz; $CDCl_3$) δ (ppm): 173.3 (*C*O_2), 156.5 (N-*C*(H)-N), 155.1 (N-*C*(H)-N), 143.3 (N-*C*=CH), 142.9 (N-*C*=CH), 137.3 (I-C=*C*H), 132 (O_2C-C=*C*H), 123 (O-C=*C*H), 122.9 (O-C=*C*H), 114.5 (N-C=*C*H), 114.4 (N-C=*C*H), 98.2 (I*C*=C), 55.8 (O*C*H_3); ***m/z*** (MALDI TOF) Calc. [M^+] $Mo_2C_{52}H_{49}N_6O_8I$ 1204.76. Found [M-H^+] 1205.07; **Elemental Anal.** Calc for $C_8H_{12}O_8Mo_2$: C 51.84; H 4.1; N 6.98. Found: C 49.15, H 3.65, N 7.89; **FT-ATR** $\nu_{max.}$ (neat) 1534, 1503, 1460, 1437, 1397, 1305, 1244, 1220, 1207, 1180, 1169, 1040, 820, 818, 763.

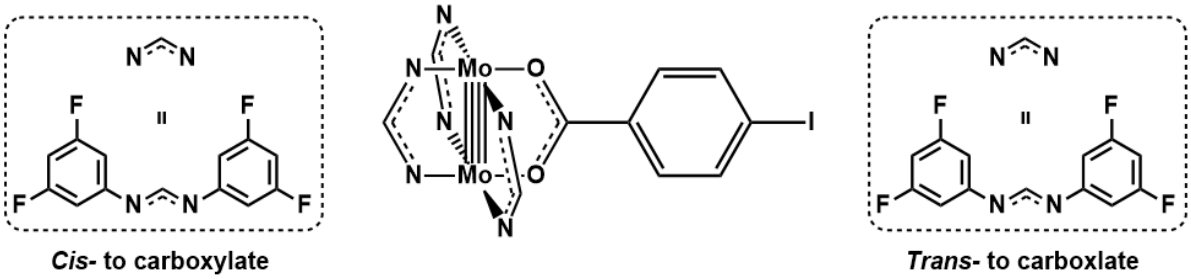

Synthesis of $Mo_2C_{46}H_{25}N_6O_2F_{12}I$ (59'b): 4-iodobenzoic acid (0.4122 g, 1.662 mmol) was added to a Schlenk flask which was then evacuated. Under inert conditions, $Mo(DFArF)_3(OAc)$ (**58'**) (0.3496 g, 0.3321 mmol) was added to the Schlenk flask. THF (22 mL) was added to the solid mixture before adding sodium methoxide in methanol (0.5 M, 1.8 mL). The solution was stirred (3 hrs). THF was removed *in vacuo*. The resulting yellow solid was dissolved in DCM until filtration *via* cannula was possible. The contents were filtered, leaving behind a white solid. The filtrate was collected and the solvent was removed *in vacuo*. The resulting yellow solid was obtained (0.2402 g, 0.1936 mmol, 58.2%) **^{1}H NMR** (400 MHz, $CDCl_3$) δ (ppm): 8.49 (1H, s, N-C(*H*)-N), 8.43 (1H, s, N-C(*H*)-N) 8.06 (2H, d, $^3J_{H,H}$ = 6.72 Hz, I-C=C*H*), 7.89 (2H, d, $^3J_{H,H}$ = 6.72 Hz, O_2C-C-C*H*), 6.52 (8H, tt, $^4J_{H,H}$ 2 Hz, $^3J_{H,F}$ = 9 Hz, FC=C(*H*)-CF), 6.39 (4H, tt, $^4J_{H,H}$ = 2 Hz, $^3J_{H,F}$ = 9 Hz, FC=C(*H*)-CF), 6.19 (16H, dd, $^4J_{H,H}$ = 2 Hz, $^3J_{H,F}$ = 9 Hz, N-C=C-*H*), 5.73 (8H, dd, $^3J_{H,F}$ = 8 Hz, N-C=C-*H*); **^{19}F NMR** (376 MHz, $CDCl_3$) δ (ppm) -107.7 (t, ^3J = 8 Hz), -108.0 (t, ^3J = 8 Hz); ***m/z*** (MALDI TOF) Calc. [M^+] $Mo_2C_{46}H_{25}N_6O_2F_{12}I$ 1240.49. Found [M-H^+] 1240.93; **FT-ATR** $\nu_{max.}$ (neat) 1619, 1591, 1538, 1464, 1417, 1397, 1319, 1291, 1140, 1124, 1120, 1036, 1007, 991, 842, 765, 681, 673.

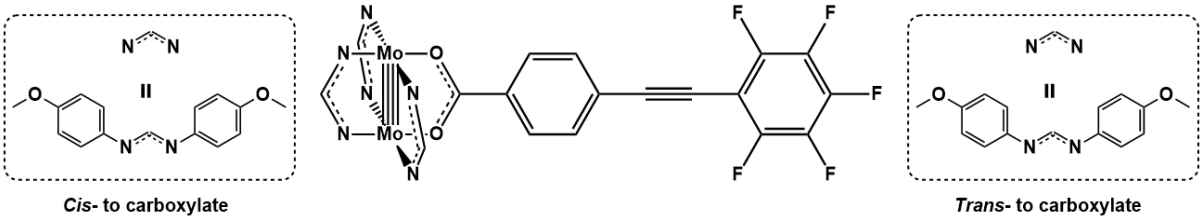

Synthesis of $Mo_2C_{60}H_{49}N_6O_8F_5$ (60a): Pentafluoroiodobenzene (0.12 mL, 0.7858 mmol) was added to an air-free Schlenk flask [1] with triethylamine (dried/degassed, 5 mL). The flask was sparged for 10 mins. $Pd(PPh_3)_2Cl_2$ (0.0127 g, 0.018 mmol), CuI (0.0109 g, 0.057 mmol) were added to a Schlenk flask [2] and dried *in vacuo*. Under inert conditions, tris-(di-p-anisylformamidine) dimolybdenum mono-4-ethynylbenzoate (**59a**) (0.2001 g, 0.181 mmol) was added to Schlenk flask [2]. Schlenk flask [2] was charged with THF (10 mL, dried/degassed). The contents in Schlenk flask [1] were transferred to Schlenk flask [2] dropwise. The resulting solution was stirred (r.t., 18 hrs). The solution was filtered through celite. The filtrate was recovered, the solvent was removed *in vacuo* and the solid residue was washed with ethanol (3×20 mL). A dark red solid was dried *in vacuo* and obtained (0.052 g, 22.6%); **^{1}H NMR** (400 MHz, $CDCl_3$) δ (ppm): 8.46 (1H, s, N-C(*H*)-N), 8.37 (2H, s, N-C(*H*)-N), 8.25 (2H, d, $^3J_{H,H}$ = 8 Hz, O_2C-C=C*H*), 7.60 (2H, d, $^3J_{H,H}$ = 8 Hz, C≡C-C=C*H*), 6.64 (4H, d, $^3J_{H,H}$ = 9 Hz, N-C=C*H*), 6.55 (4H, d, $^3J_{H,H}$ = 9 Hz, O-C=C*H*), 6.45 (4H, d, $^3J_{H,H}$ = 9 Hz, N-C=C*H*), 6.24 (2H, d, $^3J_{H,H}$ = 9 Hz), 3.72 (12H, s, OCH_3), 3.66 (6H, s); **^{19}F NMR** (376 MHz, $CDCl_3$) δ (ppm) -135.6 (dd, ^3J = 21 Hz, ^4J = 7 Hz), -152.3 (t, ^3J = 20 Hz), -161.6 (dt, ^3J = 21 Hz, ^4J = 7 Hz); ***m/z*** (MALDI TOF) Calc. [M^+] $Mo_2C_{60}H_{49}N_6O_8F_5$ 1268.94. Found [M-H^+] 1269.16; **Elemental Anal.** Calc. for $C_8H_{12}O_8Mo_2$: C 56.79; H 3.89; N 6.62. Found: C 52.06, H 2.37, N 4.33.; **FT-ATR** $\nu_{max.}$ (neat) 1599, 1583, 1536, 1499, 1460, 1419, 1399, 1313, 1287, 1246, 1217, 1175, 1107, 1032, 938, 844, 830, 785, 765, 689, 655.

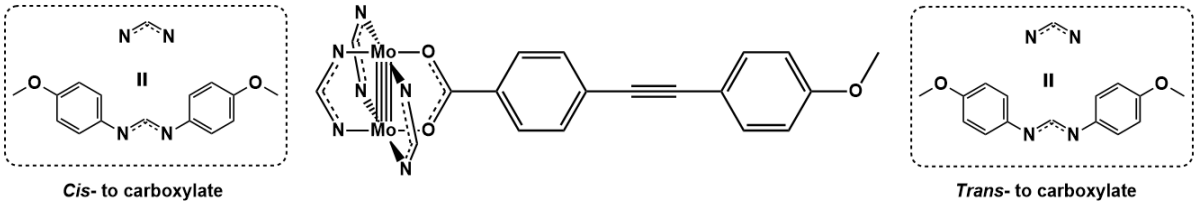

Synthesis of $Mo_2C_{61}H_{56}N_6O_8$ (60b): 4-ethynylanisole (0.35 mL, 2.6 mmol) was added to a Schlenk flask [1] with THF (dried/degassed, 5 mL). The flask was sparged for 1 hr. $Pd(PPh_3)_2Cl_2$ (0.0057 g, 0.0081 mmol), CuI (0.005 g, 0.0623 mmol) were added to a Schlenk flask [2] and dried *in vacuo*. Under inert conditions, tris-(di-p-anisylformamidine) dimolybdenum mono-4-iodobenzoate (**59b**) (0.1 g, 0.0832 mmol) was added to Schlenk flask [2]. Schlenk flask [2] was charged with triethylamine (5 mL, dried/degassed). The contents in Schlenk flask [1] were transferred to Schlenk flask [2] dropwise. The resulting solution was stirred (r.t., 18 hrs). The solution was filtered through celite. The filtrate was recovered, the solvent was removed *in vacuo* and the solid residue was washed with hexane (2×10 mL) and ethanol (3×10 mL). A solid was dried *in vacuo* and obtained (weight not recorded); **^{1}H NMR** (400 MHz, $CDCl_3$) δ (ppm): 8.46 (1H, s, N-C(*H*)-N), 8.38 (2H, s, N-C(*H*)-N), 8.25 (2H, d, $^3J_{H,H}$ = 9 Hz, O_2C-C=C*H*), 7.57 (2H, d, $^3J_{H,H}$ = 9 Hz, C≡C-C=C*H*), 7.49 (2H, d, $^3J_{H,H}$ = 9 Hz, C≡C-C=C*H*), 6.88 (2H, d, $^3J_{H,H}$ = 9 Hz, H_3CO-C=C*H*), 6.64 (8H, d, $^3J_{H,H}$ = 9 Hz, N-C=C*H*), 6.55 (8H, d, $^3J_{H,H}$ = 9 Hz, O-C=C*H*), 6.45 (4H, d, $^3J_{H,H}$ = 9 Hz, N-C=C*H*), 6.24 (4H, d, $^3J_{H,H}$ = 9 Hz, O-C=C*H*), 3.82 (3H, s, OCH_3), 3.72 (12H, s, OCH_3), 3.66 (6H, s, OCH_3); **^{13}C{^{1}H} NMR** (100 MHz, $CDCl_3$) δ (ppm) 172.6 (O_2*C*), 159.7 (156.5 (N-*C*(H)-N), 155.1 (N-*C*(H)-N), 143.4 (N-*C*=CH), 143 (N-*C*=CH), 133.3 (C≡C-C=*C*H), 132 (C≡*C*), 131.2 (C≡C-C=*C*H), 130.3 (O_2C-C=*C*H), 123 (O-C=*C*H), 122.9 (O-C=*C*H), 114.5 (N-C=*C*H), 114.4 (N-C=*C*H), 91.5 (*C*≡C), 88.2 (C≡*C*), 55.6 (O*C*H_3), 55.4 (O*C*H_3). ***m/z*** (MALDI TOF) Calc. [M^+] $Mo_2C_{61}H_{56}N_6O_8$ 1209.04. Found [M-H^+] 1209.22; **Elemental Anal.**

Calc. for $Mo_2C_{61}H_{56}N_6O_8$: C 60.6; H 4.7; N 6.9. Found: C 69.02, H 5.44, N 2.7; **FT-ATR** $\nu_{max.}$ (neat) 1644, 1607, 1538, 1499, 1462, 1440, 1395, 1311, 1289, 1242, 1213, 1177, 1107, 1032, 938, 826, 801, 765, 695, 589.

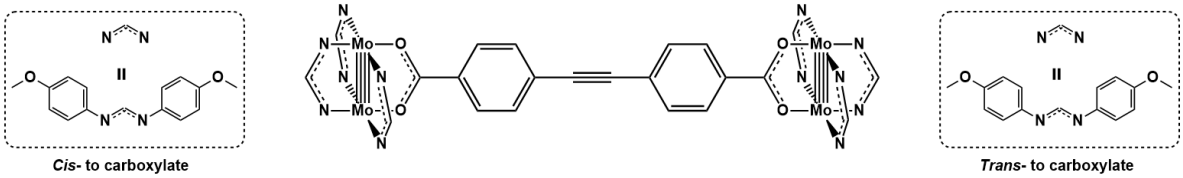

Synthesis of $Mo_4C_{106}H_{98}N_{12}O_{16}$ (61): bis(triphenylphosphine)palladium (II) dichloride (0.0058 g, 0.0083 mmol) and CuI (0.0047 g, 0.0249 mmol) were added to an oven-dried Schlenk flask. The headspace was evacuated and tris-(di-p-anisylformamidine) dimolybdenum mono-4-ethynylbenzoate (**59a**) (0.0915 g, 0.0830 mmol) and tris-(di-p-anisylformamidine) dimolybdenum mono-4-iodobenzoate (**59b**) (0.1001 g, 0.0830 mmol) were added to the flask. The contents were dissolved in THF (10 mL) and the resulting solution charged with triethylamine (5 mL) slowly while stirring. The reaction mixture was stirred (r.t., 16 hrs). The solvent was removed *in vacuo* and the resulting solid was washed with ethanol (2×10 mL) and hexane (10 mL). The washed solid was dried *in vacuo* and obtained (0.0807 g, 0.037 mmol, 44.6%); **^{1}H NMR** (400 MHz, $CDCl_3$) δ (ppm): 8.46 (1H, s, N-C(*H*)-N), 8.37 (1H, s, N-C(*H*)-N), 8.27 (4H, d, $^3J_{H,H}$ = 7 Hz, O_2C-C=C*H*), 7.61 (4H, d, $^3J_{H,H}$ = 7 Hz, C≡C-C=C*H*), 6.64 (8H, d, $^3J_{H,H}$ = 7 Hz, N-C=C*H*), 6.54 (8H, d, $^3J_{H,H}$ = 7 Hz, N-C=C*H*), 6.45 (4H, d, $^3J_{H,H}$ = 7 Hz, O-C=C*H*), 6.24 (4H, d, $^3J_{H,H}$ = 7 Hz, O-C=C*H*), 3.71 (6H, s, OCH_3); **^{13}C{^{1}H} NMR** (100 MHz, $CDCl_3$) δ (ppm) 156.4 (N-*C*(H)-N), 155.1 (N-*C*(H)-N), 143.4 (N-*C*=CH), 143 (N-*C*=CH), 132.1 (C≡C-*C*=CH), 131 (C≡C-C=*C*H), 130.1 (C≡C-C=*C*H), 123 (O-C=*C*H), 122.9 (O-C=*C*H), 114.6 (N-C=*C*H), 114.4 (N-C=*C*H), 91.3 (C≡*C*), 55.6 (CH_3). ***m/z*** (MALDI TOF) Calc. [M^+] $Mo_4C_{106}H_{98}N_{12}O_{16}$ 2179.74. Found [M-H^+] 2181.37; **Elemental Anal.** Calc. for $Mo_4C_{106}H_{98}N_{12}O_{16}$: C 58.41; H 4.53; N 7.71. Found: C 53.61, H 3.88, N 4.98; **FT-ATR** $\nu_{max.}$ (neat) 1583, 1538, 1501, 1462, 1430, 1419, 1397, 1311, 1289, 1242, 1213, 1175, 1032, 824, 783, 767, 697, 644, 589.

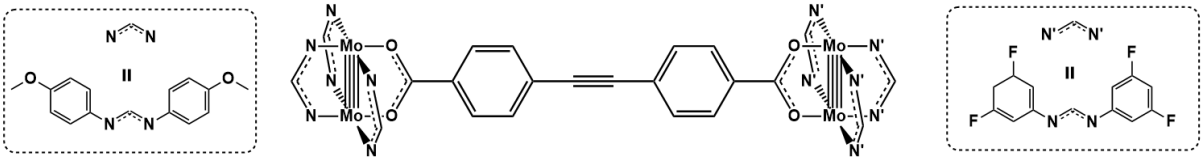

Synthesis of $Mo_4C_{100}H_{74}N_{12}O_{10}F_{12}$ (62): bis(triphenylphosphine)palladium (II) dichloride (0.0058 g, 0.0083 mmol) and CuI (0.0047 g, 0.0249 mmol) were added to an oven-dried Schlenk flask. The headspace was evacuated and tris-(di-p-anisylformamidine) dimolybdenum mono-4-ethynylbenzoate (**59a**) (0.0883 g, 0.0800 mmol) and tris-(N,N'-di-(3,5-difluoroanisyl)) dimolybdenum mono-4-iodobenzoate (**59'b)** (0.1000 g, 0.0806 mmol) were added to the flask. The contents were dissolved in THF (10 mL) and the resulting solution charged with triethylamine (5 mL) slowly while stirring. The reaction mixture was stirred (r.t., 16 hrs). The solvent was removed *in vacuo* and the resulting solid was washed with ethanol (2×10 mL) and hexane (10 mL). The washed solid was dried *in vacuo* and obtained (weight not recorded); ***m/z*** (MALDI TOF) Calc. [M^+] $Mo_4C_{100}H_{74}N_{12}O_{10}F_{12}$ 2215.47. Found [M-H^+] 2216.33; **FT-ATR** $\nu_{max.}$ (neat) 1583, 1540, 1503, 1415, 1317, 1291, 1246, 1215, 1120, 1036, 991, 857, 842, 822, 779, 697, 679**.**

References

1 J. W. Steed and J. L. Atwood, *Supramolecular Chemistry*, John Wiley & Sons, 2022.

2 D. M. D'Alessandro, B. Smit and J. R. Long, Angew. Chem. Int. Ed., 2010, **49**, 6058–6082.

3 R. Sathre and E. Masanet, *RSC Adv.*, 2013, **3**, 4964–4975.

4 M. J. Webber and R. Langer, *Chem. Soc. Rev.*, 2017, **46**, 6600–6620.

5 J. Zhou, G. Yu and F. Huang, *Chem. Soc. Rev.*, 2017, **46**, 7021–7053.

6 B. Li, H.-M. Wen, Y. Cui, W. Zhou, G. Qian and B. Chen, Adv. Mater., 2016, **28**, 8819–8860.

7 H. Li, L. Li, R.-B. Lin, W. Zhou, Z. Zhang, S. Xiang and B. Chen, *EnergyChem*, 2019, **1**, 100006.

8 A. Bavykina, N. Kolobov, I. S. Khan, J. A. Bau, A. Ramirez and J. Gascon, *Chem. Rev.*, 2020, **120**, 8468–8535.

9 D. Feng, Z.-Y. Gu, Y.-P. Chen, J. Park, Z. Wei, Y. Sun, M. Bosch, S. Yuan and H.-C. Zhou, *J. Am. Chem. Soc.*, 2014, **136**, 17714–17717.

10 J. M. Roberts, B. M. Fini, A. A. Sarjeant, O. K. Farha, J. T. Hupp and K. A. Scheidt, *J. Am. Chem. Soc.*, 2012, **134**, 3334–3337.

11 L. S. Xie, G. Skorupskii and M. Dincă, *Chem. Rev.*, 2020, **120**, 8536–8580.

12 L. Sun, T. Miyakai, S. Seki and M. Dincă, *J. Am. Chem. Soc.*, 2013, **135**, 8185–8188.

13 R. Rajak, R. Kumar, S. N. Ansari, M. Saraf and S. M. Mobin, *Dalton Trans.*, 2020, **49**, 11792–11818.

14 F. Kaiser, A. Schmidt, W. Heydenreuter, P. J. Altmann, A. Casini, S. A. Sieber and F. E. Kühn, Eur. J. Inorg. Chem., 2016, **2016**, 5189–5196.

15 M. Yoshizawa, M. Tamura and M. Fujita, *Science*, 2006, **312**, 251–254.

16 J. Kang and J. Rebek, *Nature*, 1997, **385**, 50–52.

17 C. J. Hastings, M. D. Pluth, R. G. Bergman and K. N. Raymond, *J. Am. Chem. Soc.*, 2010, **132**, 6938–6940.

18 M. D. Pluth, R. G. Bergman and K. N. Raymond, *Science*, 2007, **316**, 85–88.

19 The Nobel Prize in Physics 2010, https://www.nobelprize.org/prizes/physics/2010/summary/, (accessed 1 April 2023).

20 J. Nicks, K. Sasitharan, R. R. R. Prasad, D. J. Ashworth and J. A. Foster, Adv. Funct. Mater., 2021, **31**, 2103723.

21 A. Dhakshinamoorthy, A. M. Asiri and H. Garcia, Adv. Mater., 2019, **31**, 1900617.

22 C. Shahar, J. Baram, Y. Tidhar, H. Weissman, S. R. Cohen, I. Pinkas and B. Rybtchinski, *ACS Nano*, 2013, **7**, 3547–3556.

23 C.-F. Lee, D. A. Leigh, R. G. Pritchard, D. Schultz, S. J. Teat, G. A. Timco and R. E. P. Winpenny, *Nature*, 2009, **458**, 314–318.

24 P. L. Anelli, N. Spencer and J. F. Stoddart, *J. Am. Chem. Soc.*, 1991, **113**, 5131–5133.

25 T. Takata, *BCSJ*, 2019, **92**, 409–426.

26 S. J. Loeb, *Chem. Soc. Rev.*, 2007, **36**, 226–235.

27 T. R. Cook and P. J. Stang, *Chem. Rev.*, 2015, **115**, 7001–7045.

28 F. A. Pereira, T. Fallows, M. Frank, A. Chen and G. H. Clever, Z. Anorg. Allg Chem., 2013, **639**, 1598–1605.

29 A. Schmidt, M. Hollering, J. Han, A. Casini and F. E. Kühn, *Dalton Trans.*, 2016, **45**, 12297–12300.

30 R. A. S. Vasdev, J. A. Findlay, A. L. Garden and J. D. Crowley, *Chem. Commun.*, 2019, **55**, 7506–7509.

31 S. K. Yang and S. C. Zimmerman, Isr. J. Chem., 2013, **53**, 511–520.

32 R. P. Sijbesma, F. H. Beijer, L. Brunsveld, B. J. B. Folmer, J. H. K. K. Hirschberg, R. F. M. Lange, J. K. L. Lowe and E. W. Meijer, *Science*, 1997, **278**, 1601–1604.

33 G.-L. Li, Z. Zhuo, B. Wang, X.-L. Cao, H.-F. Su, W. Wang, Y.-G. Huang and M. Hong, *J. Am. Chem. Soc.*, 2021, **143**, 10920–10929.

34 V. Santolini, M. Miklitz, E. Berardo and K. E. Jelfs, *Nanoscale*, 2017, **9**, 5280–5298.

35 R.-J. Li, A. Tarzia, V. Posligua, K. E. Jelfs, N. Sanchez, A. Marcus, A. Baksi, G. H. Clever, F. Fadaei-Tirani and K. Severin, *Chem. Sci.*, 2022, **13**, 11912–11917.

36 S. K. Yee, J. Sun, P. Darancet, T. D. Tilley, A. Majumdar, J. B. Neaton and R. A. Segalman, *ACS Nano*, 2011, **5**, 9256–9263.

37 C. A. Bignozzi, R. Argazzi, R. Boaretto, E. Busatto, S. Carli, F. Ronconi and S. Caramori, Coord. Chem. Rev., 2013, **257**, 1472–1492.

38 C.-W. Lee, H.-P. Lu, C.-M. Lan, Y.-L. Huang, Y.-R. Liang, W.-N. Yen, Y.-C. Liu, Y.-S. Lin, E. W.-G. Diau and C.-Y. Yeh, Chem. Eur. J., 2009, **15**, 1403–1412.

39 M. Meng, Z. Tang, S. Mallick, M. H. Luo, Z. Tan, J. Liu, J. Shi, Y. Yang, C. Y. Liu and W. Hong, *Nanoscale*, 2020, **12**, 10320–10327.

40 F. J. Claire, M. A. Solomos, J. Kim, G. Wang, M. A. Siegler, M. F. Crommie and T. J. Kempa, *Nat. Commun.*, 2020, **11**, 5524.

41 F. A. Cotton, C. A. Murillo and R. A. Walton, *Multiple bonds between metal atoms [electronic resource] / edited by F. Albert Cotton, Carlos A. Murillo, Richard A. Walton.*, Springer Science and Business Media, New York, NY, 3rd ed., 2005.

42 F. A. Cotton and C. B. Harris, Inorg. Chem., 1965, **4**, 330–333.

43 R. Hrdina, *European Journal of Inorg. Chem.*, 2021, **2021**, 501–528.

44 D. Lawton and R. Mason, *J. Am. Chem. Soc.*, 1965, **87**, 921–922.

45 J. L. Eglin, L. T. Smith and R. J. Staples, Inorganica Chim. Acta, 2003, **351**, 217–224.

46 T. A. Stephenson and G. Wilkinson, J. Inorg. Nucl. Chem., 1966, **28**, 2285–2291.

47 M. Cortijo, R. González-Prieto, S. Herrero, J. L. Priego and R. Jiménez-Aparicio, Coord. Chem. Rev., 2019, **400**, 213040.

48 M. Barquín, N. Cocera, M. J. González Garmendia, L. Larrínaga, E. Pinilla and M. R. Torres, J. Coord. Chem., 2010, **63**, 2247–2260.

49 F. Hujon, R. H. D. Lyngdoh, H. F. Schaefer and R. B. King, *Inorg. Chem.*, 2021, **60**, 584–596.

50 M. H. Chisholm, in *Reactivity of Metal-Metal Bonds*, American Chemical Society, 1981, vol. 155, pp. 17–39.

51 L. A. Wilkinson, in *Organometallic Chemistry*, eds. N. J. Patmore and P. I. P. Elliott, Royal Society of Chemistry, Cambridge, 2020, vol. 43, pp. 111–143.

52 F. A. Cotton, L. M. Daniels, C. A. Murillo, I. Pascual and H.-C. Zhou, *J. Am. Chem. Soc.*, 1999, **121**, 6856–6861.

53 J. Hansen and H. M. L. Davies, Coord. Chem. Rev., 2008, **252**, 545–555.

54 H. T. Chifotides and K. R. Dunbar, *Acc. Chem. Res.*, 2005, **38**, 146–156.

55 S. L. Schiavo, P. Piraino, A. Bonavita, G. Micali, G. Rizzo and G. Neri, Sens. Actuators B Chem., 2008, **129**, 772–778.

56 M. Köberl, M. Cokoja, W. A. Herrmann and F. E. Kühn, *Dalton Trans.*, 2011, **40**, 6834–6859.

57 Y. N. Tan, T. Cheng, M. Meng, Y. Y. Zhang, C. Y. Liu, M. F. Sun, Y. Zhang and P. J. Low, *J. Phys. Chem. C*, 2017, **121**, 27860–27873.

58 S. E. Brown-Xu, M. H. Chisholm, C. B. Durr, T. L. Gustafson and T. F. Spilker, *J. Am. Chem. Soc.*, 2014, **136**, 11428–11435.

59 R. H. Cayton, M. H. Chisholm, J. C. Huffman and E. B. Lobkovsky, *J. Am. Chem. Soc.*, 1991, **113**, 8709–8724.

60 F. A. Cotton, C. Lin and C. A. Murillo, *Journal of the Chemical Society, Dalton Trans.*, 1998, 3151–3154.

61 M. H. Chisholm and A. M. Macintosh, *J. Chem. Soc., Dalton Trans.*, 1999, 1205–1208.

62 M. H. Chisholm, F. A. Cotton, L. M. Daniels, K. Folting, J. C. Huffman, S. S. Iyer, C. Lin, A. M. Macintosh and C. A. Murillo, *J. Chem. Soc., Dalton Trans.*, 1999, 1387–1392.

63 F. A. Cotton, L. M. Daniels, C. Lin and C. A. Murillo, *J. Am. Chem. Soc.*, 1999, **121**, 4538–4539.

64 F. A. Cotton, C. Lin and C. A. Murillo, *Inorg. Chem.*, 2001, **40**, 478–484.

65 F. A. Cotton, C. Lin and C. A. Murillo, *Inorg. Chem.*, 2001, **40**, 575–577.

66 F. A. Cotton, C. Lin and C. A. Murillo, *Inorg. Chem.*, 2001, **40**, 472–477.

67 F. Albert Cotton, L. M. Daniels, C. Lin, C. A. Murillo and C. A. Murillo, *Chem. Commun.*, 1999, 841–842.

68 C. Creutz and H. Taube, *J. Am. Chem. Soc.*, 1969, **91**, 3988–3989.

69 R. F. Winter, *Organometallics*, 2014, **33**, 4517–4536.

70 M. B. Robin and P. Day, in *Advances in Inorganic Chemistry and Radiochemistry*, eds. H. J. Emeléus and A. G. Sharpe, Academic Press, 1968, vol. 10, pp. 247–422.

71 B. Thompson, MRes Thesis, University of York, 2022.

72 F. A. Cotton, L. M. Daniels, E. A. Hillard and C. A. Murillo, *Inorg. Chem.*, 2002, **41**, 1639–1644.

73 I. A. Z. Squire, C. A. Goult, B. C. Thompson, E. Alexopoulos, A. C. Whitwood, T. F. N. Tanner and L. A. Wilkinson, *Inorg. Chem.*, 2022, **61**, 19144–19155.

74 J. Hicks, S. P. Ring and N. J. Patmore, *Dalton Trans.*, 2012, **41**, 6641–6650.

75 M. H. Chisholm and N. J. Patmore, *Acc. Chem. Res.*, 2007, **40**, 19–27.

76 L. E. Wilson, C. Hassenrück, R. F. Winter, A. J. P. White, T. Albrecht and N. J. Long, Angew. Chem. Int. Ed., 2017, **56**, 6838–6842.

77 F. A. Cotton, J. P. Donahue, C. Lin and C. A. Murillo, *Inorg. Chem.*, 2001, **40**, 1234–1244.

78 E. D. Becker, *High Resolution NMR : Theory and Chemical Applications*, San Diego, CA : Academic Press, 3rd ed., 2000.

79 F. A. Cotton, J. P. Donahue and C. A. Murillo, *J. Am. Chem. Soc.*, 2003, **125**, 5436–5450.

80 T. E. Concolino, J. L. Eglin and R. J. Staples, *Polyhedron*, 1999, **18**, 915–921.

81 J. L. Eglin, Comments Inorg., 2002, **23**, 23–43.

82 F. A. Cotton, C. Y. Liu and C. A. Murillo, *Inorg. Chem.*, 2004, **43**, 2267–2276.

83 F. A. Cotton, C. Y. Liu, C. A. Murillo, D. Villagrán and X. Wang, *J. Am. Chem. Soc.*, 2003, **125**, 13564–13575.

84 F. A. Cotton, J. P. Donahue and C. A. Murillo, *Inorg. Chem.*, 2001, **40**, 2229–2233.

85 F. A. Cotton, C. Y. Liu, C. A. Murillo and X. Wang, *Inorg. Chem.*, 2003, **42**, 4619–4623.

86 F. A. Cotton, Z. Li, C. Y. Liu and C. A. Murillo, *Inorg. Chem.*, 2007, **46**, 7840–7847.

87 M. H. Chisholm and N. J. Patmore, *Dalton Trans.*, 2006, 3164–3169.

88 E. Neofotistou, C. D. Malliakas and P. N. Trikalitis, *Inorg. Chem.*, 2007, **46**, 8487–8489.

89 M. J. Han, C. Y. Liu and P. F. Tian, *Inorg. Chem.*, 2009, **48**, 6347–6349.

90 A. Aviram and M. A. Ratner, Chem. Phys. Lett., 1974, **29**, 277–283.

91 X. Xiao, C. Y. Liu, Q. He, M. J. Han, M. Meng, H. Lei and X. Lu, *Inorg. Chem.*, 2013, **52**, 12624–12633.

92 W. Y. Yu, M. Meng, H. Lei, X. D. He and C. Y. Liu, *J. Phys. Chem. C*, 2016, **120**, 12411–12422.

93 T. Cheng, M. Meng, H. Lei and C. Y. Liu, *Inorg. Chem.*, 2014, **53**, 9213–9221.

94 T. Ren, *Chem. Rev.*, 2008, **108**, 4185–4207.

95 W.-Z. Chen and T. Ren, *Organometallics*, 2004, **23**, 3766–3768.

96 W.-Z. Chen and T. Ren, *Organometallics*, 2005, **24**, 2660–2669.

97 G.-L. Xu and T. Ren, *Organometallics*, 2005, **24**, 2564–2566.

98 G.-L. Xu and T. Ren, *Inorg. Chem.*, 2006, **45**, 10449–10456.

99 S. E. Brown-Xu, M. H. Chisholm, C. B. Durr and T. F. Spilker, *J. Am. Chem. Soc.*, 2013, **135**, 8254–8259.

100 S. E. Brown-Xu, M. H. Chisholm, C. B. Durr, T. F. Spilker and P. J. Young, *Chem. Sci.*, 2015, **6**, 1780–1791.

101 P. F. Barbara, A. J. Gesquiere, S.-J. Park and Y. J. Lee, *Acc. Chem. Res.*, 2005, **38**, 602–610.

102 W. J. Ramsay, F. J. Rizzuto, T. K. Ronson, K. Caprice and J. R. Nitschke, *J. Am. Chem. Soc.*, 2016, **138**, 7264–7267.

103 J. Park, Y.-P. Chen, Z. Perry, J.-R. Li and H.-C. Zhou, *J. Am. Chem. Soc.*, 2014, **136**, 16895–16901.

104 T. F. Spilker, Ph.D. Thesis, The Ohio State University, 2014.

105 P. Siemsen, R. C. Livingston and F. Diederich, Angew. Chem. Int. Ed., 2000, **39**, 2632–2657.

106 R. H. Cayton, S. T. Chacon, M. H. Chisholm and K. Folting, *Polyhedron*, 1993, **12**, 415–422.

107 C. Lin, J. D. Protasiewicz, E. T. Smith and T. Ren, *Inorg. Chem.*, 1996, **35**, 6422–6428.

108 N. Elgrishi, K. J. Rountree, B. D. McCarthy, E. S. Rountree, T. T. Eisenhart and J. L. Dempsey, *J. Chem. Educ.*, 2018, **95**, 197–206.